BINARY COMBINATIONS OF HPMA COPOLYMER BOUND ANTICANCER DRUG CONJUGATES

JARUNEE HONGRAPIPAT

**A THESIS SUBMITTED IN PARTIAL FULFILLMENT
OF THE REQUIREMENTS FOR
THE DEGREE OF DOCTOR OF PHILOSOPHY
(PHARMACEUTICS)
FACULTY OF GRADUATE STUDIES
MAHIDOL UNIVERSITY
2008**

Title
Entitled

BINARY COMBINATIONS OF HPMA COPOLYMER BOUND ANTICANCER DRUG CONJUGATES

.....
Miss Jarunee Hongrapipat
Candidate

.....
Prof. Dr. Sompol Prakongpan, Ph.D.
Major-Advisor

.....
Prof. Dr. Jindřich Kopeček, Ph.D.
Co-Advisor

.....
Assoc. Prof. Dr. Pimolpan Pithayanukul, Ph.D.
Co-Advisor

.....
Prof. Banchong Mahaisavariya, M.D.
Dean
Faculty of Graduate studies

.....
Prof. Dr. Ampol Mitrevej, Ph.D.
Chair
Doctor of Philosophy Programme
in Pharmaceutics
Faculty of Pharmacy

Title
Entitled

BINARY COMBINATIONS OF HPMA COPOLYMER BOUND ANTICANCER DRUG CONJUGATES

was submitted to the Faculty of Graduate Studies, Mahidol University
For the degree of Doctor of Philosophy (Pharmaceutics)
on
20 May, 2008

.....
Miss Jarunee Hongrapipat
Candidate

.....
Prof. Dr. Pavla Kopečková, Ph.D.
Chair

.....
Prof. Dr. Sompol Prakongpan, Ph.D.
Member

.....
Prof. Dr. Jindřich Kopeček, Ph.D.
Member

.....
Assoc. Prof. Dr. Pimolpan Pithayanukul, Ph.D.
Member

.....
Prof. Banchong Mahaisavariya, M.D.
Dean
Faculty of Graduate studies
Mahidol University

.....
Prof. Dr. Ampol Mitrevej, Ph.D.
Dean
Faculty of Pharmacy
Mahidol University

ACKNOWLEDGEMENTS

A number of people have contributed to the completion of this thesis, and I would like to offer my gratitude for their assistance.

Firstly, appreciation is given to my advisor, Prof. Dr. Sompol Prakongpan for his help and supporting my work in every possible way throughout my study.

I am deeply grateful to my oversea co-advisors, Prof. Dr. Jindřich Kopeček for giving me opportunity to join his research group, and his guidance, scientific expertise, encouragement and support throughout the research.

My special thank belongs to Prof. Dr. Pavla Kopečková for her invaluable help, encouragement, suggestion and her care in research, as well as her advice with the HPMA copolymer synthesis and characterization.

I would like to acknowledge to Dr. Alexander (Sasha) Malugin, Dr. Huaizhong Pan, Dr. Jihua Liu and Dr. Jiyuan (Jane) Yang for their excellent assistance and many helpful discussion.

I would like to thank my friends and colleagues at University of Utah, Monika Sima, Russell Johnson, Jon Callahan, Vaikunth Cuchelkar, Larisa Radu, Kuangshi Wu, Weiwei Yuan for being helpful, and providing the great time and enjoyable environment in lab.

In particular, a big thank you goes to Pad Chivukula for being patient in training my English language and taking good cares of me during I was in USA.

I also would like to thank Ph.D. candidate of Mahidol University, Ms. Jiraporn Leanpolchareanchai for organizing everything in Mahidol University during I was abroad.

Finally, I owe special thanks to my mom, my sisters and my brother for all their loves, plentiful supports and encouragements.

The research was supported in part by the NIH grant CA51578 from the National Cancer Institute, and by the Thailand Research Fund (TRF) through the Royal Golden Jubilee Ph.D. Program (Grant No. PHD/0176/2545).

Doxorubicin was a kind gift from Dr. A. Suarato (Pfizer, Milano, Italy). SOS-thiophene was kindly supplied by the Drug Synthesis and Chemistry Branch, Developmental Therapeutics Program, Division of Cancer Treatment and Diagnosis, National Cancer Institute.

JARUNEE HONGRAPIPAT

BINARY COMBINATIONS OF HPMA COPOLYMER BOUND ANTICANCER DRUG CONJUGATES

JARUNEE HONGRAPIPAT 4537354 PYPT/D

Ph.D. (PHARMACEUTICS)

THESIS ADVISORS: SOMPOL PRAKONGPAN, Ph.D., JINDŘICH KOPEČEK, Ph.D., PIMOLPAN PITHAYANUKUL,Ph.D.

ABSTRACT

The main goal of this study was to determine the biological activities and the drug interactions in anticancer effect toward (*A*) human ovarian carcinoma OVCAR-3 cells by single agents and sequential combinations of SOS thiophene (SOS) and mesochlorin e_6 monoethylenediamine (Mce_6) in the form of free drugs, non-targeted *N*-(2-hydroxypropyl)methacrylamide (HPMA) copolymer-drug conjugates, and Fab'-targeted HPMA copolymer-drug conjugates; and (*B*) human renal carcinoma A498 cells by single agents and binary simultaneous combinations of free SOS, doxorubicin (DOX), and Mce_6 and their HPMA copolymer-drug conjugates. The cytotoxic activities were determined using a modified MTT assay. The median-effect analysis and the determination of the combination index (CI) were used to describe the drug interaction and quantify the synergism, antagonism, or additivity in anticancer effects. The results of experiment (*A*) showed that (*i*) the sequential combinations toward OVCAR-3 cells of free drugs SOS+Mce_6 and non-targeted HPMA copolymer-drug conjugates P-GFLG-SOS+P-GFLG-Mce_6 (P is the HPMA copolymer backbone and GFLG is the glycylphenylalanylleucylglycine spacer) displayed very strong synergism to synergism in the entire range of cell inhibition levels (f_a = 0.5-0.95); and (*ii*) the Fab'-targeted HPMA copolymer-drug conjugates (Fab' from OV-TL16 antibodies complementary to CD47) P-(GFLG-SOS)-Fab'+P-(GFLG-Mce_6)-Fab' exhibited a strong synergism for f_a values up to about 0.85, but showed synergistic effect and nearly additive effect at f_a = 0.9 and 0.95, respectively. The results of experiment (*B*) demonstrated that (*i*) as single agents SOS and P-GFLG-SOS were significantly more effective than the other agents evaluated; (*ii*) the combination of SOS+DOX proved to be synergistic over all cell growth inhibition levels; (*iii*) the SOS+Mce_6 and P-GFLG-SOS+P-GFLG-Mce_6 combinations displayed synergism up to f_a values of about 0.8 and reached slight antagonism and nearly additive effect at f_a = 0.95, respectively; (*iv*) all other combinations exhibited synergism in a wide range of drug effect levels up to f_a < 0.9 and were additive at higher f_a values. The observations from both experiments support the continuation of *in vivo* investigations of these conjugates for the treatment of ovarian and renal cancers.

KEY WORDS: *N*-(2-HYDROXYPROPYL)METHACRYLAMIDE COPOLYMER/ 2,5-*bis*(6-HYDROXYMETHYL-2-THIENYL) FURAN/ MESOCHLORIN e_6 MONOETHYLENEDIAMINE/ DOXORUBICIN/ COMBINATION INDEX

115 P.

การเพิ่มฤทธิ์ในการต้านการเจริญเติบโตของมะเร็งโดยการใช้ยาเชื่อมต่อพอลิเมอร์ HPMA สองตัวร่วมกัน

(BINARY COMBINATIONS OF HPMA COPOLYMER BOUND ANTICANCER DRUG CONJUGATES)

จารุณี หงส์รพิพัฒน์ 4537354 PYPT/D

ปร.ด. (เภสัชการ)

คณะกรรมการควบคุมวิทยานิพนธ์: สมพล ประคองพันธ์, Ph.D., JINDŘICH KOPEČEK, Ph.D., พิมลพรรณ พิทยานุกูล, Ph.D.

บทคัดย่อ

วัตถุประสงค์ของการศึกษานี้เพื่อศึกษาฤทธิ์ทางชีวภาพในการต้านเซลล์มะเร็งรังไข่ OVCAR-3 ของการให้ยาตัวเดียวและ 2 ตัวและปฏิกิริยาระหว่างยาเมื่อให้ยา 2 ตัวแบบต่อเนื่องกัน โดยการให้ยา SOS thiophene (SOS) และ mesochlorin e_6 monoethylenediamine (Mce_6) ในรูปแบบยาอิสระ, ยาเชื่อมต่อพอลิเมอร์ *N*-(2-hydroxypropyl)methacrylamide (HPMA) และยาเชื่อมต่อพอลิเมอร์ HPMA กับชิ้นส่วนแอนติบอดี้ Fab' ซึ่งมาจากแอนติบอดี้ OV-TL16 ซึ่งมีความสามารถในการจับกับ CD47 บนเซลล์มะเร็งรังไข่ ผลการศึกษาพบว่าการให้ยาแบบเดี่ยวและแบบต่อเนื่อง SOS+Mce_6 ในรูปแบบยาอิสระและยาเชื่อมต่อพอลิเมอร์ HPMA สามารถต้านการเจริญเติบโตของเซลล์มะเร็งรังไข่และยาทั้งสองเสริมฤทธิ์ซึ่งกันและกันตลอดระดับการต้านการเจริญเติบโตของเซลล์ (5-95%) รวมทั้งการให้ยาแบบต่อเนื่อง SOS+Mce_6 ในรูปแบบยาเชื่อมต่อพอลิเมอร์ HPMA กับชิ้นส่วนแอนติบอดี้ Fab' สามารถเสริมฤทธิ์กันในระดับ 5-90% แต่สามารถรวมฤทธิ์กันในระดับ 95% นอกจากนี้การศึกษาฤทธิ์ทางชีวภาพและปฏิกิริยาระหว่างยาเมื่อให้ยา 2 ตัวแบบพร้อมกันในการต้านเซลล์มะเร็งไต A498 โดยการให้ยา SOS, Mce_6 และ doxorubicin (DOX) ในรูปแบบยาอิสระและยาเชื่อมต่อ HPMA ผลการศึกษาพบว่าการให้ยา SOS หรือ SOS เชื่อมต่อ HPMA ตัวเดียวสามารถยับยั้งการเจริญเติบโตของเซลล์มะเร็งไตได้ดีกว่ายา Mce_6 และ DOX ทั้งในสองรูปแบบและการให้ยา SOS+DOX รวมกันก็สามารถเสริมฤทธิ์กันได้ตลอดระดับการต้านการเจริญเติบโตของเซลล์ รวมทั้งการให้ยาพร้อมกันของ SOS+Mce_6 และ DOX+Mce_6 ในรูปแบบยาอิสระ และยาเชื่อมต่อ HPMA แสดงฤทธิ์แบบเสริมกันในระดับประมาณ 5-90% และแสดงฤทธิ์รวมกันในระดับ 95% การศึกษาทั้งสองนี้แสดงให้เห็นว่าการให้ ยาเชื่อมต่อ HPMA แบบ 2 ตัวที่ใช้ในการทดลองนี้ควรได้รับเลือกในการศึกษาฤทธิ์ทางชีวภาพในสัตว์ทดลองต่อไป

115 หน้า

CONTENTS

CONTENTS (continued)

LIST OF TABLES

LIST OF FIGURES

LIST OF FIGURES (continued)

LIST OF ABBREVIATIONS

°C	degree celcius
%	percent
% v/v	percent of volume by volume
% w/v	percent of weight by volume
% w/w	percent of weight by weight
ε	extinction coefficient
µg	microgram(s)
µL	microliter(s)
µm	micrometer(s)
µM	micromolar(s)
µmol	micromole(s)
nm	nanometer(s)
AIBN	2,2'-azobisisobutyronitrile
APMA	*N*-(3-aminopropyl)methacrylamide hydrochloride
CI	combination index
cm	centimeter(s)
D	dose (concentration)
Da	dalton
DEAE	diethylaminoethyl
DI	deionized
DIPEA	*N*,*N*´-diisopropylethylamine
D_m	median-effect dose (median-effect concentration)
DMAP	4-dimethylaminopyridine
DMF	*N*,*N*-dimethylformamide
DMSO	dimethylsulfoxide
d_n	dose of the agent in combination that produce the *x*% effect

LIST OF ABBREVIATIONS (continued)

D_n	dose of the individual agent that produce the *x*% effect
DOX	doxorubicin
DRI	dose-reduction index
$(D)_n$	dose of drug n used in combination that inhibit a system *x*%
$(D_x)_n$	dose of drug n alone that inhibit a system *x*%
ED	effective dose
EDTA	ethylenediaminetetraacetic acid
e.g.	exempli gratia (for example)
et al.	et alii (and others)
ESI-MS	electrospray ionization mass spectrometry
f_a	fraction of cells affected after drug exposure
Fa-CI plot	combination index plot (or CI plot)
FITC	fluorescein-5-isothiocyanate
FPLC	fast performance liquid chromatography
f_u	fraction of cells unaffected after drug exposure
GG	glycylglycine (Gly-Gly)
GFLG	glycylphenylalanylleucylglycine (Gly-Phe-Leu-Gly)
gp	glycoprotein
h	hour
HDM-2	human double minute-2
HPMA	*N*-(2-hydroxypropyl)methacrylamide
IAP	integrin-associated protein (CD47 or OA-3)
IC_{50}	concentration that inhibits cell growth by 50% as compared with control cell growth
IFN-α	interferon alpha
IL-2	interleukin-2

LIST OF ABBREVIATIONS (continued)

Ka	affinity constant
kDa	kilodalton
m	coefficient denoting the shape of the dose-effect curve (or slope of the median-effect plot)
M	molar
MA	methacryloyl
mAb	monoclonal antibody
MA-GFLG-Drug	*N*-methacryloylglycylphenylalanylleucylglycine containing drug at side chain termini via GFLG linker
MA-GFLG-Mce_6	*N*-methacryloylglycylphenylalanylleucylglycine containing Mce_6 at side chain termini via GFLG linker
MA-GFLG-ONp	*N*-methacryloylglycylphenylalanylleucylglycine *p*-nitrophenyl ester
MA-GFLG-SOS	*N*-methacryloylglycylphenylalanylleucylglycine containing SOS at side chain termini via GFLG linker
MAL	maleimide group
Mce_6	mesochlorin e_6 monoethylene diamine
MDM-2	mouse double minute-2
MES	2-(*N*-morpholino)ethanesulfonic acid
mg	milligram(s)
mL	milliliter(s)
mM	milimolar(s)
mmol	milimole(s)
mol%	mole percent
MTT	3-(4,5-dimethylthiazol-2-yl)-2,5-diphenyltetrazoliumbromide
M_w	weight-average molecular weight

LIST OF ABBREVIATIONS (continued)

M_w/M_n	polydispersity (the ratio of weight-average to number-average molecular weight)
MWCO	molecular weight cut off
$^1O_2$	singlet oxygen
ONp	*p*-nitrophenyl ester
P	HPMA copolymer backbone
PBS	phosphate buffered saline
PEG	poly(ethyleneglycol)
PDT	photodynamic therapy
P-GFLG-DOX	HPMA copolymer bound DOX via GFLG linker
P-GFLG-Drug	HPMA copolymer bound drug via GFLG linker
P-GFLG-Mce_6	HPMA copolymer bound Mce_6 via GFLG linker
P-(GFLG-Mce_6)-Fab'	Fab' fragment-targeted HPMA copolymer-Mce_6 conjugate
P-(GFLG-Mce_6)-FITC	fluorescein-labeled non-targeted HPMA copolymer-Mce_6 conjugate
P-(GFLG-Mce_6)-(Fab'-FITC)	fluorescein-labeled Fab' fragment-targeted HPMA copolymer-Mce_6 conjugate
P-(GFLG-Mce_6)-MAL	HPMA copolymer-Mce_6 conjugate containing maleimide groups
P-(GFLG-Mce_6)-NH_2	HPMA copolymer-Mce_6 conjugate containing amine groups
P-GFLG-ONp	HPMA precursor with *N*-methacryloyl glycylphenylalanylleucylglycine *p*-nitrophenyl ester groups
P-GFLG-SOS	HPMA copolymer bound SOS via GFLG linker
P-(GFLG-SOS)-Fab'	Fab' fragment-targeted HPMA copolymer-SOS conjugate

LIST OF ABBREVIATIONS (continued)

P-(GFLG-SOS)-FITC	fluorescein-labeled non-targeted HPMA copolymer-SOS conjugate
P-(GFLG-SOS)-(Fab'-FITC)	fluorescein-labeled Fab' fragment-targeted HPMA copolymer-SOS conjugate
P-(GFLG-SOS)-MAL	HPMA copolymer-SOS conjugate containing maleimide groups
P-(GFLG-SOS)-NH_2	HPMA copolymer-SOS conjugate containing amine groups
PK1	HPMA copolymer bound DOX via a GFLG linker (FCE28068)
PK2	HPMA copolymer bound DOX via a GFLG linker containing side-chains terminated in *N*-acylated galactosamine (FCE28069)
r	linear correlation coefficient
RITA	reactivation of p53 and induction of tumor cell apoptosis
SAMSA	5-((2-(and-3)-*S*-(acetylmercapto)succinoyl)amino)fluorescein
SEC	size exclusion chromatography
5-SFX	6-(fluorescein-5-carboxamido) hexanoic acid succinimidyl ester
SMCC	succinimidyl *trans*-4-(maleimidomethyl) cyclohexane-1-carboxylate
SOS	2,5-bis(5-hydroxymethyl-2-thienyl) furan (SOS thiophene, NSC 652287)
THF	tetrahydrofuran
TLC	thin-layer chromatography
wt.%	weight percent

PUBLICATIONS AND PRESENTATIONS

PUBLICATIONS

Hongrapipat J, Liu J, Kopečková P, Prakongpan S, Kopeček J. Combination chemotherapy and photodynamic therapy with Fab' fragment targeted HPMA copolymer conjugates in human ovarian carcinoma cells. Submitted.

Hongrapipat J, Kopečková P, Prakongpan S, Kopeček J. Enhanced antitumor activity of combinations of free and HPMA copolymer-bound drugs. Int J Pharm 2008;351(1-2):259-70.

POSTER PRESENTATIONS

Hongrapipat J, Kopečková P, Prakongpan S, Kopeček J. Combination treatment of human ovarian carcinoma cells with Fab'-targeted HPMA copolymer - SOS thiophene and - Mce_6 conjugates. Poster presented at The 13^{th} International Symposium on Recent Advances in Drug Delivery Systems, Feb 26-28, 2007, Salt Lake City, Utah.

Hongrapipat J, Kopečková P, Prakongpan S, Kopeček J. Enhanced antitumor activity of combinations of free and HPMA copolymer-bound drugs. Poster presented at RGJ Seminar Series LIX: Nanotechnology in Drug Delivery, Mar 20, 2008, Faculty of Pharmacy, Bangkok, Thailand.

CHAPTER I
INTRODUCTION

In the United States and other developed countries, cancer is presently responsible for about 25% of all deaths. According to the World Health Organization (WHO), there were 10.9 million new cases being diagnosed every year, 6.7 million people died of cancer, and 24.6 million people living with cancer worldwide (within 5 years of diagnosis) (1). Cancers can be divided broadly into two groups: solid tumor cancers, which are characterized by the growth of malignant tumors within the body in areas such as brain, lung, liver, breast or prostate cancer, and hematological or blood-borne cancers, such as leukemia.

The most conventional ways for treating cancer are surgery, radiation therapy and chemotherapy. These treatments may be given as stand-alone treatments or, more commonly, in some combinations with one another. These treatments are variously combined in order to optimize therapeutic indices for that individual patient. Surgery and radiation are the local treatment methods which the tumor is either directly removed through surgery or irradiated with the objective of destroying the cancer cells. Chemotherapy is a systemic treatment method which involves the administration of drugs with the objective of killing cancer cells anywhere in the body, including any remaining cancer cells that were not destroyed by local treatment. Chemotherapeutic agents can damage healthy cells and cause systemic effects. Because these agents circulate throughout the entire body through the bloodstream and most of these agents do not make a distinction between cancerous cells and noncancerous cells (1). Nevertheless, the nonspecific cytotoxicity of chemotherapeutic agents is another obstacle that needs to be overcome. However, as cancer research develops, the treatments are becoming more specific for different types of cancer. There has been significant progress in the development of targeted therapy drugs that act specifically on certain cancers, and which minimize damage to normal cells.

To increase the selectivity of therapeutic agents to cancer cells, the drug delivery systems have been designed by using various carriers, such as polymeric carriers, liposomes, and nanoparticles. The creation of proposed drug delivery systems was based on the specific pathophysiological characteristics of most solid cancers that are not observed in normal tissues called "enhanced permeability and retention (EPR) effect". The EPR effect means that macromolecules are selectively trapped by tumor tissues and stay there for a longer period of time because of the following characteristics of tumor tissues: (*a*) high neovascular density; (*b*) larger intercellular space (100-200 nm) in defective vascular architecture; (*c*) vascular hyperpermeability due to the increased production of vascular permeability factor; and (*d*) ineffective lymphatic drainage (2, 3). Due to this effect, the use of macromolecular drug delivery systems facilitates the uptake and transport of therapeutic agents and creates a dose-differentiation between the treatment target and the rest of the body (2). The enhanced drug accumulation in tumor tissue increases the therapeutic effect while reducing non-specific side effects (4-6). Moreover, it is well known that macromolecular drug delivery systems have the potential to overcome multidrug resistance. The exclusion of the polymer-drug conjugates from the cytoplasm of the cell, due to the fact that intracellular trafficking occurs within membrane-limited organelles, renders efflux pumps ineffective (7). Experimental data on sensitive (A2780) and resistant (A2780/AD) human ovarian carcinoma cells showed that, in contrast to free doxorubicin (DOX), *N*-(2-hydroxypropyl)methacrylamide (HPMA) copolymer bound DOX conjugate overcame pre-existing MDR1-gene-encoded multidrug resistance, and did not induce it *de novo* after acute or chronic exposure *in vitro* (8, 9). Similar results were obtained in solid tumor mice models of DOX sensitive and resistant human ovarian carcinoma. Free DOX was effective only in sensitive tumors, while HPMA copolymer bound DOX conjugate was effective in both sensitive and drug-resistant tumors (10).

In addition of the passive targeting of the drug at the tumor site by macromolecular carriers, active targeting can be usually achieved by adding to the drug delivery system a ligand moiety specifically directed to certain types of binding sites on cancer cells (11). These binding sites, such as antigens or receptors, are either uniquely expressed or overexpressed on the target cells relative to normal cells.

Several different targeting moieties were examined, including sugars (12, 13), lectins (14, 15), receptor ligands (16, 17), and antibodies (18, 19) and their fragments, such as Fab' (20, 21). To obtain such multifunctional capabilities, macromolecular carriers have been designed to consist of (*a*) a non-immunogenic and biocompatible water-soluble polymer backbone such as PEG or HPMA copolymers (22), (*b*) therapeutically active molecules, (*c*) linkers between the polymer backbone and the active molecule that are stable in blood circulation and release the free drug at target sites, and (*d*) a targeting moiety to mediate biomolecular recognition (23, 24).

Water-soluble synthetic HPMA copolymer is one of the drug delivery systems that many researchers have been using as carrier of anticancer agents (7, 25, 26). Several HPMA copolymers bound drug(s) are currently in preclinical and clinical trials, such as HPMA copolymer-doxorubicin (27), HPMA copolymer-platinate (28) and HPMA copolymer-TNP-470 (29). For decades HPMA-drug conjugates have been studied and reported that can increase the passive accumulation of the drug at the tumor site by EPR effect (30), and overcome efflux pump-mediated mechanism of drug resistance (8-10). Furthermore, the incorporation of targeting moieties, such as monoclonal antibodies (mAb) and antibody fragments, to HPMA copolymers can allow the specific delivery and the actively accumulation of drugs at the tumor site by their association with antigens that are overexpressed on the target cells relative to normal tissues (5, 11, 31, 32). Consequently, the intracellular concentration of the polymeric conjugates is enhanced with concomitant increase in antitumor activity (32). These modifications of mAb and antibody fragments also reduce their immunogenicity and extend their circulating half-lives (33, 34). Moreover, the polymer modification of antibody fragments provides a better control of the structure of HPMA copolymer conjugates compared to full-length mAb. The unique sulfhydryl group near the C terminus of Fab' fragments has provided a convenient way for coupling to HPMA copolymers containing maleimide groups and allow the antigen-binding site to be more approachable (20, 35).

Often, a combination of chemotherapy drugs, the use of two or more drugs with different mechanisms of action, is used due to some drugs work better together than alone when given either simultaneously or in sequence. Other than the

improvement of the therapeutic outcome, the combination may reduce the side effects because of minimizing the doses of chemotherapy drugs.

Based on the rationale mentioned above, the combination of HPMA copolymer-drug conjugates appears to be a novel and successful strategy for cancer treatments. The purpose of the present work was to investigate the binary combinations of anticancer agents against two different cancer cell lines, human ovarian carcinoma and human renal carcinoma cell lines. Three anticancer agents chosen in these studies were SOS [2,5-bis(5-hydroxymethyl-2-thienyl) furan, SOS thiophene, NSC 652287], Mce_6 (mesochlorin e_6 monoethylene diamine) and DOX. These agents represent low-molecular weight (M_w) compounds possessing different sites and/or mechanisms of action. To integrate the virtues of polymeric carrier, anticancer agent and/or targeting moiety, the polymer bound drug conjugates and Fab'-targeted polymer bound drug conjugates were synthesized. The experiments were designed to examine the cytotoxic effect of anticancer agents and polymer conjugates as single agents and in combinations. To compare their *in vitro* cell inhibitory activities, the drug concentration that inhibited cell growth by 50% compared with control cells (IC_{50}) was determined using a modified 3-(4,5-dimethylthiazol-2-yl)-2,5-diphenyltetrazoliumbromide (MTT) assay. MTT assay is the widely accepted colorimetric assay was used to measure the cell viability after drug exposure. The yellow tetrazolium MTT reagent is reduced by metabolically active cells, in part by the action of dehydrogenase enzymes, to generate reducing equivalents such as NADH and NADPH. The resulting intracellular purple formazan can be solubilized and quantified by spectrophotometric means. The MTT reagent yields low background absorbance values in the absence of cells. For each cell type the linear relationship between cell number and signal produced is established, thus allowing an accurate quantification of the percentage of cell viability (36).

Moreover, the drug combinations were evaluated using the median-effect analysis. This method is the most commonly used method to evaluate drug combinations *in vitro*, based on the Loewe additivity model, as originally proposed by Chou and Talalay (37-39). The median-effect method assesses the drug-drug interaction by a term called the "combination index" (CI), which is based on the concentration-response relationship. The CI value was used to classify the synergism,

antagonism, and additive effects of drug combinations. These experiments were expected to demonstrate that the combinations of these agents may produce synergistic effects and thereby reduce effective doses, compared to the doses required for each agent alone to produce a given drug effect level.

CHAPTER II
LITERATURE REVIEW

1. Cancer

Cancer is a group of diseases or disorders characterized by uncontrolled cell proliferation and the spread ability of abnormal cells to other parts of body (40). These rapid growing cells may form a clump of cells that are called tumors. Tumors can be benign (non-cancerous) or malignant (cancerous). Benign tumors are tumors that remain self-contained and not spread to other parts of the body. Malignant tumors, or cancers, are not self-contained. They can invade neighboring tissues and organs, or spread to other parts of the body. Cancers are capable of scattering through the body by two mechanisms: invasion and metastasis. Invasion is the direct migration and penetration by cancer cells into surrounding tissues. Metastasis refers to the ability to spread by sending off seedlings of cancer cells into lymphatic and blood vessels, and settle in normal tissues elsewhere in the body (41). More than two-hundred distinct varieties of cancers have been described (42). Five broad categories of cancer types may be classified according to type of cell in which they originate and the degree of differentiation, as carcinoma, sarcoma, leukemia, lymphoma, and melanoma. Carcinomas are solid tumors that originate in epithelial tissues, such as liver, lung, bladder, kidney, breast, ovary, uterus, intestinal tract and skin. Approximately 80% to 90% of all cancer cases are carcinomas. Sarcomas are rare solid tumors, representing less than 2% of all cancers and originate in the supporting tissues, such as connective tissues, bone, muscle, cartilage, and fat. Leukemias are cancers of blood-forming organs that result from abnormal white blood cells production in the bone marrow; they account for 2% of all cancers. Lymphomas are cancers of the lymphocytes that originate in the lymphatic system, e.g. lymph nodes. Lymphomas constitute about 5% of cancer. Melanomas are cancers that originate in melanocytes, the pigment cells in the skin (43). It usually starts with any change in size, shape or color of the spot or mole on the skin.

In these researches two different tumor models, ovarian carcinoma and renal carcinoma, were chosen to study the *in vitro* cytotoxicities of therapeutic agents as single agents and in combinations.

1.1 Ovarian Cancer

Among all the gynecologic cancers, ovarian malignancies represent the greatest clinical challenge. Ovarian cancer is cancer that forms in tissues of ovary, part of female reproductive system. It is the eighth most common cancer in women and ranks fifth as the cause of cancer-related deaths. There are three broad types of ovarian cancer including epithelial ovarian cancer, germ cell cancer, and stromal cell cancer each with different etiologies and clinical behavior. Epithelial ovarian cancer is the most common type and comprises about 90% of all ovarian cancer cases. It forms on the surface of the ovary in the epithelial cells (44, 45). Ovarian cancer is usually asymptomatic until they have metastasized, patients present with advanced disease in more than two-third of the cases. Ovarian cancer has an overall five-year survival rate of only 30%. This poor prognosis is largely because three-fourth of cases are accompanied with extra-ovarian disease, which reflects the absence of symptoms in early-stage ovarian cancer (46). Moreover, ovarian cancer lacks any clear early detection or screening test, meaning that most cases are not diagnosed until they have reached advanced stages. Ovarian cancer represents a major surgical challenge, and requires intensive and often complex therapies (47). The main treatments for ovarian cancer are surgery and chemotherapy. In some cases the combination of these treatments will be recommended (48).

1.2 Renal Cancer

Renal cancer is the seventh most common malignancy among men and the ninth among women, accounting for about 3% of adult malignancies. There are several different types of renal cancer cells. The most common called conventional or clear cell is found in about 75% of renal cancers. The second most common, called papillary, is found in about 12% of renal cancers. Other types, which occur rarely, include chromophobe (4%), oncocytoma (4%), collecting duct (<1%), and unclassified (3-5%) (49). Clear renal cell carcinoma develops from the proximal renal tubular

epithelium (49, 50). It is by far the most frequent neoplasm arising from the kidney. The prognosis for advanced stage renal carcinoma is poor. The low efficiency of chemotherapeutic agents is due to high levels of *p*-glycoprotein expression in normal renal proximal tubules and renal carcinoma cells (51, 52). Furthermore, nearly one-third of patients develop metastatic disease after nephrectomy (50), and about 30% of those treated for localized disease eventually relapse (53). The treatment options for patients with metastatic renal cell carcinoma are few. Conventional chemotherapy and radiotherapy rarely result in clinically beneficial responses. Recently, the immunotherapy, a method of using substances that induce the body's natural immune defense to fight cancer, has become the only standard treatment for metastatic renal cell cancer. Studies showed that two such substances, interleukin-2 (IL-2) and interferon alpha (IFN-α) can shrink the tumor size more than 50% (54, 55). However, the immunotherapy only works in only 15-20% of patients, and IL-2 and IFN-α often cause severe side effects, such as extreme fatigue, influenza-like symptoms, intestinal bleeding, heart attacks, and myocardial infarction (56, 57). Evidently, novel approaches in the treatment of renal carcinoma are needed.

2. Cancer Treatments

A definitive diagnosis usually requires the histological examination of a tissue biopsy specimen. Once diagnosed, cancer can be treated by surgery, chemotherapy, radiation therapy or other methods. The choice of therapy depends on the specific type, location, and stage of cancer, as well as the general state of the patient. Complete removal of the cancer without damage to the rest of the body is the goal of treatment. Surgery is especially appropriate for certain types of cancer, such as breast cancer, where tumors are often well-defined and surgically accessible. However, many types of solid tumors, including those affecting brain, spine, lungs and various other organs, present significant challenges to a surgical approach. Surgery is highly invasive because it requires entering the body by incision, painful and involves significant operative and post-operative risks, including risks associated with anesthesia, infection and other complications. Sometimes surgery is used to reduce the size of a tumor before using other therapies to eliminate any remaining cancer cells in the area surrounding the tumor. Damage during surgery may occur when healthy

tissue surrounding the tumor is removed to make sure that all of the cancer cells are removed. Radiation therapy has been used not only to treat the area around a tumor site, typically as an adjunct to surgery after the tumor has been removed, but also to directly target the tumor when surgery is not possible. However, normal tissues that are either right in or close to the intended treatment area may receive substantial radiation causing other adverse side effects. The surgery and radiation methods are local cancer treatments, which can cause side effects due to damage of surrounding tissues. In contrast, chemotherapy a systemic cancer treatment method by using drugs that can slow or stop the growth and reproduction of cancer cells, which causes systemic side effects by damaging healthy cells throughout the entire body (1).

3. Anticancer Agents

3.1 Photosensitizing Compounds

Photodynamic therapy (PDT), a three-component therapy consisting of a photosensitizer, visible light and oxygen, is a minimally invasive procedure that has great potential for the treatment of malignant disease. It is a relatively new cancer treatment modality that employs light excitation of a photosensitizer to yield cytotoxic oxygen-related species (58, 59). It also depends on the retention of photosensitizers in tumor tissue and irradiation of the tumor with visible light (60).

Mce_6 (Figure 1A) is one of the second-generation synthetic photosensitizing compounds. The initiating step of the photosensitizing mechanism is the absorption of a light photon in the red region of spectrum (640-700 nm) by the sensitizer, causing the activation of drug molecule from its ground state to the extremely unstable excited singlet state with a half life in range of 10^{-6} to 10^{-9} seconds. The singlet excited photosensitizer either decays back to the ground state, resulting in the fluorescence or undergoes intersystem crossover to the longer lived (10^{-3} second) tripled excited state. The interaction of the triplet sensitizer with surrounding molecules results in two types of photooxidative reaction. Type I pathway involves electron or hydrogen atom transfer, producing radical forms of the photosensitizer or the substrate. These intermediates may react with oxygen to form peroxides, superoxide ions, and hydroxyl radicals, which initiate free radical chain reactions. Type II mechanism is mediated by

the energy transfer process with ground state oxygen and to the return of the sensitizer to its ground state. The *in situ* generation of singlet oxygen ($^1O_2$) via type II pathway appears to play the central role in photodynamic cytotoxicity because of the highly efficient interaction of the $^1O_2$ species with different biomolecules, resulting in irreversible photodamage to the cells, cell destruction, and cell death (59, 61-64). However, the photodamage is limited within <0.02 μm of radius of action, mainly because of the limited diffusion of the extremely short-lived singlet oxygen in biologic systems (<0.04 μs) (65, 66). Due to this fact, the effect of photosensitizer is dependent on its cellular accumulation (67). Nevertheless, various delivery systems, such as copolymer conjugates (68), lipoproteins (69) and microspheres (70), have been suggested to enhance the accumulation of photosensitizers into tumor tissue and reduce the non-specific damage to normal tissue.

3.2 Reactivation of p53 and Induction of Tumor Cell Apoptosis (RITA) Compounds

RITA compounds, such as nutlins (71, 72) and chalcone B-1 (73), are small-molecule inhibitors of p53-HDM-2 interaction and are sought as tumor-selective drugs. The function of HDM-2 (human double minute-2) is binding to the N-terminal transactivation domain of p53 resulting in p53 proteasomal degradation (74). Following RITA molecule inhibits p53-HDM-2 interaction, thereby preventing HDM-2-mediated degradation of p53, consequently p53 levels rise, and causing cell cycle arrest or apoptosis.

The synthetic dithiophene compound SOS (Figure 1B), is novel RITA compound that exhibit the most potent and selective antitumor activity against several tumor cell lines expressing wild-type p53, especially the A498 human renal carcinoma cell line. Studies suggested that SOS induces DNA damage and promotes the formation of DNA-DNA and DNA-protein cross-links (75) and interrupts the p53–HDM-2 interaction (76). These effects lead to p53 stabilization and activation resulting in G_0-G_1 and G_2-M cell cycle arrest, thereby strongly inducing apoptosis. *In vivo* studies of SOS in mice with xenografts derived from different drug-sensitive cell lines, including renal A498, renal CAKI-1, melanoma UACC-257, ovarian OVCAR-5, colon HCC-2998 (77), colon HCT116 expressing wild-type p53 and its derivative p53-

null HCT116 (76), showed that SOS possessed strong antitumor activity. It produced complete tumor regression of A498 tumor xenografts, and possessed a moderate or minimal antitumor activity to other cell lines, but had no effect on p53-null HCT116 xenografts.

3.3 Anthracycline

DOX (Figure 1C) is one of the most effective anthracycline antitumor agents. It has shown an excellent anticancer activity in various solid and hematopoietic cancers, including breast cancer, ovarian cancer, prostate cancer, bladder cancer, small and non-small cell lung cancers, Hodgkin's and non-Hodgkin's lymphoma, acute and chronic leukemias, multiple myeloma, and soft tissue and bone sarcomas (78). The multiple mechanisms of action of DOX include: intercalating DNA (79), inhibiting DNA-topoisomerase II interaction (80), and inducing the generation of singlet oxygen and other oxygen radicals (81). These mechanisms lead to DNA strand breaks, DNA damage, and damage to cellular membranes, resulting in G_1 and G_2 cell cycle arrest and cell death (82-84). However, the usefulness of DOX is limited by side effects, particularly cumulative dose-dependent cardiotoxicity (85). Previous studies in mice have demonstrated that the severe cardiotoxicity of DOX can be reduced by conjugating it to HPMA copolymers (86). Similar results have been observed in clinical trials (27).

4. Macromolecular Drug Delivery System

Many macromolecules, such as poly(ethyleneglycol) (PEG) (87), poly(glutamic acid) (88), and HPMA copolymers (27, 89), have been utilized as drug carriers in an attempt to enhance tumor accumulation of macromolecules within tumor sites due to the leakiness of angiogenic tumor blood vessels by the EPR effect (90). The features of macromolecules are essential for effective design (5). The macromolecules must be non-toxic and non-immunogenic, and the molecular mass of macromolecules must be high enough to ensure long circulation (this must be <40,000 g/mol for non-biodegradable macromolecules to ensure eventual renal elimination of the carrier), but low enough to ensure endocytic internalization (typically <100,000 g/mol) (91-93). Moreover, the macromolecules must be able to carry an adequate

A

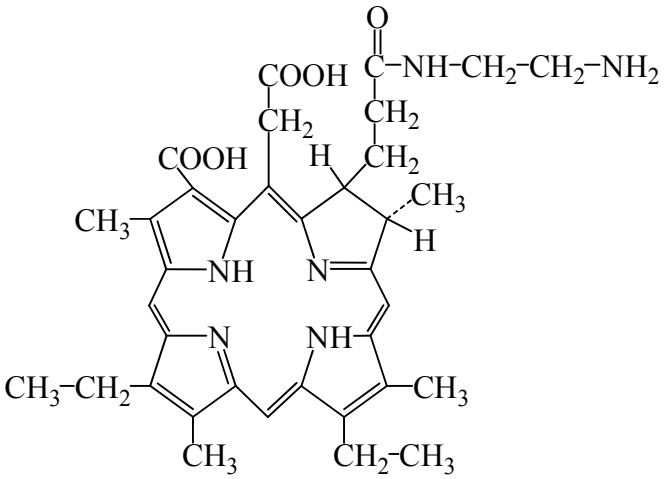

B

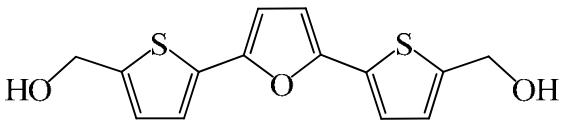

C

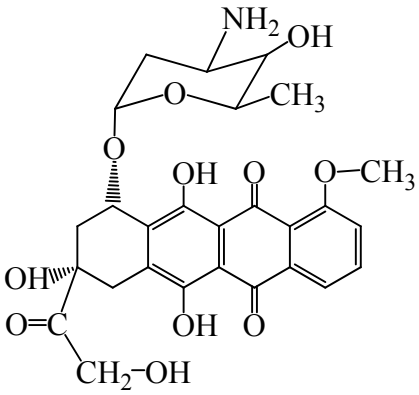

Figure 1. Chemical structure of (**A**) mesochlorin e_6 monoethylene diamine (Mce_6), (**B**) 2,5-bis(5-hydroxymethyl-2-thienyl) furan (SOS thiophene, SOS), and (**C**) doxorubicin (DOX).

payload in relation to drug potency and the linker between drug and macromolecule must be stable during transport in blood circulation, but able to release drug at an optimum rate on arrival at the target site.

Macromolecules are widely used platforms in the formulation of small molecule drugs. Macromolecules may simply improve the physicochemical stability of drug, and can produce long-circulating conjugates and enhance the efficacy of a therapeutic agent by limiting cellular uptake to the endocytic route (5, 94). Whereas the low-M_w drugs enter the cell by diffusion via the plasma membrane and subsequently distribute to all the subcellular compartments, the entry of macromolecules is restricted to endocytosis with ultimate location in the lysosomal compartment of the cell (95). Endocytosis in the case of macromolecules can occur by three different mechanisms depending on their structure: fluid-phase endocytosis, adsorptive endocytosis, and receptor-mediated endocytosis (7, 25). Fluid-phase endocytosis (also known as bulk-fluid endocytosis) occurs when no interaction between the macromolecule and the cell surface takes place. Consequently, macromolecules are taken up slowly depending on their concentration in the extracellular fluid (96). The incorporation of hydrophobic molecules (97) or positively charged moieties (98) into the macromolecule not only can promote substantial non-specific membrane binding due to the net negative charge of the plasma membrane and the hydrophobic nature of the constituent lipids, but also results in a concomitant increase in the rate of macromolecular uptake. This process is known as adsorptive endocytosis. Incorporation of moieties in the macromolecular structure, which specifically bind to cell surface molecules (receptors or antigens), renders the conjugate biorecognizable and initiates endocytotic processes. The macromolecules are internalized specifically by a select subset of cells, thus resulting in not only an increased rate of internalization as compared to fluid phase endocytosis, but also a substantially altered body distribution (99, 100). Therefore, the conjugation of drug or drug and targeting ligand to macromolecule can reduce access to normal cells or sites of toxicity and overcome multidrug resistance, and increase the therapeutic efficacy of a parent anticancer compound (101, 102).

4.1 HPMA Copolymers

HPMA is the most investigated and advanced polymer used in therapeutics due to its versatility as a vehicle. Uncharged, highly biocompatible HPMA homopolymer was designed and synthesized in Czechoslovakia as a plasma expander (24, 103). HPMA being hydrophilic, increases water solubility of the drugs, such as paclitaxel, and has proven to be non-toxic (7, 104). HPMA also can be decorated with multiple agents, such as anticancer agents (5), targeting moieties (11), and imaging agents (105, 106), and can facilitate the delivery of these agents to target site. It is well known that HPMA copolymer drug conjugates have the potential to overcome existing drug efflux pumps located in the plasma membrane of cancer cells and prevent de novo development of multidrug resistance (8-10). In contrast, free low-M_w drugs activated the multidrug resistance mechanisms, such as cellular detoxification mechanisms, antioxidant defense systems, and other non-specific cellular defensive mechanisms. The conjugates internalized into the cancer cells by endocytosis are transported through the cellular cytoplasm in membrane bound organelles, which are not permeable to macromolecules (107). The exclusion of the conjugates from the cytoplasm rendered the efflux pumps ineffective. In addition, this protects the drugs from cellular detoxification enzymes and preserves their high anticancer activity. Thus polymeric drug conjugates bypass some of the common mechanisms of multidrug resistance.

Following internalization, HPMA copolymer conjugates are first localized in mildly acidic endosomes (pH 5.0–6.5) and then ended up in lysosomes, where high levels of lysosomal enzymes and much lower pH are present. Incorporation of linkers degradable in the lysosomal environment can allow for release of free drug and subsequent drug redistribution in the cell. Consequently, the design of the drug attachment/release spacer connecting drug to the polymer backbone was based on the lysosomal environment. Linkers that could be used include acid-labile linkers, disulfide bonds and lysosomal enzyme-sensitive linkers. Acid-labile linkers, such as hydrazone linkages (108) and *cis*-acotinyl spacers (109), are rapidly hydrolyzed at the pH in the endosomal and lysosomal compartments. The problem is that the difference of two pH units between the blood stream and the lysosomal compartment is not high enough to ensure both the stability in the blood stream and fast hydrolysis in

lysosomal compartments. Disulfide bonds linking the drug to the polymer are nonspecifically degraded in the blood stream and at the cell membrane, resulting in the non-specific release of free drug and thus the development of side effects (110). Lysosomal enzyme-sensitive linkers, such as oligopeptide sequences, are stable in circulation and can be specifically cleaved in the lysosome releasing the free drug. Detailed studies with various oligopeptide spacers have been performed to determine optimal linker sequences (111, 112). The commonly used tetrapeptidyl linker glycylphenylalanylleucylglycine (Gly-Phe-Leu-Gly, GFLG) was designed to be stable in the bloodstream and interstitial space but susceptible to cleavage by lysosomal cysteine proteinases, particularly cathepsin B, within the lysosomal compartment resulting in active drug liberation into lysosome and transfer to cytoplasm (113-115). Furthermore, the M_w and M_w distribution are important factors in a polymer carrier's biocompatibility. Based on early studies that evaluated the M_w dependency of endocytosis and biodistribution, an optimal HPMA copolymer M_w of ~30,000 g/mol was chosen (91-93). HPMA copolymers are non-biodegradable in the main chain, so this M_w was chosen and the M_w distribution of synthetic carriers has to be below the renal threshold to ensure the elimination of the carrier from the body.

An HPMA copolymer with DOX conjugated with GFLG peptidyl linker (PK1, FCE28068) was the first synthetic polymer conjugate to enter phase I trials in 1994. The structure is shown in Figure 2. PK1 demonstrated antitumor activity in refractory cancers without polymer-related toxicity. The obtained data strongly indicated the biocompatibility of the HPMA copolymer carrier (27). It also demonstrated that HPMA copolymer-DOX conjugates can induce endocytosis for the delivery of drugs into the solid tumor models and improve *in vivo* antitumor activity with less toxicity when compared to the free drug (116). A detailed investigation showed that high-M_w HPMA copolymer bound drugs accumulated preferentially in solid tumors, due to EPR-mediated tumor accumulation (passive targeting), with only trace amounts of drugs detected in healthy organs, such as liver, heart, lungs, spleen and kidneys. In contrast, significant amount of free drugs were found in the healthy organs. Therefore, the conjugation of low-M_w anticancer drug to HPMA copolymer substantially limited adverse side effects to healthy organs compared to free drugs (7-9).

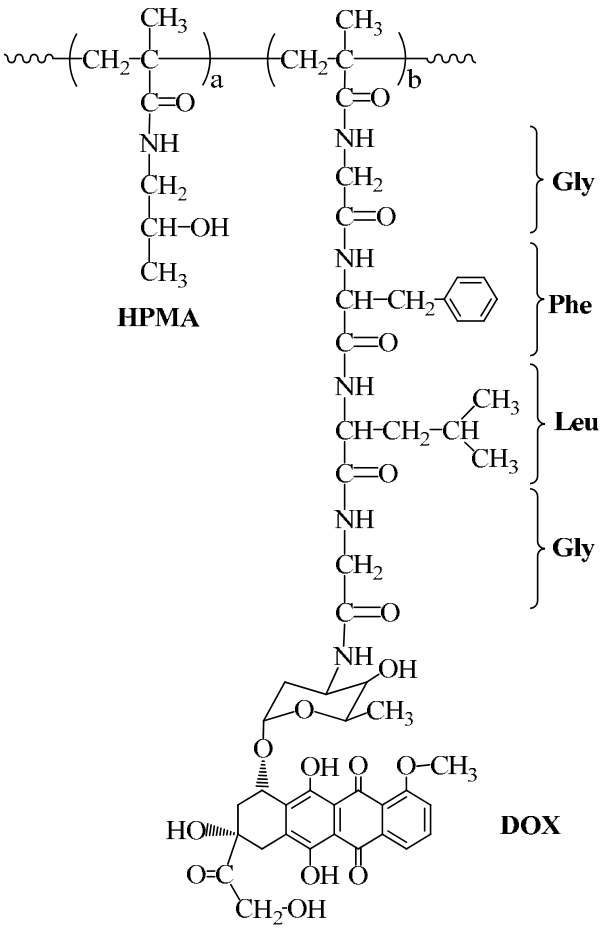

Figure 2. Chemical structure of HPMA polymer bound DOX conjugate (PK1).

4.2 Targeted-HPMA Copolymer Conjugates

Various targeting moieties (complementary to molecules on the surface of the cell, such as carbohydrates (117, 118), vitamins or analogs (119, 120), hormones or analogs (121), proteins (122, 123), and antibodies (34, 99), can be incorporated into the polymeric conjugates to achieve the biorecognizability of conjugates at the plasma membrane of the target cells. . Incorporation of targeting moieties to HPMA copolymer conjugates can improve the cell surface binding of conjugates. This enhances the amount of the conjugates being internalized by receptor-mediated endocytosis, further increases the rate of cellular uptake and increases the intracellular concentration (as compared to fluid phase or adsorptive endocytosis) (20, 32, 89).

The targeting moieties can be classified into two major categories: non-antibody ligands and antibody ligands (11). Non-antibody ligands are inexpensive and stable but non-selective and low-binding affinity, for example galactosamine (124) and folate (120) which target the asialoglycoprotein receptors on hepatoma cells and the folate receptors overexpressed on cancer cells, respectively. Contrary to antibody ligands (monoclonal antibodies or antibody fragments) that have high-binding affinity and high degree of specificity, such as anti-Thy 1.2 antibodies which target the Thy 1.2 antigens on mouse splenocytes (125), and OV-TL 16 whole antibodies (32, 99) and OV-TL 16 antibody Fab' fragments (20, 21) which target the OA-3 surface antigens on ovarian cancer cells.

PK2 or FCE28069 is the first targetable HPMA copolymer conjugate evaluated in Phase I/II clinical trial. It contains DOX bound to HPMA copolymer via a GFLG sequence and in addition side-chains terminated in galactosamine (Figure 3). This conjugate was designed to target the liver using the hepatocyte asialoglycoprotein receptor to promote liver specific receptor-mediated targeting (active targeting) and may, therefore, be useful in the treatment of primary or metastatic liver cancer (89, 124). In addition of PK1 and PK2 conjugates, other HPMA conjugates that have been evaluated in clinical trials are listed in Table 1.

Another two targetable HPMA copolymer conjugates containing OV-TL 16 whole antibody and OV-TL 16 antibody Fab' fragment as targeting ligands, and DOX and Mce_6 as anticancer drugs, were studied both in *in vitro* and *in vivo* (32, 99). The cellular internalization studies showed that the targeted copolymer was internalized

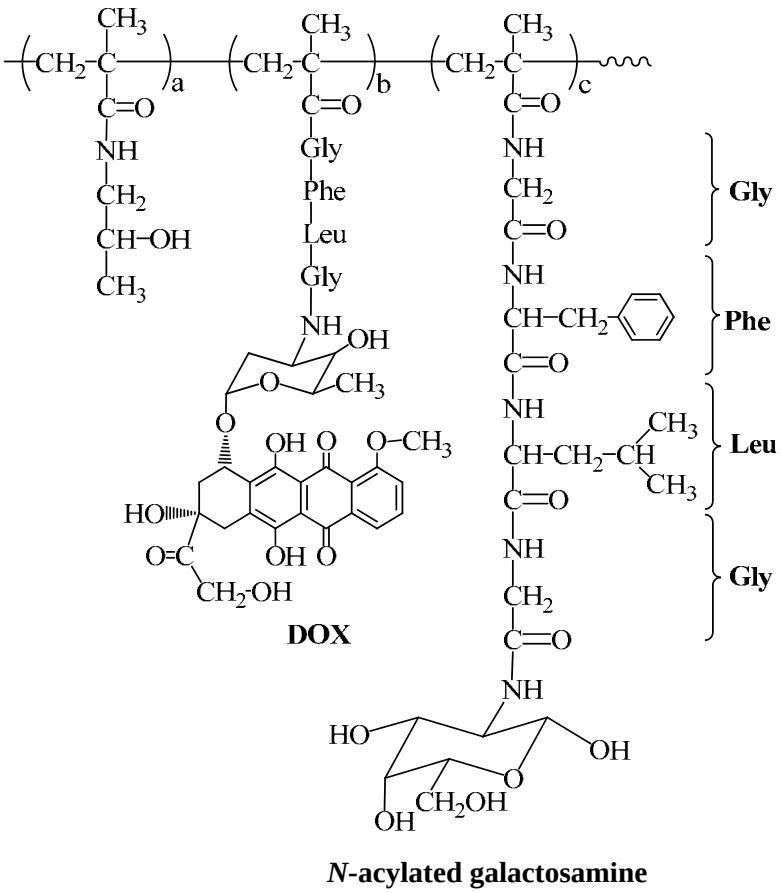

Figure 3. Chemical structure of HPMA copolymer bound DOX conjugate contains side-chain terminated in *N*-acylated galactosamine (PK2).

Table 1. HPMA copolymer bound drug conjugates in clinical trials.

HPMA copolymer-drug conjugates	**Name**	**Phase of clinical trial**	**References**
HPMA copolymer-Doxorubicin	PK1, FCE28069	II	(27, 126)
HPMA copolymer-Doxorubicin-Galactosamine	PK2, FCE28069	I/II	(89, 127)
HPMA copolymer-Paclitaxel	PNU166945	I	(128)
HPMA copolymer-Camptothecin	PNU166148, MAG-CPT	I	(129-132)
HPMA copolymer-*cis*-Platinate	AP5280	I/II	(28)
HPMA copolymer-DACH-platinate	AP5346; ProLindac	I/II	(133, 134)

more efficiently than the non-targeted copolymer. This internalization can be inhibited by the presence of free OV-TL16 antibody in the culture medium, indicating the role of receptor-mediated endocytosis. Cytotoxicity studies demonstrated that the targeted conjugates exhibited higher cytotoxicity toward OVCAR-3 cells than the non-targeted conjugates and nearly restored the cytotoxicity to that of free drugs. This is related to the different mechanisms of cell uptake (receptor-mediated endocytosis for targeted conjugates as compared to fluid phase/adsorptive endocytosis for non-targeted conjugates and diffusion for free drugs) (99).

5. Synthetic Procedures of HPMA Copolymer Conjugates

Generally, there are two possible methods for the preparation of HPMA copolymer bound drugs, or for the incorporation of drugs, targeting moieties, or other functional groups into HPMA copolymer conjugates:

(*a*) polymeranalogous reaction: coupling of drug molecule with a copolymer precursor possessing reactive groups; and

(*b*) copolymerization of a polymerizable drug derivative with suitable comonomers.

Both synthetic methods can yield similar polymer-drug conjugates when using the same drug. The selection of synthesis methods depends on the individual requirements in each case (24, 25).

5.1 Polymeranalogous Reactions

This involves the attachment of drug to a preformed polymeric carrier. The prerequisite of this method is the match of the reactive groups on the polymer backbone and the drug. Polymer backbone can be synthesized with reactive groups at side chain termini that are complementary to functional groups on the drug molecule. The polymer can then be reacted with the drug, resulting in the formation of a polymer-drug conjugate. For example, a polymer containing side-chains terminated in carboxyl groups that are complementary to the hydroxyl or amino group, the ester or amide bond may be formed, respectively, between the drug molecule and polymer backbone.

Another example is a polymer backbone containing reactive *p*-nitrophenyl ester groups at side chain termini that can be reacted with drug molecules bearing a reactive amino group by aminolysis forming amide bond (Figure 4). However, it may be essential to modify the reactive groups (either on the drug or polymer side chains) to enable the reaction to proceed in certain cases (135, 136).

5.2 Copolymerization of Polymerizable Drug Derivatives with Monomers

An essential feature in this method involves the synthesis of a polymerizable drug derivative by reacting the drug with a polymerizable molecule (monomer). This derivative can be then copolymerized with a suitable monomer to form the polymer-drug conjugate (Figure 5). This method may be used when the drug molecule is stable during the polymerization process. An advantage of this method is the avoidance of side reactions that sometimes occur during polymeranalogous reactions.

6. Attachment of Targeting Moieties

The incorporation of targeting moieties into the structure of the polymer-drug conjugate can also be done using techniques similar to polymeranalogous or copolymerization reactions depending on the structure of the targeting moiety. In the case of polymeranalogous techniques, polymer-drug conjugates can be synthesized with pendant reactive groups on side-chain termini. Reactive groups are selected such that they can specifically bind the targeting moieties. For example, HPMA copolymer conjugates containing *N*-acetylated galactosamine can be synthesized by aminolyzing the reactive copolymer precursor containing *p*-nitrophenyl ester with galactosamine.

When using antibodies as targeting moieties, antibodies may be bound directly to anticancer agents; however, this approach may lead to loss of antibody activity (137). The polymer intermediate is used to conserve the bioactivity of antibody and also to increase the specific toxicity of the conjugates (138). Antibodies can be attached to polymer backbones using three different methods. First, antibodies contain a large number of accessible surface lysine residues. Their ε-amino groups may be used for binding to active ester groups on polymer side-chains of polymeric carriers by aminolysis (34, 125). The disadvantage of this method is the possibility of

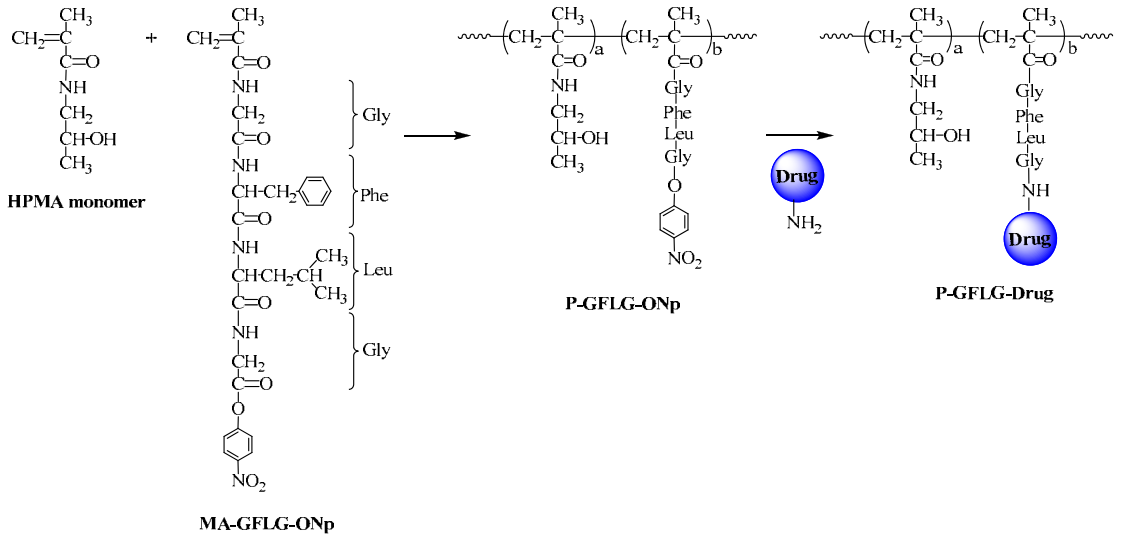

Figure 4. Synthetic scheme for the HPMA copolymer conjugate with drug bound via a biodegradable GFLG spacer (P-GFLG-Drug) using polymeranalogous technique in a two-step method. The first step involves the synthesis of a polymer precursor containing reactive *p*-nitrophenyl ester groups at GFLG side chain termini (P-GFLG-ONp where P is the HPMA copolymer backbone) by copolymerizing HPMA with *N*-methacryloylglycylphenylalanylleucylglycine *p*-nitrophenyl ester (MA-GFLG-ONp). The second step is the reaction of the drug molecule containing a reactive amino group with the polymer precursor (139).

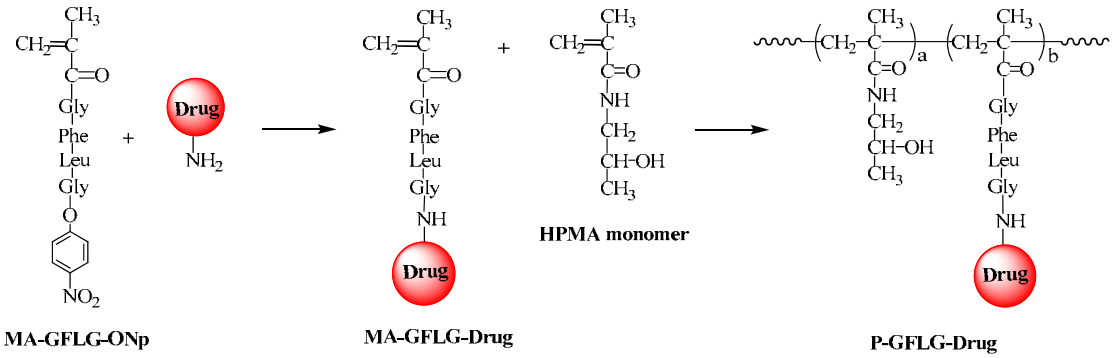

Figure 5. Synthetic scheme for the HPMA copolymer-drug conjugate (P-GFLG-Drug) using copolymerization technique. First, a monomer containing drug molecule at side chain termini via GFLG linker (MA-GFLG-Drug) is synthesized by reacting drug with MA-GFLG-ONp. Second, the MA-GFLG-Drug is copolymerized with HPMA monomer to yield P-GFLG-Drug (139).

attachment of multiple copolymer chains to one antibody molecule, which may restrict the flexibility of antibodies and reduce the bioactivity of antibody. Second, the carbohydrates near the hinge region of antibodies can be oxidized by sodium periodate to produce aldehyde groups. These groups can be reacted with hydrazide reactive groups on side chains of the polymers and hence formed hydrazone linkages. Third, antibody can also be reduced to Fab' fragments containing sulfhydryl groups, which may be reacted with maleimide groups on side-chain termini of polymers via thioether bonds. The last two methods may cause minor modifications to antibody structure and afford better control over biological activity, when compared to the aminolysis method (140).

Another strategy to synthesize the antibody-targeted conjugates is the use of copolymerization reaction technique. The polymerizable derivatives of whole antibody or Fab' fragment can be synthesized by reacting the antibody or Fab' fragment with a polymerizable monomers. The incorporation of these derivatives in copolymerization reactions can yield targeted conjugates. However, this technique should be performed under mild conditions to avoid denaturation of antibodies and Fab' fragments (20, 141).

7. Combination Therapy

The treatment options for cancer are surgery, radiation, chemotherapy, hormone therapy, biological therapy, targeted therapy, and also combination of these therapies (50, 142). Nowadays, it is well established that the clinical standard treatment in many types of cancer is optimized using combination therapy that has contributed to increasing survival and cure rates. The principles for the development of combination treatment are the therapeutic agents should be individually active with different mechanisms of action and non-overlapping toxicity profiles (143). The combination of multiple drugs may not only target multiple targets, multiple subpopulations, or multiple diseases simultaneously, but also direct the effect against single target or a disease and treat it more effectively. The drug combinations are currently used in an attempt to (*a*) enhance the efficacy of the therapeutic effect; (*b*) reduce the dosage to avoid unwanted side effects but increase or maintain the same efficacy; and (*c*) minimize or slow down the development of drug resistance. From

these benefits, the drug combinations have been widely used and became the leading choice for the treatment of cancer. For example, combinations of chemotherapies using agents with different mechanisms of action (144, 145); chemotherapy in combination with PDT (146-148); chemotherapy and immunotherapy (149); PDT and radiotherapy (150); and radioimmunotherapy with radiotherapy (151).

Recently, a novel concept of combining chemotherapy and PDT, using HPMA copolymer bound drugs has been developed (152). The *in vivo* combination studies on two cancer models, Neuro 2A neuroblastoma induced in A/J mice (153) and human ovarian carcinoma heterotransplanted in nude mice (32, 154, 155), demonstrated that combination therapy with HPMA copolymer-bound DOX (P-GFLG-DOX) and HPMA copolymer-bound Mce_6 (P-GFLG-Mce_6) produced tumor cures which could not be obtained with monotherapy either chemotherapy or PDT alone. Additionally, significantly lower nonspecific toxicities were observed when compared to low-M_w drugs. Furthermore, the biodistribution study of P-GFLG-Mce_6 and P-GFLG-DOX revealed the optimum time lag between the administration of both conjugates and irradiation of the tumor (156).

The additional enhancement of therapeutic efficacy may be reached using targeted combination chemotherapy and PDT with OV-TL16-HPMA copolymer-DOX and OV-TL16-HPMA copolymer-Mce_6 conjugates. These immunoconjugates accumulated preferentially in human ovarian carcinoma OVCAR-3 xenografts in nude mice resulting in increasing of therapeutic efficacy when compared with non-targeted conjugates (P-GFLG-DOX and P-GFLG-Mce_6). The targeted conjugates suppressed tumor growth for the entire period of the experiment (32).

8. The *In Vitro* Combination Study

Many *in vitro* drug combination studies have been performed to quantitatively evaluate the possibilities for synergistic or antagonistic effects being mediated by mixtures of chemicals. *In vitro* studies are very useful in initial studies of the detection of the potential of chemicals to produce cytotoxicity. Experimental conditions for drug combination *in vitro* can be easily defined, or fixed, and the drug concentrations can be maintained constant during the course of the experiment. They also have the advantage that a large number of combinations of chemicals can be

assayed within a short time frame and at relatively low cost. Therefore, most drug combination studies in biomedical literature have been conducted *in vitro*, with dose-effect curves each consisting of five to eight data points for each drug alone and their combinations. The *in vitro* combination studies not only lead to conserving the use of laboratory animals, but also reducing the cost of using animals for animal purchasing, maintenance, facilities, and equipment. Moreover, mathematical analysis of these *in vitro* studies is potentially powerful because many binary drug combinations can be explored computationally.

Compared with *in vitro* studies, determining synergism or antagonism *in vivo* using animals is obviously more time consuming and more costly and greater variability in measurements will be encountered. However, the combined effects demonstrated *in vitro* should be confirmed *in vivo* due to the potential differences in the biological processes of *in vitro* and *in vivo*. Therefore, *in vivo* drug combination studies are usually carried out only for selected drugs, after *in vitro* combination studies, and/or before clinical development (37, 157).

9. Drug-Drug Interaction and *In Vitro* Drug Interaction Evaluation Methods

The studies of interactions among agents are of fundamental interest and practical importance in all areas of medicine and, in particular, in cancer chemotherapy where combination therapy is commonly used. The agent may interact with one another and modify the magnitude of the therapeutic effect. The interactions may result in three different combined effects. The term ‘‘additivity’’ is used when several (two or more) compounds act without any mutual interactions and the total effect of a combination does not differ from what can be expected from the dose-effect relations of the individual agents. The terms ‘‘synergism’’ and ‘‘antagonism’’ are used when there is an interaction among compounds, e.g. when the total effect is greater and less than expected, respectively (158).

The nature and quantitative extent of drug-drug interactions is usually determined in *in vitro* studies. Two reviews described the various interaction assessment approaches (159, 160). These appraoches were categorized into two main models of the drug interaction evaluation, e.g. the Bliss independence model and the Loewe additivity model.

9.1 The Bliss Independence Model

This model is also called effect multiplication or the fractional product. It assumes that the agents can bind simultaneously and mutually nonexclusively (e.g., totally independent mechanisms) and the combined effect of two agents equals the multiplication product of the effects of individual agents. This assumption is valid only for linear drug concentration-effect relationship (e.g., drug effect increases linearly with its concentration). Therefore, this model has limited applicability. However, this assumption illustrates that all substances that have a partial overlapping action cannot be properly tested with this model. The widely accepted approach for this model is the fractional product method of Webb (161). The disadvantages of this method include: (*a*) it is inconsistent; there is a possibility to reach the opposite conclusion than that found with the isobologram method (as described below); and (*b*) there is no quantitative measurement that summarizes the intensity of synergism or antagonism (160, 162, 163).

9.2 The Loewe Additivity Model

This model is based on the assumption that a drug can not interact with itself. It assumes that two agents act on a target through a similar mechanisms or modes of actions (mutually exclusive) and is valid for nonlinear drug concentration-effect relationship such as the commonly observed sigmoidal curve. Hence, this model is more appropriate for evaluating drugs demonstrating such a relationship. Methods are based on the Loewe additivity model, such as the isobolographic method and the median effect method as described below.

9.2.1 The Isobolographic Method

This method is the classic commonly used method for detecting and characterizing departures from additivity between combinations of drugs or chemicals whether a combination dose is synergistic or antagonistic. It evaluates the interaction at a chosen effect level and is useful to inspect the *in vitro* drug interaction at the corresponding concentration, often the median effect concentration (or dose) required to inhibit (or to affect) a system by 50% (IC_{50} or D_m) (39). The isobologram was introduced as a graphical approach by Fraser (164). It is a plot of a contour line

representing equally effective doses of two or more agents for a single effect level with the doses of each agent as each coordinate axis (157). The particular effect level, such as IC_{50}, is selected; however IC_{50} can be extended for the *x*% effect. Figure 6 presents the illustration of possible isobolograms for the combinations of two drugs/chemicals. In the isobologram one or several lines (isoboles) are shown connecting different dose combinations that produce the same selected effect. The doses of each agent alone that give this effect are plotted as axial points and the straight diagonal line connecting these points is called the line of additivity. This line is the locus of points (dose pairs) that will produce this effect in a simply additive combination and allows a comparison with the dose pairs of different combinations that produce this effect level experimentally. It is notable that the dose combinations may be antagonistic while others are either synergistic or additive (165). If the values lie above or to the right of the additivity line then the mixture is antagonistic. If the values that cause the selected effect lie below or to the left of the additivity line then the mixture is synergistic (Figure 6A). Moreover, the dose pairs may be represented by the isoboles of different combinations that cause the selected effect. Hence, if the isobole is below the line of additivity, a synergism is demonstrated, whereas if the isobole is above the line of additivity, an antagonism is claimed (Figure 6B).

Berenbaum (166) introduced Equation 1 to calculate a CI value. This enables calculation of the effects of combinations directly from dose effect relationships of the individual compounds, regardless of the particular types of dose effect relations involved.

$$CI = \frac{d_1}{D_1} + \frac{d_2}{D_2} + \frac{d_n}{D_n} \qquad (1)$$

where d_1, d_2, … d_n are the doses of the agents in combination that produce the *x*% effect and D_1, D_2, … D_n are the doses of the individual agents producing the same effect. CI value is 1, less than 1, or more than 1 when the combinations show no interaction (additivity), synergy, or antagonism, respectively.

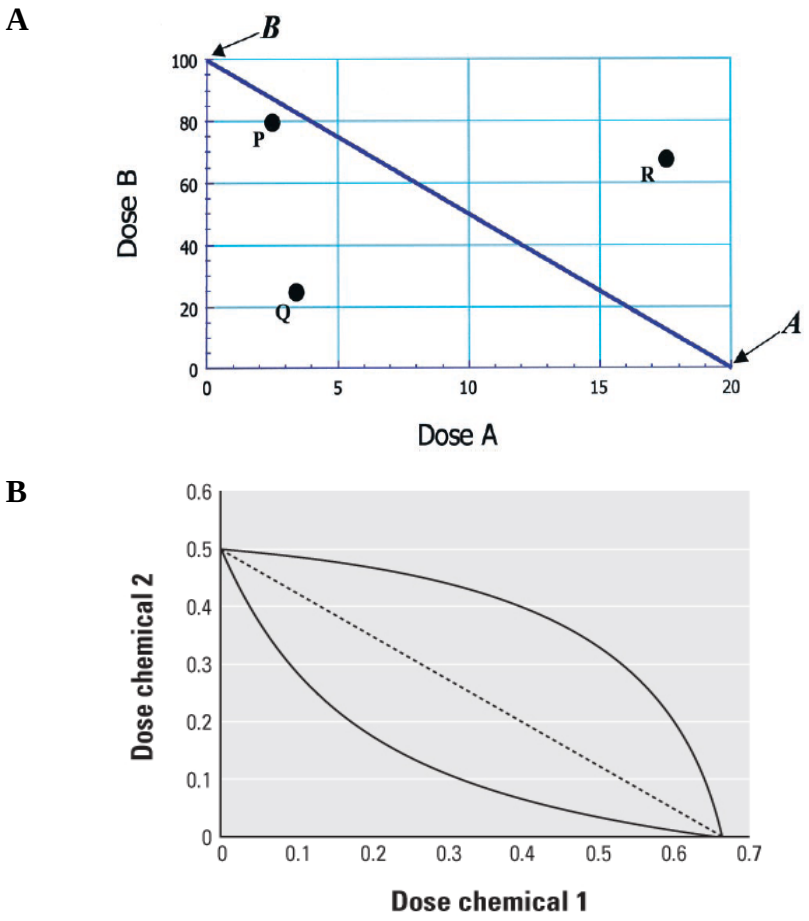

Figure 6. The isobolograms of combinations of two drugs/chemicals for 50% of the maximum effect (IC_{50}). (**A**) The isobologram in which the line of additivity was linked between the IC_{50} doses of drug *A* alone is 20 and drug *B* alone is 100. If the values lay to the right or the left of the additivity line then the mixture is antagonistic or synergistic, respectively. Points P, Q, and R represent the IC_{50} doses from the three different combinations of drugs *A* and *B*. Point Q is a dose pair of drug *A* at 3.4 and drug *B* at 25 which means lesser quantities of drugs *A* and *B* are required to give the 50% of the maximum effect and display synergistic effect. On the contrary, the dose pair denoted by point R, required greater drug quantities and is therefore antagonistic. Point P that appears near the line would probably be simply additive effect (165). (**B**) The dashed line connecting two intercept points is the line of additivity. This line is formed by linking the IC_{50} doses of individual agent (Chemical 1 and Chemical 2) that calculated from the dose-response curves. When the isobole falls below or above the line of additivity, a synergism or an antagonism is demonstrated, respectively (167).

The advantages of the isobologram method include: (*a*) it is simple, flexible and inexpensive; (*b*) it is widely accepted; and (*c*) many newer, more rigorous methods are based on the isobologram approach, such as the median-effect method by Chou and Talalay (1984). However, the isobolographic method has some practical limitations to the study of combinations of two or three agents. First, an isobologram has two dimensions which is convenient for two-agent combinations. For three-agent combinations, it is not convenient to construct a three-dimensional isobologram, and even if it were constructed, it would not be easy to read. Second, the two-drug isobolograms might be shown in multiple effect levels, which usually only three or fewer effect levels will be readable as shown in Figure 7. However, if an isobologram was constructed for four or more effect levels, it would be very difficult to read and may lead to a false conclusion because of data point overlapping or scattering (37). Furthermore, the isobolographic method lacks many of the good characteristics of objective statistical procedures and also lacks a summary measure of the intensity of interaction.

9.2.2 The Median-Effect Method

The median effect method is the most widely used one to evaluate drug interactions *in vitro* based on the Loewe additivity theory (37-39). This method is similar to isobologram analysis and provides qualitative information on the nature of drug interaction. The median-effect equation (37, 168, 169) describes dose-effect relationships in the following form, which is expressed by

$$\frac{f_a}{f_u} = \left(\frac{D}{D_m}\right)^m \qquad (2)$$

where f_a and f_u are the fraction of cells affected [calculated from: 1 - (absorbance of treatment well - average of absorbance of blanks) / (average of absorbance of untreated cell wells - average of absorbance of blanks)] and unaffected ($f_u = 1 - f_a$) after drug exposure by the dose or concentration D, D_m is the median-effect dose (IC_{50}) that inhibits the cell growth by 50%, and *m* is the coefficient denoting the

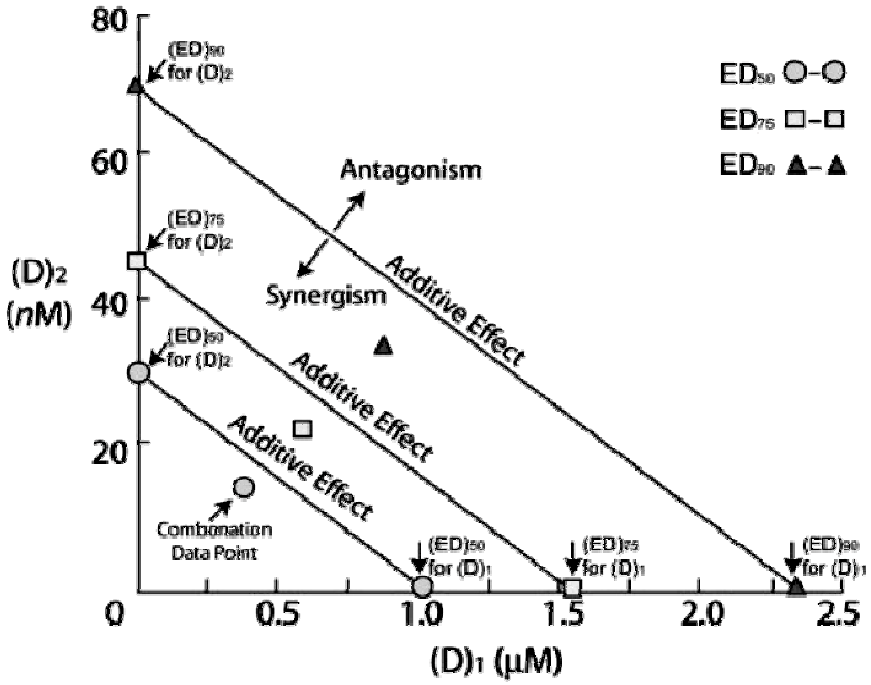

Figure 7. The isobologram at three effect levels including ED_{50}, ED_{75}, and ED_{90} (where ED is the effective dose) (37).

shape of the dose-effect curve, which is determined by the slope of the median-effect plot. Equation 2 can be rearranged and illustrated by

$$D = D_m \left(\frac{f_a}{(1-f_a)} \right)^{1/m} \quad (3)$$

Based on the logarithmic transformation of Equation 2 (168),

$$\log \left(\frac{f_a}{f_u} \right) = m \log (D) - m \log (D_m) \quad (4)$$

where m is the slope of the median-effect plot of $x = \log (D)$ versus $y = \log (f_a/f_u)$. An example for transforming the dose-effect curves for each drug and for combination into linear forms by the median-effect plots is given in Figure 8. Note that Equation 4 has the form of a classic straight line equation ($y = mx + b$). In the median-effect plot, D_m is the anti-log of the x-intercept, which can be easily determined.

The median effect equation for a single drug (Equation 2) can be extended to multiple drugs. Thus, for a two-drug combination, the multiple drug-effect equation is:

$$\left(\frac{(f_a)_{1,2}}{(f_u)_{1,2}} \right)^{1/m} = \left(\frac{(f_a)_1}{(f_u)_1} \right)^{1/m} + \left(\frac{(f_a)_2}{(f_u)_2} \right)^{1/m} = \frac{(D)_1}{(D_m)_1} + \frac{(D)_2}{(D_m)_2} \quad (5)$$

The preceding equation is based on the generalized assumption that two drugs share the similar modes of action (e.g., effects are mutually exclusive), which is in complete agreement with the assumption of the classic isobologram. $(f_a)_1$, $(f_a)_2$ and $(f_a)_{1,2}$ are the fractions affected by drug 1 and drug 2 and their combination, respectively. For two drugs that have totally different modes of actions (e.g., effects are purely mutually nonexclusive), then the resulting equation should have a third term, thus,

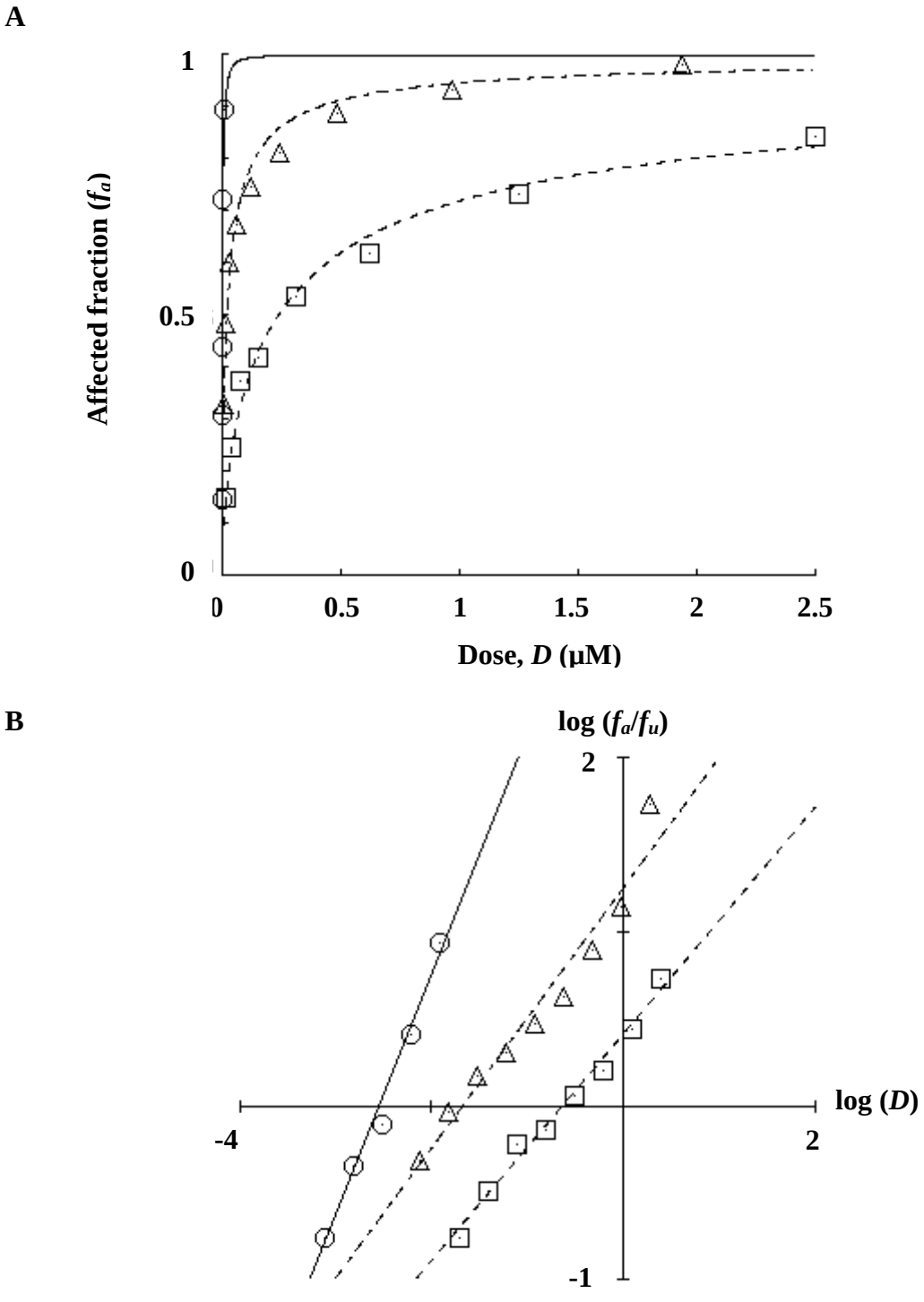

Figure 8. (**A**) Dose-effect curves and (**B**) the median-effect plots of Drug A (○), Drug B (□), and combination of Drug A and Drug B (△), according to Equations 2-4.

$$\left(\frac{(f_a)_{1,2}}{(f_u)_{1,2}}\right)^{1/m} = \frac{(D)_1}{(D_m)_1} + \frac{(D)_2}{(D_m)_2} + \frac{(D)_1(D)_2}{(D_m)_1(D_m)_2} \qquad (6)$$

Because partially exclusive or partially nonexclusive (e.g., two drugs that have some overlapping mechanisms of action) cases may exist and Equation 6 may underestimate synergistic drug interactions. It is concluded that Equation 5 should be used as the "base equation". If any partially exclusive condition exists, the third term of Equation 6 should be considered as a contributing factor for the intrinsic synergistic effect under the assumption of Equation 5 (37, 170).

Based on Equation 5, Chou and Talalay (171) introduced the term "CI" value to describe the interaction between two drugs and to quantify the extent of drug interaction, such as synergism, antagonism or additive effects, at a particular effect (e.g., percentage of growth. Theoretically, CI is the ratio of the combination dose to the sum of the single-agent doses at an isoeffective level. The CI is determined by the equation:

$$CI = \frac{(D)_1}{(D_x)_1} + \frac{(D)_2}{(D_x)_2} \qquad (7)$$

where $(D_x)_1$ and $(D_x)_2$ are the doses of drug 1 alone and drug 2 alone that inhibit a system (the cell growth) *x*%, respectively. The $(D_x)_1$ and $(D_x)_2$ can be determined from median-effect equation (Equation 3). $(D)_1$ and $(D)_2$ are for doses of drug 1 and drug 2 used in combination that also inhibit *x*%. The CI values for different values of f_a (e.g. for different degrees of cell growth inhibition) were calculated by solving Equation 7 with the CompuSyn software (ComboSyn Inc, Paramus, NJ). A plot of CI on the *y*-axis as a function of effect levels (f_a) on the *x*-axis is called Fa-CI plot or CI plot (Figure 9). Owing to the complexity of whole-cell biological system, the CompuSyn program automatically analyzes a data set using both the mutually exclusive and mutually nonexclusive assumptions. The CI equation determines the effect of drug combinations, such as additivity, synergism (greater-than-the-expected-additive effect), and antagonism (less-than-an-expected-additive

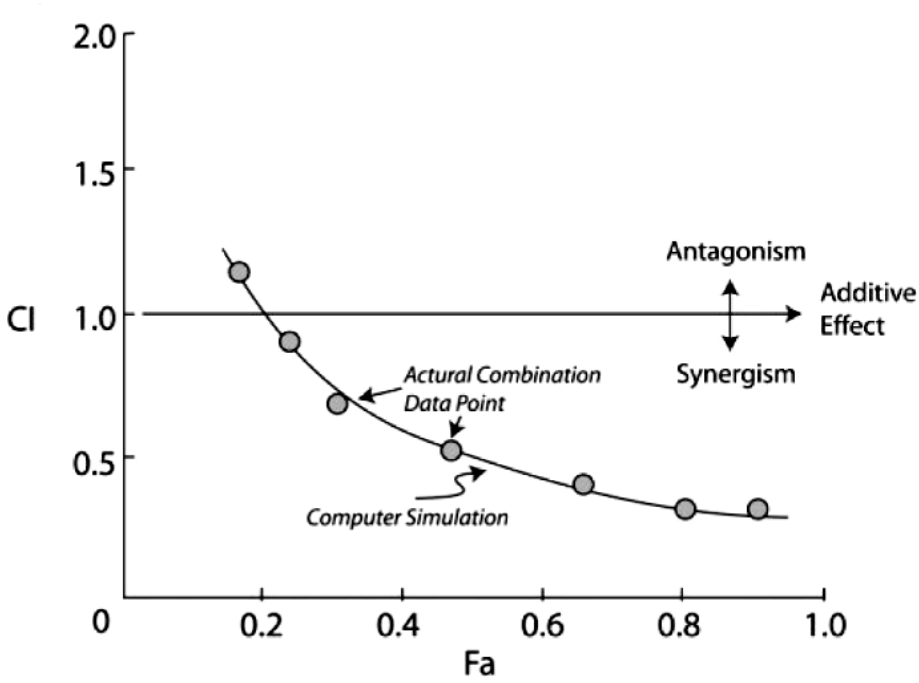

Figure 9. Fa-CI plot based on the Chou and Talalay combination index theorem can be generated by using CompuSyn (37).

effect). Thus, in the Fa-CI plot, CI < 1, = 1, and > 1 indicate synergism, additivity, and antagonism, respectively. The precise biological significance of various degrees of synergism or antagonism remains to be defined, but it has been proposed that CI values be interpreted as follows (37, 170):

<0.1	very strong synergism
0.1 - 0.3	strong synergism
0.3 - 0.7	synergism
0.7 - 0.9	moderate to slight synergism
0.9 - 1.1	nearly additive
1.1 - 1.45	slight to moderate antagonism
1.45 - 3.3	antagonism
3.3 - 10	strong antagonism
>10	very strong antagonism

Numerous anticancer agent combinations had been analyzed using the median-effect method. Examples include: combination therapy for chronic myelogenous leukemia with imatinib and γ-irradiation or alkylating agents (busulfan and treosulfan) (172); the combination treatment of lung adenocarcinoma cell line using perifosine and 7-hydroxystaurosporine (173); and combination treatment using irofulven and 5-fluorouracil or cisplatin against human colon and ovarian carcinoma cells (174).

CHAPTER III
MATERIALS AND METHODS

MATERIALS

The substances and reagents used in the present study are listed below.

1. Model Drugs

1.1 Mce_6 disodium salt (Porphyrin Products, Logan, UT)

1.2 SOS (Drug Synthesis and Chemistry Branch, Developmental Therapeutics Program, Division of Cancer Treatment and Diagnosis, National Cancer Institute)

1.3 DOX hydrochloride was a gift from Dr. A. Suarato, Pfizer, Milano, Italy

2. Cell Lines

2.1 Human ovarian carcinoma cell line OVCAR-3 (American Type Culture Collection, Manassas, VA)

2.2 Human renal carcinoma cell line A498 (American Type Culture Collection, Manassas, VA)

3. Chemicals

3.1 RPMI 1640 medium (Sigma Chemical Co., St. Louis, MO)

3.2 EMEM medium (American Type Culture Collection, Manassas, VA)

3.3 Insulin (Sigma Chemical Co., St. Louis, MO)

3.4 Fetal bovine serum (HyClone Laboratories, Logan, UT)

3.5 Serum free hybridoma medium (Gibco Life Sciences, Carlsbad, CA)

3.6 Pepsin (Sigma Chemical Co., St. Louis, MO)

3.7 Cysteine (Sigma Chemical Co., St. Louis, MO)

3.8 *N*-(3-aminopropyl)methacrylamide hydrochloride (Polysciences, Inc., Warrington, PA)

3.9 Succinimidyl *trans*-4-(maleimidomethyl) cyclohexane-1-carboxylate (Soltec Ventures, Beverly, MA)

3.10 6-(fluorescein-5-carboxamido) hexanoic acid, succinimidyl ester (Molecular Probes, Eugene, OR)

3.11 Cyclodextrin (Sigma Chemical Co., St. Louis, MO)

3.12 Dibasic sodium phosphate (Sigma Chemical Co., St. Louis, MO)

3.13 Monobasic potassium phosphate (Sigma Chemical Co., St. Louis, MO)

3.14 Sodium chloride (Sigma Chemical Co., St. Louis, MO)

3.15 Potassium chloride (Sigma Chemical Co., St. Louis, MO)

3.16 Ethylenediaminetetraacetic acid (Sigma Chemical Co., St. Louis, MO)

3.17 Sodium acetate (Sigma Chemical Co., St. Louis, MO)

3.18 Acetic acid (Sigma Chemical Co., St. Louis, MO)

3.19 Sodium citrate (Sigma Chemical Co., St. Louis, MO)

3.20 Citric acid (Sigma Chemical Co., St. Louis, MO)

3.21 Sodium hydroxide (Sigma Chemical Co., St. Louis, MO)

3.22 Tris (hydroxymethyl) aminomethane hydrochloride (Sigma Chemical Co., St. Louis, MO)

3.23 Acetone (Sigma Chemical Co., St. Louis, MO)

3.24 Ether (Sigma Chemical Co., St. Louis, MO)

3.25 Methanol (Sigma Chemical Co., St. Louis, MO)

3.26 Hexane (Sigma Chemical Co., St. Louis, MO)

3.27 *N,N*-dimethylformamide (Sigma Chemical Co., St. Louis, MO)

3.28 *N,N′*-diisopropylethylamine (Sigma Chemical Co., St. Louis, MO)

3.29 Dimethylsulfoxide (Sigma Chemical Co., St. Louis, MO)

3.30 4-Dimethylaminopyridine (Sigma Chemical Co., St. Louis, MO)

3.31 2,2′-Azobisisobutyronitrile (Sigma Chemical Co., St. Louis, MO)

3.32 1-Amino-2-propanol (Sigma Chemical Co., St. Louis, MO)

3.33 *tert*-Octylpyrocatechine wa provided by Pavla Kopečková)

3.34 Tetrahydrofuran (Sigma Chemical Co., St. Louis, MO)

3.35 4-Dimethylaminopyridine (Sigma Chemical Co., St. Louis, MO)

3.36 2-(*N*-morpholino)ethanesulfonic acid (Sigma Chemical Co., St. Louis, MO)

3.37 Bis(2-hydroxyethyl)-imino-tris(hydroxymethyl)-methane (Sigma Chemical Co., St. Louis, MO)

3.38 Paraformaldehyde (Sigma Chemical Co., St. Louis, MO)

3.39 Anti-fade reagent (Molecular Probes, Eugene, OR)

3.40 TrypLE^{TM} Express (Gibco Invitrogen Corporation, Carlsbad, CA)

3.41 3-(4,5-Dimethylthiazol-2-yl)-2,5-diphenyltetrazoliumbromide (Sigma Chemical Co., St. Louis, MO)

3.42 Sodium dodecyl sulfate (Sigma Chemical Co., St. Louis, MO)

EQUIPMENT

1. Cellulosic-MPS cartridge bioreactor (Spectrum Labs, Rancho Dominguez, CA)
2. Ultracentrifuge (Baxter, Deerfield, IL)
3. Cell culture flask (Greiner bio-one, Monroe, NC)
4. 24-well plate (Greiner bio-one, Monroe, NC)
5. 96-well plate (Greiner bio-one, Monroe, NC)
6. Lab-Tek®II chamber slide, 8 wells (Electron Microscopy Sciences, Hatfield, PA)
7. Protein G Sepharose 4 Fast Flow column (Pharmacia, Piscataway, NJ)
8. Superdex 200 column (Pharmacia, Piscataway, NJ)
9. Superose 6 column (Pharmacia, Piscataway, NJ)
10. Sephadex G-25 (Pharmacia, Piscataway, NJ)
11. Sephadex LH-20 column (GE Healthcare, Chalfont St. Giles, Buckinghamshire)
12. Silica gel column (Sigma Chemical Co., St. Louis, MO)
13. DEAE Sepharose Fast Flow ion exchange column (GE Healthcare, Chalfont St. Giles, Buckinghamshire)
14. TLC (Merck KGaA, Darmstadt, Germany)
15. Dialysis tube (Spectrum Laboratories, Rancho Dominguez, CA)
16. Rotary evaporator (Buchi, Flawil, Sankt Gallen)
17. Desiccator (Wheaton, Millville, NJ)
18. UV/Visible spectrophotometer (Variant, Les Ulis, Essonne)
19. Microplate reader (Bio-Rad, Hercules, CA)
20. Shaking water bath (Thermo Fisher Scientific, Waltham, MA)
21. Balance (Mettler, Greifensee, Zürich)
22. Micropipette (Eppendorf, Hamburg, Germany)
23. Pyrex culture tube (Greiner bio-one, Monroe, NC)
24. Zeiss LSM 510 confocal imaging system (Carl Zeiss, Thornwood, NY)
25. FACScan instrument (Becton Dickinson, Franklin Lakes, NJ)
26. ENH bulb 250W 120V halogen lamps (Ushio, Cypress, CA)

METHODS

1. Experiment A: Combination Treatment of Human Ovarian Carcinoma Cells with Fab'-Targeted HPMA Copolymer Bound Drug Conjugates

1.1 Cell Culture

The human ovarian carcinoma OVCAR-3 cells were cultured in RPMI 1640 medium containing 10 μg/mL insulin supplemented with 10% fetal bovine serum, at 37°C in a humidified atmosphere of 5% CO_2 (v/v).

1.2 OV-TL16 Antibody Production

The OV-TL16 antibody was produced as described previously (21). Briefly, the OV-TL16 antibody was produced by *in vitro* cartridge bioreactor (Cellulosic-MPS, Spectrum Labs, Rancho Dominguez, CA) culture of OV-TL16 hybridoma cells with serum free hybridoma medium. The antibody-containing cell suspension harvested from bioreactor was centrifuged. The antibody-containing supernatant was collected and serially filtered through filter membrane 11 μm, 1 μm, 0.7 μm, 0.45 μm and 0.2 μm. The antibody was purified by applying the supernatant on a protein G Sepharose 4 Fast Flow column (Pharmacia, Piscataway, NJ), equilibrated with binding buffer (0.01 M Na_2HPO_4, 0.15 M NaCl, 0.01 M EDTA pH 7.2). The OV-TL16 antibody was eluted with 0.5 M acetate buffer pH 3.0. The pH of antibody fraction was adjusted to ~7 using 1 N NaOH. The antibody was dialyzed (MWCO 6-8 kDa) against phosphate buffered saline (PBS) overnight at 4°C.

1.3 Preparation of Fab' Fragment

The antibody Fab' fragment was prepared freshly as described previously (20, 21). The OV-TL16 antibody in 0.1 M citric buffer pH 4.0 was digested by 10% (w/w) pepsin for 2.5 h at 37°C to give $F(ab')_2$. The digestion reaction was monitored by size exclusion chromatography (SEC) on a Superdex 200 column. The $F(ab')_2$ was reduced to Fab' with 20 mM cysteine in 20 mM Tris buffer pH 8.5 for 1 h at 37°C, pH 8.5. Excess cysteine was removed on a Sephadex G-25 (PD-10 column, Pharmacia).

1.4 Synthesis of Non-Targeted HPMA Copolymer Conjugates

1.4.1 Non-Targeted HPMA Copolymer-Mce_6 Conjugate (P-GFLG-Mce_6)

P-GFLG-Mce_6 was also prepared as described previously (153, 175). Briefly, the conjugate was synthesized using a polymeranalogous reaction in two steps. First, the polymer precursor P-GFLG-ONp was prepared by radical precipitation copolymerization of HPMA and MA-GFLG-ONp (139, 176). Second, Mce_6 was bound to P-GFLG-ONp precursor, containing 5.1 mol% of active ester groups; molecular weight (M_w) = 22 kDa; polydispersity (M_w/M_n) = 1.2. The procedure is shown in Figure 10. Mce_6 (160 mg, 0.234 mmol) was dissolved in *N*,*N*-dimethylformamide (DMF; ~3 mL). P-GFLG-ONp (750 mg, 0.230 mmol ONp groups) was dissolved in DMF (~2.5 mL). The suspension of Mce_6 was added dropwise into polymer precursor solution while stirring. The reaction mixture was stirred for 1 h until the mixture was completely dissolved. *N*,*N*′-diisopropylethylamine (DIPEA; 40 µL, 0.229 mmol) was added under stirring. The solution was stirred overnight in the dark at room temperature. The solution was precipitated into a mixture of acetone: ether (3:2 (v/v), ~500 mL). The precipitate was collected by filtration and dried under vacuum. The product was dissolved in methanol (~10 mL) and purified twice on a Sephadex LH-20 column with methanol/0.5% acetic acid as the elution solvent. The polymer band was collected and evaporated to dryness. The product was dissolved in deionized (DI) water (~20 mL), dialyzed overnight and lyophilized.

1.4.2 Non-Targeted HPMA Copolymer-SOS Conjugate (P-GFLG-SOS)

P-GFLG-SOS was synthesized by binding of SOS to the P-GFLG-ONp polymer precursor via an ester linkage (177). The reactions are shown in Figure 11. Briefly, P-GFLG-ONp contained 4.15 mol% of active ester groups; M_w = 23 kDa; M_w/M_n = 1.3 (450 mg, 0.116 mmol ONp groups) was dissolved in DMF (~4 mL) and mixed with 1 mL DMF solution of SOS (71 mg, 0.243 mmol). 4-Dimethylaminopyridine (DMAP; 40 mg, 0.327 mmol) was added into the reaction

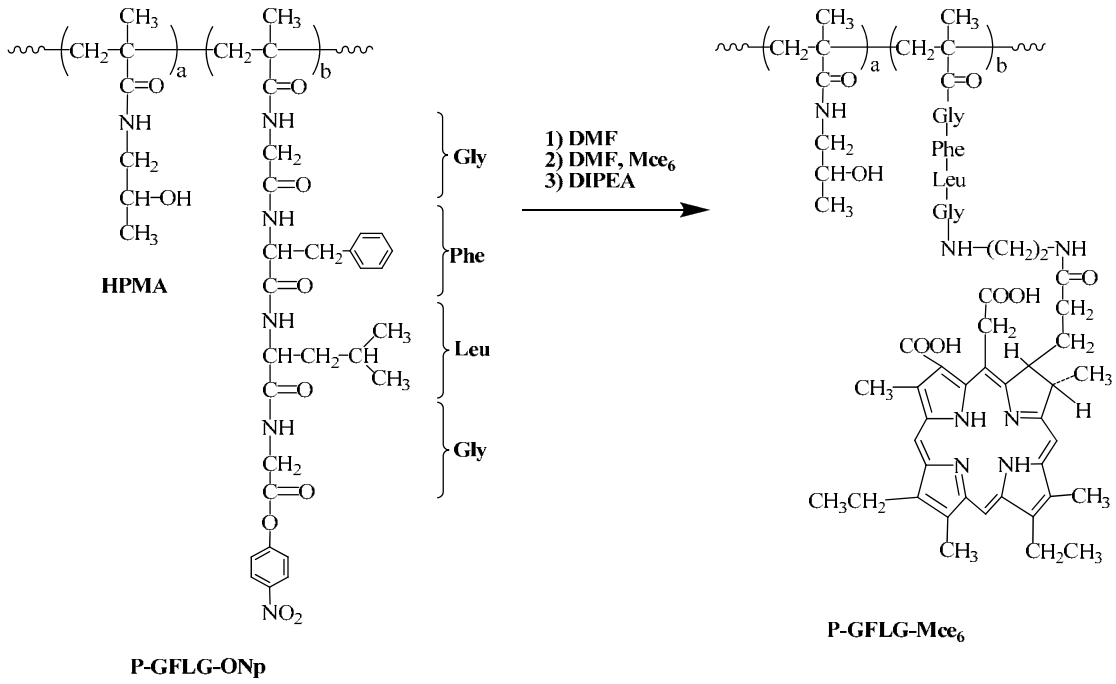

Figure 10. Synthetic scheme for the HPMA copolymer-Mce_6 conjugates containing GFLG spacers (P-GFLG-Mce_6).

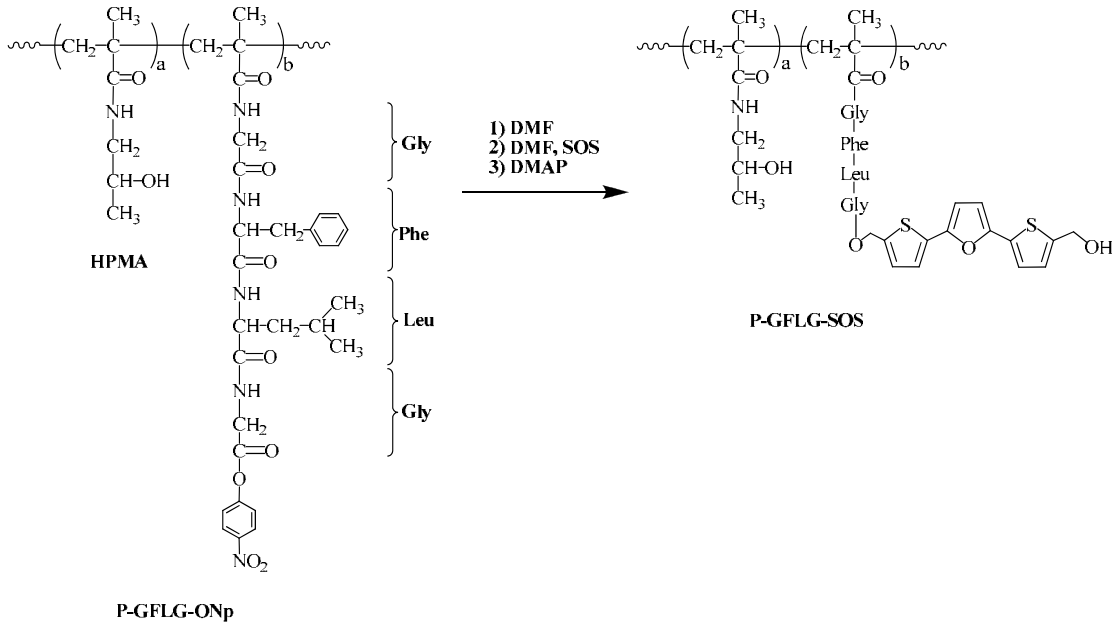

Figure 11. Synthetic scheme for the HPMA copolymer-SOS conjugates containing GFLG spacers (P-GFLG-SOS).

mixture. The reaction solution was bubbled with N_2 and allowed to proceed for 72 h in the dark at room temperature. The product was isolated, after reduction of volume, by precipitation into a mixture of acetone: ether (3:1 (v/v), ~550 mL). The precipitate was collected by filtration, washed with acetone (~50 mL) and ether (~50 mL), and dried under vacuum. To purify the product was dissolved in methanol (~3 mL) and applied to a Sephadex LH-20 column with methanol as the mobile phase. The polymer band was collected, concentrated under reduced pressure and re-precipitated. The product was a yellowish powder.

1.5 Synthesis of HPMA Copolymer Conjugates Containing Maleimide Groups

1.5.1 HPMA Copolymer-Mce_6 Conjugate Containing Maleimide Groups [P-(GFLG-Mce_6)-MAL]

This copolymer precursor was prepared in three steps. The reactions are shown in Figure 12. First, a polymerizable derivative of Mce_6, *N*-methacryloylglycylphenylalanylleucylglycine Mce_6 (MA-GFLG-Mce_6) (20) was synthesized by reacting MA-GFLG-ONp (60 mg, 0.103 mmol) with Mce_6 (63.5 mg, 0.093 mmol) in DMF (~2 mL). The reaction solution was stirred at room temperature in dark for 2 h. DIPEA (18 μL, 0.103 mmol) was added and stirring continued overnight. 1-Amino-2-propanol (~8 μL, 0.103 mmol) and small amount of *tert*-octylpyrocatechine were added and DMF removed under reduced pressure. The residue was isolated using a Sephadex LH-20 column with acetone: methanol: acetic acid (2:1:0.1) as the mobile phase. The fractions were collected and checked on TLC. The product fraction was evaporated to dryness, washed with ether, collected by filtration, and dried under vacuum. The M_w of MA-GFLG-Mce_6 was 1083.6 Da as determined by electrospray ionization mass spectrometry (ESI-MS). The product yield was 90 mg (73%). Second, the polymeric precursor P-(GFLG-Mce_6)-NH_2 was prepared by radical copolymerization of HPMA (103) (107.6 mg, 0.751 mmol), *N*-(3-aminopropyl)methacrylamide hydrochloride (APMA, 16.27 mg, 0.091 mmol), and MA-GFLG-Mce_6 (76.9 mg, 0.068 mmol) in methanol (~1.8 mL) at 50°C for 48 h, using 2,2′-azobisisobutyronitrile (AIBN; 19.27 mg) as the initiator. The

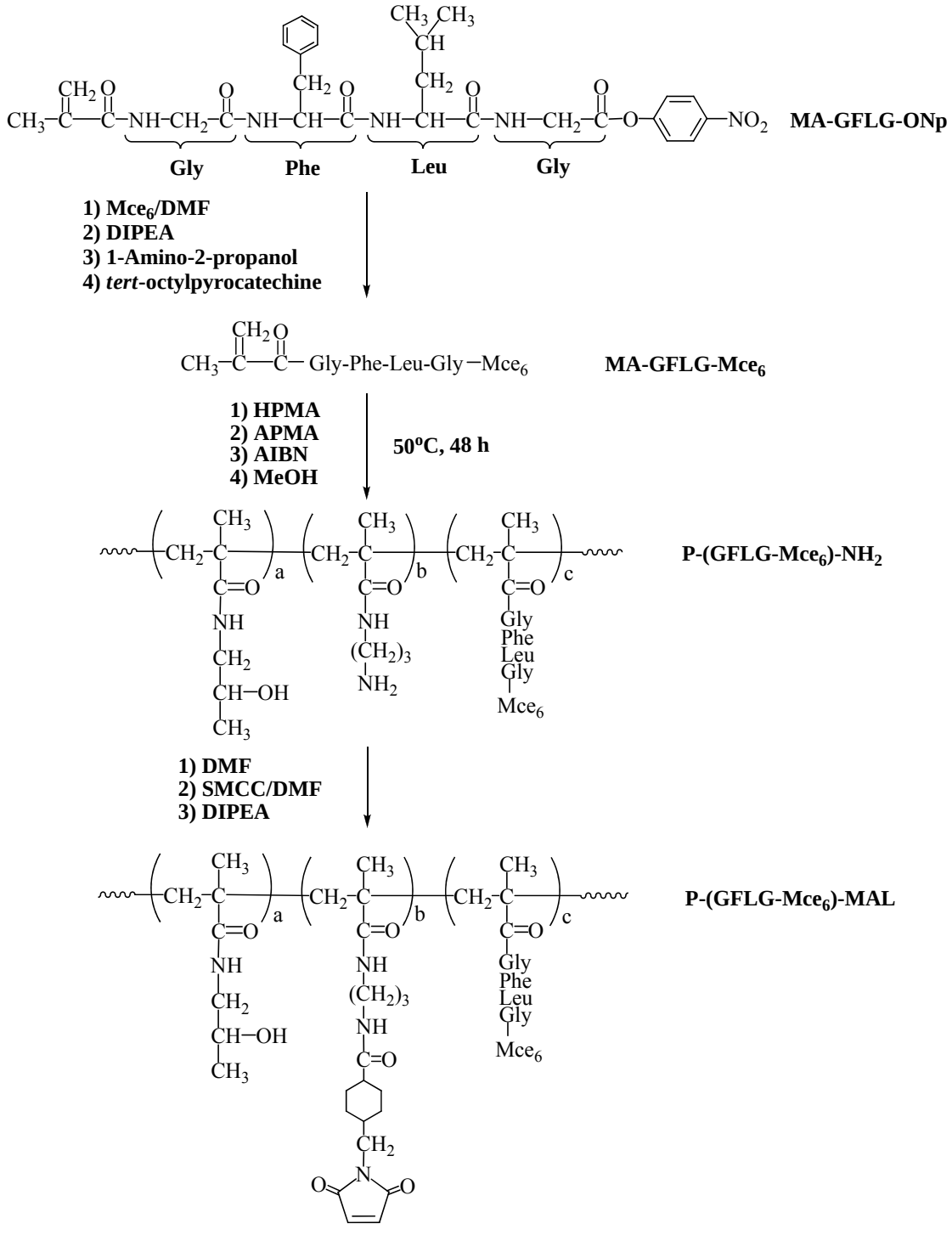

Figure 12. Synthetic scheme for the HPMA copolymer-Mce_6 conjugates containing maleimide groups [P-(GFLG-Mce_6)-MAL].

polymerization mixture contained 12.5 wt% of monomers and 1.2 wt% of AIBN. The mole ratio of HPMA: APMA: MA-GFLG-Mce_6 was 82.5:10:7.5. The reaction mixture was purified on a Sephadex LH-20 column eluted with methanol. The polymer fraction was collected and methanol was evaporated. The residue was precipitated in a mixture of acetone: ether (1:2 (v/v)). The precipitate was dissolved in water, dialyzed (MWCO 6-8 kDa) against DI water and lyophilized. Third, polymeric precursor P-(GFLG-Mce_6)-MAL was prepared by reacting P-(GFLG-Mce_6)-NH_2 (55 mg, 0.026 mmol NH_2 group) with succinimidyl *trans*-4-(maleimidomethyl) cyclohexane-1-carboxylate (SMCC; 17.36 mg, 0.052 mmol) and DIPEA (~13 µL, 0.078 mmol). The mole ratio of NH_2: SMCC: DIPEA was 1:2:3. P-(GFLG-Mce_6)-NH_2 was dissolved in 0.3 mL DMF and SMCC in 0.9 mL DMF. The polymer solution was added into the SMCC solution. DIPEA was added dropwise. The reaction solution was stirred overnight at room temperature. The DMF was removed under reduced pressure to dryness. The residue was dissolved in a small volume of methanol and purified on a Sephadex LH-20 column eluted with a mixture of methanol and 0.1% acetic acid. The copolymer band was collected, evaporated and precipitated into a mixture of acetone: ether (1:1).

1.5.2 HPMA Copolymer-SOS Conjugate Containing Maleimide Groups [P-(GFLG-SOS)-MAL]

This copolymer precursor was also prepared by a three-step reaction (Figure 13). First, MA-GFLG-ONp (278.6 mg, 0.480 mmol) and SOS (200 mg, 0.68 mmol) were dissolved in tetrahydrofuran (THF; ~15 mL). DMAP (44.6 mg, 0.370 mmol) was added. The reaction mixture was stirred at room temperature in dark for 72 h. The mixture was concentrated under reduced pressure. The residue was isolated using silica gel column chromatography. The excess free drug was recovered by elution with acetone: hexane (2:1) and the fractions were collected by eluting with acetone and then with methanol. The fractions were checked on TLC. The product-containing fraction was evaporated and recrystallized with THF/hexane. The M_w of MA-GFLG-SOS was 734.2 Da as determined by ESI-MS. The product yield was 130 mg (27%). Second, polymeric precursor, P-(GFLG-SOS)-NH_2, was synthesized by copolymerization of HPMA (141.3 mg, 0.987 mmol), APMA (14.2 mg, 0.079 mmol),

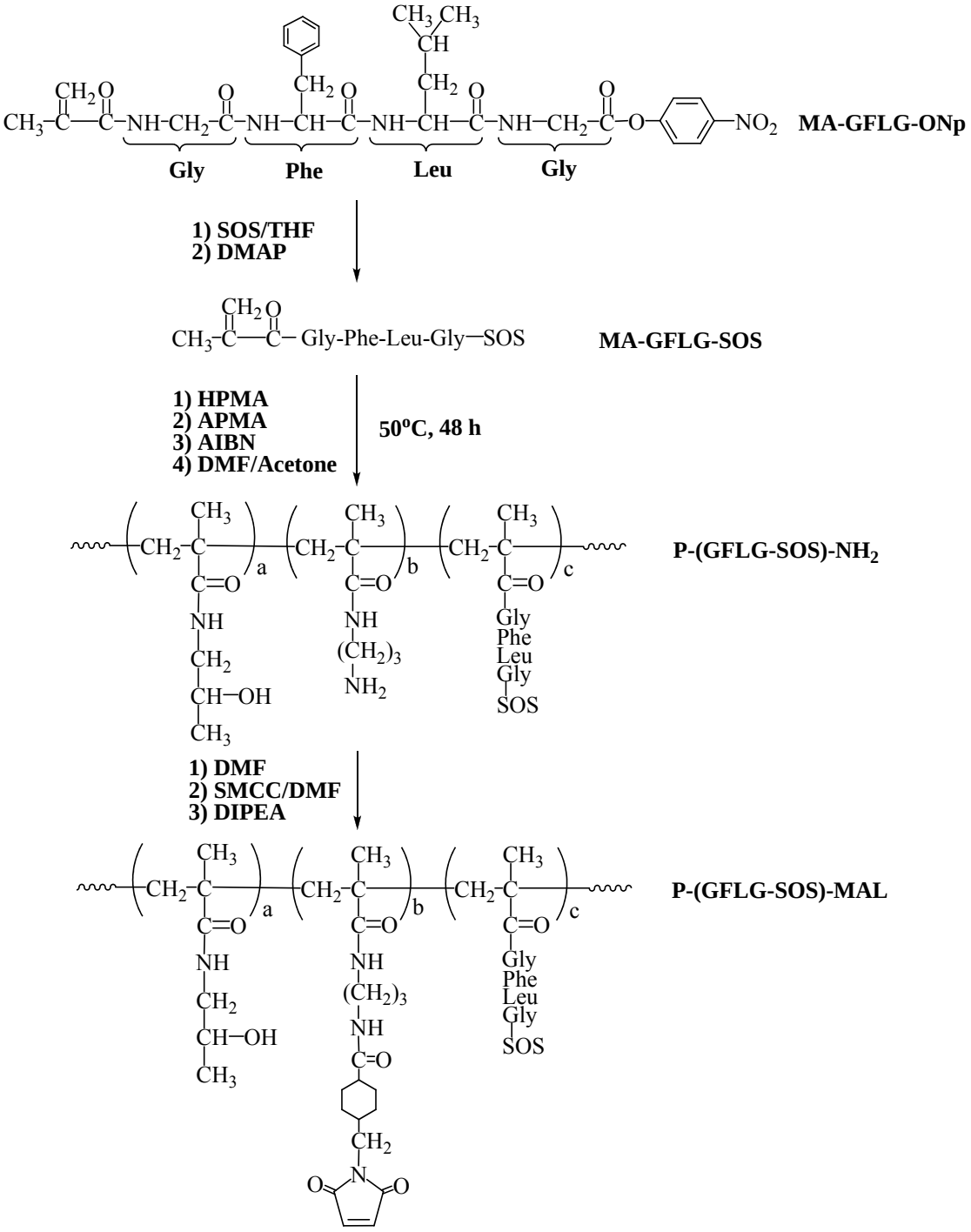

Figure 13. Synthetic scheme for the HPMA copolymer-SOS conjugates containing maleimide groups [P-(GFLG-SOS)-MAL].

and MA-GFLG-SOS (50 mg, 0.068 mmol) in DMF (1 mL) and acetone (0.5 mL) at 50°C for 48 h, using AIBN (19.7 mg) as the initiator. The mole ratio of HPMA: APMA: MA-GFLG-SOS was 87:7:6. The reaction mixture was purified on a Sephadex LH-20 column eluted with methanol. The polymer fraction was collected and evaporated to the viscous residue. The residue was precipitated into acetone: ether (1:1). Third, polymeric precursor P-(GFLG-SOS)-MAL was prepared by using the same procedure as for P-(GFLG-Mce_6)-MAL. P-(GFLG-SOS)-NH_2 (145 mg, 0.040 mmol NH_2 groups) and SMCC (26.41 mg, 0.079 mmol) were dissolved separately in DMF (~2.5 mL and ~0.5 mL, respectively). DIPEA (~21 μL, 0.119 mmol) was used. The product was applied on Sephadex LH-20 column and eluted with methanol without acetic acid. The product was precipitated and filtered off.

1.6 Preparation of Antibody Fab' Fragment-Targeted HPMA Copolymer-Mce_6 or -SOS Conjugates [P-(GFLG-Mce_6)-Fab' and P-(GFLG-SOS)-Fab']

The targeted conjugates were prepared by dissolving P-(GFLG-Mce_6)-MAL or P-(GFLG-SOS)-MAL precursor in 20 mM 2-(*N*-morpholino)ethanesulfonic acid (MES) buffer pH 6.5 and reacting with freshly prepared Fab' fragment (polymer: Fab' weight ratio = 1:2) overnight in dark at 4°C. The product was purified on a DEAE (diethylaminoethyl) Sepharose Fast Flow ion exchange column (Pharmacia), eluted using 20 mM Bis-Tris buffer pH 6.5 with a gradient NaCl concentration of 0-0.5 M. The fraction corresponding to conjugate was confirmed by size exclusion chromatography using Superose 6 (HR 10/30) column. The structure of polymer conjugates is showed in Figure 14.

1.7 Preparation of Fluorescein-Labeled Non-Targeted HPMA Copolymer-Mce_6 or -SOS Conjugates [P-(GFLG-Mce_6)-FITC and P-(GFLG-SOS)-FITC]

6-(fluorescein-5-carboxamido) hexanoic acid succinimidyl ester (5-SFX; ~0.1 mg, 0.170 μmol) was dissolved in dimethylsulfoxide (DMSO; 25 μL) and DI water (100 μL). The polymer precursor P-(GFLG-Mce_6)-NH_2 or P-(GFLG-SOS)-NH_2 (~3 mg, ~1 μmol NH_2) was dissolved in DI water (~300 μL). The 5-SFX solution was

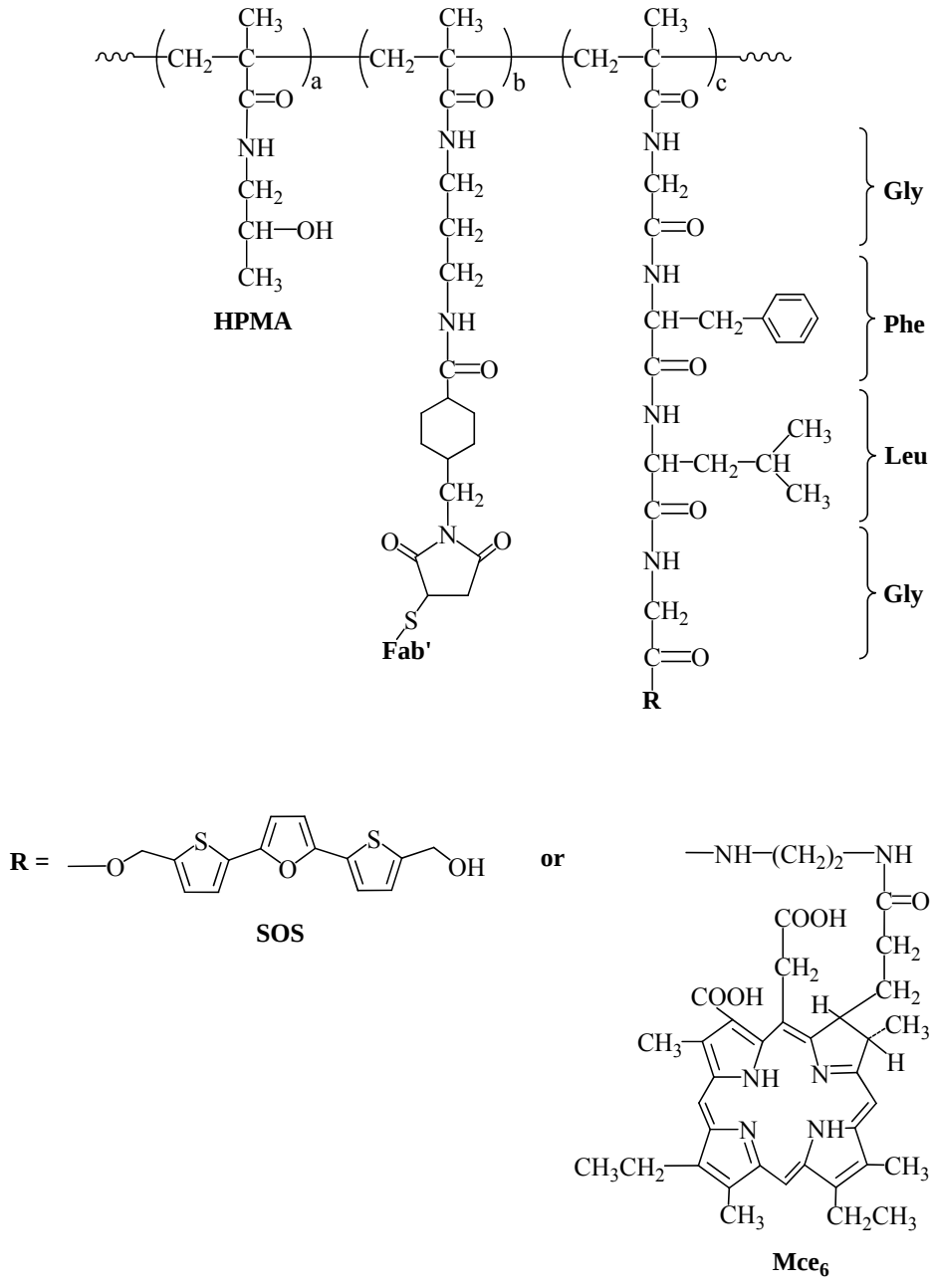

Figure 14. Chemical structures of the Fab'-targeted HPMA copolymer-Mce_6 or -SOS conjugates [P-(GFLG-Mce_6)-Fab' or P-(GFLG-SOS)-Fab')].

added into the polymer solution. DIPEA (~1 drop) was added into the reaction solution while stirring. The mixture was stirred at room temperature in dark for 1 h. Saturated Na_2HPO_4 (~20 μL) was added to stop the reaction. The product was separated on a PD-10 column and eluted with PBS.

1.8 Preparation of Fluorescein-Labeled Fab'-Targeted HPMA Copolymer-Mce_6 or -SOS Conjugates [P-(GFLG-Mce_6)-(Fab'-FITC) and P-(GFLG-SOS)-(Fab'-FITC)]

P-(GFLG-Mce_6)-Fab' and P-(GFLG-SOS)-Fab' (~1 mg of Fab', 0.017 μmol) were reacted with 5-SFX (~0.1 mg, 0.170 μmol). The mole ratio of Fab'-targeted HPMA copolymer bound drug conjugates: 5-SFX was 1:10. The procedure was as described for P-(GFLG-Mce_6)-FITC and P-(GFLG-SOS)-FITC.

1.9 Drug Stock Solution Preparations

SOS was dissolved in PBS containing cyclodextrin (5% (w/v) cyclodextrin in PBS/1 mg of SOS) to enhance the solubility of SOS (178). P-GFLG-SOS, P-(GFLG-Mce_6)-Fab', and P-(GFLG-SOS)-Fab' were prepared in PBS. Other samples (Mce_6 and P-GFLG-Mce_6) were prepared in DI water. All stock solutions were sterile-filtered. Drug contents were determined by UV spectrophotometry. All stock solutions were freshly prepared and gradually diluted with RPMI 1640 culture medium before use.

1.10 Confocal Microscopy

Fifty thousand OVCAR-3 cells were subcultured into an eight-chamber slide and incubated for 2 days at 37°C in a humidified atmosphere of 5% CO_2. The cells in each chamber were exposed to fluorescein-labeled copolymer conjugates (at 20 μM FITC equivalent) at 37°C for 1 h in dark. Cells were fixed with 2% paraformaldehyde for 20 min at room temperature and washed twice with PBS. The chamber slide was covered with cover slide utilizing anti-fade reagent. The cell internalization of fluorescently labeled HPMA copolymer conjugates was imaged using a Zeiss (Thornwood, NY) LSM 510 confocal imaging system.

1.11 Flow Cytometry

OVCAR-3 cells (75,000 cells/well) were seeded into 24-well plate and incubated 24 h at 37°C in a humidified atmosphere of 5% CO_2. Cells in each well were exposed to the fluorescein-labeled copolymer conjugates (at 20 μM FITC equivalent) at 37°C for 1 h in dark. The medium was removed. The cell monolayer was rinsed twice with ice-cold PBS and detached from the well surface by incubation with TrypLE^{TM} Express for 2 min. All steps were carried out on ice to minimize efflux of the sample. The cells were suspended with ice-cold PBS containing 0.2% fetal bovine serum, maintained in suspension on ice in the dark and processed for flow cytometry utilizing FACScan instrument (Becton Dickinson). Twenty thousand events were collected per sample. Control cells were not exposed to the sample to assess the endogenous fluorescence of the cells.

1.12 Cytotoxicity Bioassays

The drug concentration that inhibited cell growth by 50% compared with control cells (IC_{50}) was determined using a modified MTT assay (36). Cells were seeded in 96-well flat bottom microplates at a density of 10,000 cells/well in 200 μL of RPMI 1640 medium and allowed to grow for ~30 h. The cells were then exposed to various concentrations of each free drug alone (Mce_6 and SOS), each non-targeted copolymer conjugate (P-GFLG-Mce_6 and P-GFLG-SOS), each targeted copolymer conjugate [P-(GFLG-Mce_6)-Fab' and P-(GFLG-SOS)-Fab'], or their sequential combinations (n=6 in single experiment). The different treatment protocols are shown in Figure 15. During the cells exposure to drug(s), they were incubated at 37°C in a humidified atmosphere of 5% CO_2 and in the dark condition. After 4 days of exposure for SOS and its conjugates or 1 day of exposure for Mce_6 and its conjugates, the drugs were removed, cells were washed with warm PBS and the medium (300 μl) replaced. For cell growth inhibition studies using Mce_6, P-GFLG-Mce_6, or P-(GFLG-Mce_6)-Fab' (alone or in combinations), the cells were irradiated with three tungsten halogen lamps through a 650 nm band pass filter at 3.0 mW/cm^2 for 30 min. After additional 1 day or 4 days in culture for SOS and its conjugates or for Mce_6 and its conjugates, respectively, medium was removed and replaced with 100 μL of fresh medium and 10 μL of sterile-filtered MTT solution (5mg/mL in PBS). After incubating for 24 h, 150

μL of 20% (w/v) sodium dodecyl sulfate in water was added to each well and incubated overnight. The following day, the absorbance of each well was read at 570 nm with a reference wavelength at 630 nm. Untreated cells served as a 100% cell viability control and the media served as background reference. Growth inhibition was expressed as the growth of drug-treated cells related to that of untreated control cells.

1.13 Determination of Drug Interaction and Combination Index

In combination treatment studies, OVCAR-3 cells were treated with a dose range of SOS for 4 days followed by a dose range of Mce_6 for 1 day, and irradiated for 30 min (n=6 in single experiment), as shown in Figure 15. After each step the drug was removed and the cells were washed with warm PBS. The drug interaction and CI were determined using median-effect analysis according to the method of Chou and Talalay, as described previously in Chapter II (37, 38).

1.14 Statistical Analysis

All mean values are presented as means ± standard deviation (n=6 in single experiment).

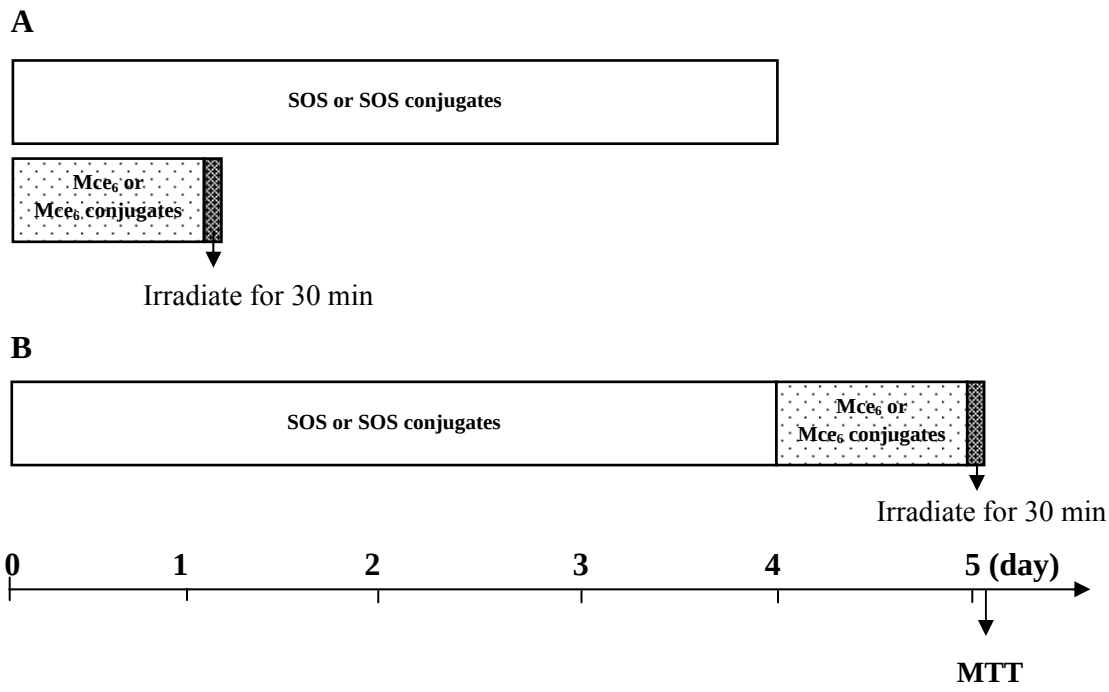

Figure 15. Scheme for the experimental protocols used in the cytotoxicity study. (**A**) Cells were treated with single agents - different concentrations of Mce_6, SOS, or their conjugates. (**B**) Cells were treated with sequential combinations of SOS or HPMA copolymer-SOS conjugates, followed by treatment with Mce_6 or HPMA copolymer - Mce_6 conjugates.

2. Experiment B: Combination Treatment of Human Renal Carcinoma Cells with Free Drugs and HPMA Copolymer Bound Drug Conjugates

2.1 Cell Culture

The human renal carcinoma A498 cells were grown as monolayer cultures in EMEM medium supplemented with 10% fetal bovine serum, at 37°C in a humidified atmosphere of 5% CO_2 (v/v).

2.2 Synthesis of HPMA Copolymer-Drug Conjugates

2.2.1 HPMA Copolymer-Mce_6 or -SOS Conjugates (P-GFLG-Mce_6 and P-GFLG-SOS)

P-GFLG-Mce_6 and P-GFLG-SOS were prepared as previously described eariler, and its chemical structure is shown in Figures 10 and 11.

2.2.2 HPMA Copolymer-DOX Conjugate (P-GFLG-DOX)

P-GFLG-DOX was prepared as described previously (153, 176). Briefly, the conjugate was synthesized by conjugating DOX to P-GFLG-ONp precursor, containing 5.5 mol% of active ester groups; M_w = 22 kDa; M_w/M_n = 1.2. The procedure is shown in Figure 16. DOX (127 mg, 0.220 mmol) and P-GFLG-ONp (1 g, 0.330 mmol ONp groups) were dissolved in DMSO (~4 mL). The reaction mixture was stirred to complete dissolution for 20 min. DIPEA (48 μL, 0.275 mmol) was added while stirring. The reaction mixture was stirred overnight in the dark at room temperature. Then, 1-amino-2-propanol (~15 μL) was added under stirring. The reaction mixture was precipitated into a mixture of acetone: ether (3:1 (v/v), ~500 mL)). The precipitate was collected by filtration, washed with a mixture of acetone: ether (3:1 (v/v)) and ether, and dried under vacuum. The product was dissolved in methanol (~10 mL) and purified twice on a Sephadex LH-20 column with methanol/0.5% acetic acid as the mobile phase. The polymer band was then collected and evaporated to dryness. The product was dissolved in DI water (~20 mL), dialyzed overnight against DI water and lyophilized.

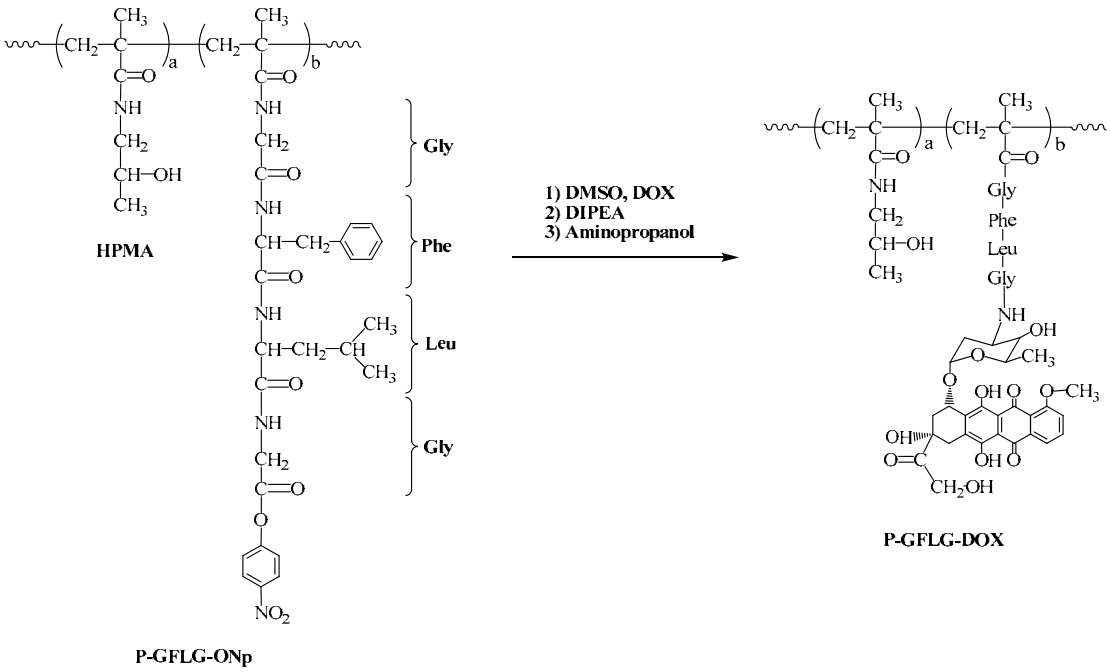

Figure 16. Synthetic scheme for the HPMA copolymer-DOX conjugates (P-GFLG-DOX) containing GFLG spacers.

2.3 Drug Stock Solution Preparations

SOS was dissolved in PBS containing cyclodextrin (5% (w/v) cyclodextrin in PBS/1 mg of SOS) to enhance the solubility of SOS (178). Other samples (DOX, Mce_6, P-GFLG-SOS, P-GFLG-DOX, and P-GFLG-Mce_6) were prepared in DI water. All stock solutions were filtered using a 0.22 μm sterile filter and kept in sterilized Eppendorf tubes. Drug contents were determined by UV spectrophotometry. All stock solutions were freshly prepared and gradually diluted with EMEM culture medium before use.

2.4 *In Vitro* Growth Inhibition Bioassays

The IC_{50} was determined using a modified MTT assay (36). Cells were seeded in 96-well flat bottom microplates at a density of 5,000 cells/well in 200 μL of EMEM medium and allowed to grow for 36 h. The cells were then exposed to various concentrations of each free drug alone (SOS, DOX, and Mce_6), each copolymer conjugate (P-GFLG-SOS, P-GFLG-DOX, and P-GFLG-Mce_6), or their binary combinations (n=6). After 16 h of exposure, the drugs were removed, cells were washed with warm PBS and the medium (300 μL) replaced. For the cell growth inhibition studies using Mce_6 or P-GFLG-Mce_6 (alone or in combinations), the cells were irradiated with three tungsten halogen lamps through a 650 nm band pass filter at 3.0 mW/cm^2 for 30 min. After an additional 3 days in culture, medium was removed and replaced with 100 μL of fresh medium and 10 μL of sterile-filtered MTT solution (5mg/mL in PBS). After incubating for 24 h, 150 μL of 20% (w/v) sodium dodecyl sulfate in water was added to each well and incubated overnight. The following day, the absorbance of each well was read at 570 nm with a reference wavelength at 630 nm. Untreated cells served as a 100% cell viability control and the media served as background reference. Growth inhibition was expressed as the growth of drug-treated cells related to that of untreated control cells.

2.5 Dose-Effect Analysis and Determination of Combination Index

In binary combination treatment studies, A498 cells were treated with a dose range of SOS, DOX, Mce_6, P-GFLG-SOS, P-GFLG-DOX, and P-GFLG-Mce_6 simultaneously for 16 h (n=6). Drug interactions and CI values were analyzed using

median-effect principle according to the method of Chou and Talalay (37, 38) as described previously in Chapter II.

The concept of the dose-reduction index (DRI) was formally introduced by Chou JH and Chou TC in 1988 (179) and has since been used in many publications. The DRI (37, 180) is a determination of how many -fold the dose of each drug in a synergistic combination may be reduced at a given effect level compared with the doses of each drug alone. The DRI is important in clinical situations, in which dose reduction leads to reduced toxicity toward the host or normal cells while the desired therapeutic efficacy is retained or increased. The DRI value for each corresponding drug was calculated by the following simple equation:

$$DRI = \frac{(D_x)_1}{(D)_1} + \frac{(D_x)_2}{(D)_2} \quad (8)$$

where $(D_x)_1$ and $(D_x)_2$ are the doses of drug 1 alone and drug 2 alone that inhibit the cell growth *x*%, respectively. $(D)_1$ and $(D)_2$ are for doses in combination that also inhibit *x*%.

2.6 Statistical Analysis

All mean values are presented as means ± standard deviation. The Student's *t*-test (two tailed) was used to evaluate the statistical significance of any differences in mean values in the experimental groups. The ANOVA test was used to assess the differences in means between single agents and combination treatments. In all statistical analyses, *p*-values < 0.05 were considered to indicate statistical significance.

CHAPTER IV
RESULTS AND DISCUSSION

1. Combination Treatment of Human Ovarian Carcinoma Cells with Fab'-Targeted HPMA Copolymer Bound Drug Conjugates

In this study, Fab'-targeted and non-targeted HPMA copolymer-drug (SOS and Mce_6) conjugates for combination chemotherapy and PDT against human ovarian OVCAR-3 carcinoma cells were synthesized. The antibody Fab' fragment was prepared from OV-TL16 antibody, which recognizes the OA-3 surface antigen, also known as CD47 or IAP (integrin-associated protein) (181, 182), overexpressed on most human ovarian carcinoma cells (183, 184). It was hypothesized that a combination of these agents may produce synergistic effects and has higher efficiency than each agent alone. Accordingly, the efficiency of free, non-targeted, and Fab' fragment-targeted HPMA copolymer-bound SOS and Mce_6 against OVCAR-3 cells as single agents and in combination was evaluated. The CI analysis was used to quantify the synergism, antagonism, and additive effects of drug combinations (37-39).

1.1 Characteristics of HPMA Copolymer-Mce_6 or -SOS Conjugates

The structures of HPMA copolymer conjugates, P-GFLG-Mce_6, P-GFLG-SOS, P-(GFLG-Mce_6)-Fab', and P-(GFLG-SOS)-Fab', are shown in Figures 10, 11 and 14. The drugs, Mce_6 and SOS, were bound to the HPMA copolymer backbone via a GFLG spacer, stable in the bloodstream, but susceptible to enzymatically catalyzed hydrolysis in the lysosomal compartment of the cells (112, 114, 115). For Fab' attachment, the amino groups of APMA monomer units in HPMA copolymer precursors were first converted to maleimido groups by reaction with a heterobifunctional agent, SMCC (Figures 12 and 13), followed by attachment of Fab' via thioether bonds. In some experiments, fluorescently labeled conjugates were synthesized. In non-targeted conjugates, the 5-SFX was attached to amino groups of

APMA monomer units. The Fab'-targeted conjugates were labeled by the reaction of 5-SFX with the final conjugates.

The characteristics of HPMA copolymer precursors, non-targeted HPMA copolymer conjugates, Fab'-targeted HPMA copolymer conjugates, and fluorescently labeled conjugates are summarized in Tables 2-4. P-GFLG-Mce_6, P-GFLG-SOS, P-(GFLG-Mce_6)-Fab', and P-(GFLG-SOS)-Fab' conjugates contained 2.9, 3.4, 2.0, and 5.0 drug molecules per macromolecule, respectively. P-(GFLG-Mce_6)-Fab' and P-(GFLG-SOS)-Fab' had drug: polymer: Fab' molecular ratios of approximately 2:1:1 and 5:1:1, respectively. The M_w of Fab'-targeted copolymer conjugates were 2.2 to 2.8 times higher than that of non-targeted conjugates.

1.2 Intracellular Uptake of Fluorescein-Labeled Fab'-Targeted HPMA Copolymer Conjugates.

Unlike low-M_w drugs that enter cells by diffusion through the plasma membrane, macromolecules are internalized within membrane-limited vesicles in the process of endocytosis. Several basic internalization mechanisms, clathrin-mediated endocytosis, caveolae-mediated endocytosis, clathrin- and caveolin-independent endocytosis, and macropinocytosis have been identified (185, 186). To a greater or lesser extent, two or more distinct mechanisms co-exist when a single cell type internalizes macromolecule-drug conjugates (187).

Studies on the subcellular fate of HPMA copolymer-drug conjugates demonstrated that the conjugates are lysosomotropic and will accumulate in the lysosomal compartment of the cell. Tijerina *et al.*, using subcellular fractionation, determined the localization of a considerable fraction of HPMA copolymer-Mce_6 conjugates in the lysosomal compartment of human ovarian carcinoma A2780 cells (68). Omelyanenko *et al.* used pH dependent fluorescence of FITC to display the lysosomotropism of FITC-labeled HPMA copolymers containing *N*-acylated galactosamine in HepG2 hepatocarcinoma cells (188).

Recently, the uptake mechanism of HPMA copolymer-DOX conjugate in human ovarian carcinoma OVCAR-3 cells was studied by confocal fluorescence microscopy and by co-localization experiments with substrates specific for a particular

Table 2. Characterization of non-targeted HPMA copolymer conjugates and polymeric precursors.

Structures	**Mol% of side-chains[a]**	**mmol ligand per g polymer conjugate**	**Number of ligand per polymer chain (conjugate)**	**Apparent M_w (kDa)[b]**	**%Yield**
P-GFLG-Mce_6	2.04	0.125	2.9	23	69
P-GFLG-SOS	1.62	0.106	3.4	32	61
P-(GFLG-Mce_6)-NH_2	2.62 8.11[c]	0.153 (Mce_6) 0.472 (NH_2)	1.7 (Mce_6)	11	32
P-(GFLG-SOS)-NH_2	4.60 4.70[c]	0.270 (SOS) 0.272 (NH_2)	2.7 (SOS)	10	73
P-(GFLG-Mce_6)-MAL	2.60 6.02[d]	0.142 (Mce_6) 0.329 (MAL)	2.0 (Mce_6)	14	[e]
P-(GFLG-SOS)-MAL	4.14 3.36[d]	0.236 (SOS) 0.192 (MAL)	5.2 (SOS)	22	76

[a] Determined by UV spectrophotometry in methanol: extinction coefficient at 395 nm (ε_{395}) = 158000 M^{-1} cm^{-1} for Mce_6, ε_{358} = 33000 M^{-1} cm^{-1} for SOS.

[b] Apparent molecular weight (M_w) of polymers was estimated by size exclusion chromatography using ÄKTA/FPLC (fast performance liquid chromatography) (Pharmacia) system equipped with a Superose 6 column, calibrated with polyHPMA fractions. PBS buffer pH 7.3 + 30% (v) acetonitrile and 0.1 M acetate buffer pH 5.5 + 30% (v) acetonitrile were used for polymer conjugates containing Mce_6 and polymer conjugates containing SOS, respectively.

[c] Determined by ninhydrin assay.

[d] Determined by 5-((2-(and-3)-*S*-(acetylmercapto)succinoyl)amino)fluorescein assay (SAMSA assay).

[e] Not determined.

Table 3. Characterization of Fab'-targeted HPMA copolymer-Mce_6 or -SOS immunoconjugates.

Structures	**wt.%** **drug : polymer : Fab'**[a]	**Molecular ratio** **drug : polymer : Fab'**	**M_w** **(kDa)**[b]
P-(GFLG-Mce_6)-Fab'	2.1 : 21.1 : 76.8	2 : 1 : 1	64
P-(GFLG-SOS)-Fab'	1.6 : 23.5 : 74.9	5 : 1 : 1	72

[a] Mce_6 and SOS contents determined by UV spectrophotometry in methanol: ε_{395} = 158000 M^{-1} cm^{-1} for Mce_6, ε_{358} = 33000 M^{-1} cm^{-1} for SOS. Protein content was determined by Lowry assay.

[b] Calculated from the composition of polymer (molecular ratio of drug, polymer, and Fab').

Table 4. Characterization of fluorescently labeled HPMA copolymer conjugates.

Structures	**mmol FITC per g polymer conjugate**[a]	**Number of FITC per polymer chain (conjugate)**
P-(GFLG-Mce_6)-FITC	0.060	1.0
P-(GFLG-SOS)-FITC	0.038	0.6
P-(GFLG-Mce_6)-(Fab'-FITC)[b]	0.063	3.1 (per conjugate)
P-(GFLG-SOS)-(Fab'-FITC)[b]	0.050	2.5 (per conjugate)

[a] Determined by spectrophotometric determination of FITC (ε_{497} = 73 000 M^{-1} cm^{-1} in 0.1 M sodium borate buffer).

[b] Fluorescently labeled targeted conjugates were prepared by reacting P-(GFLG-Mce_6)-Fab' and P-(GFLG-SOS)-Fab' (Table 3) with 5-SFX.

internalization mechanism. The results suggested that the HPMA copolymer-DOX conjugate is internalized via both clathrin- and caveolae-mediated endocytosis (187).

The biorecognition and cellular uptake of P-(GFLG-Mce_6)-(Fab'-FITC) and P-(GFLG-SOS)-(Fab'-FITC) was studied using confocal microscopy and flow cytometry. Non-targeted conjugates, P-(GFLG-Mce_6)-FITC and P-(GFLG-SOS)-FITC, served as controls. The confocal microscopy images and flow cytometry profiles of OVCAR-3 cells exposed to conjugates are shown in Figures 17 and 18, respectively. After a 1-h exposure of cells to HPMA copolymer conjugates, the intracellular concentrations of targeted polymer conjugates containing Mce_6 and SOS were significantly higher when compared to non-targeted conjugates. Both confocal microscopy images and flow cytometry profiles displayed very similar results. These results indicated the biorecognition of HPMA copolymer conjugates containing the Fab' antibody fragment by OVCAR-3 cells. The results of confocal microscopy are consistent with the internalization of targeted HPMA copolymer conjugates via receptor-mediated endocytosis, and of the non-targeted conjugates, containing hydrophobic drugs, by fluid-phase pinocytosis and adsorptive pinocytosis, concurrently.

The data are consistent with previous data on the determination of binding constants of OV-TL16 antibody targeted HPMA copolymers toward OVCAR-3 cells (140). The affinity constant, K_a of free antibody was 8×10^{-8} M^{-1}, whereas the K_a for the P-(GG-Mce_6)-Fab' was 3×10^{-8} M^{-1}. The minor decrease in the affinity may be a result of chemical modification and/or steric hindrance of the polymer chain upon the formation of the antibody - antigen complex.

1.3 *In Vitro* Inhibition of OVCAR-3 Cell Growth by Drugs as Single Agents.

The growth inhibitory effects of Mce_6, SOS, P-GFLG-Mce_6, P-GFLG-SOS, P-(GFLG-Mce_6)-Fab', and P-(GFLG-SOS)-Fab' as single agents on OVCAR-3 cells were evaluated after drug exposure using the MTT assay. The IC_{50} values for the free drugs, non-targeted and targeted HPMA copolymer conjugates are shown in Table 5. The 1-day Mce_6 exposure and 4-day SOS exposure have been selected based on

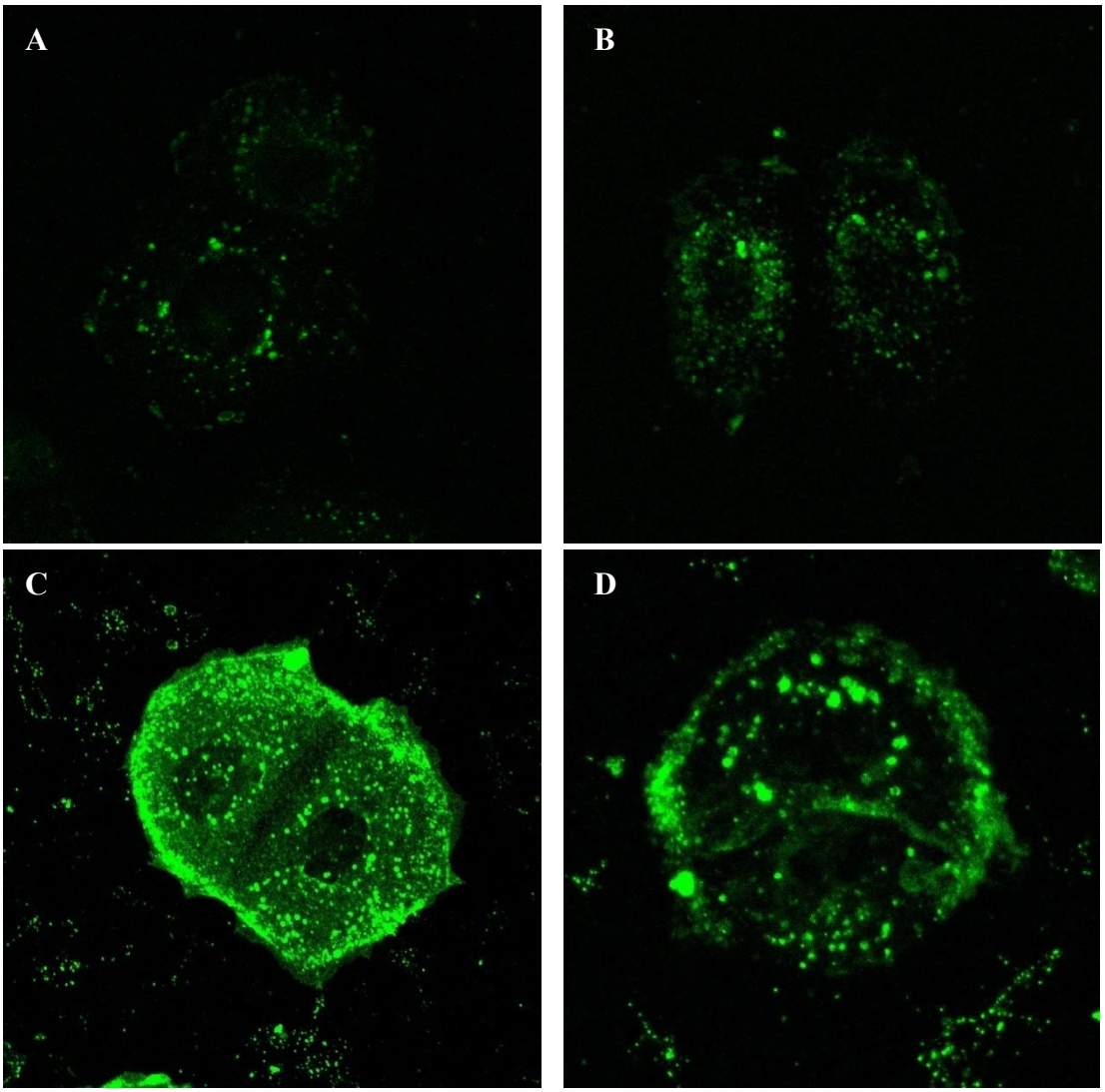

Figure 17. Confocal image of fixed OVCAR-3 cells incubated with fluorescein-labeled HPMA copolymer conjugates in RPMI 1640 culture medium for 1 h in the dark. (**A**) P-(GFLG-Mce_6)-FITC, (**B**) P-(GFLG-SOS)-FITC, (**C**) P-(GFLG-Mce_6)-(Fab'-FITC), and (**D**) P-(GFLG-SOS)-(Fab'-FITC).

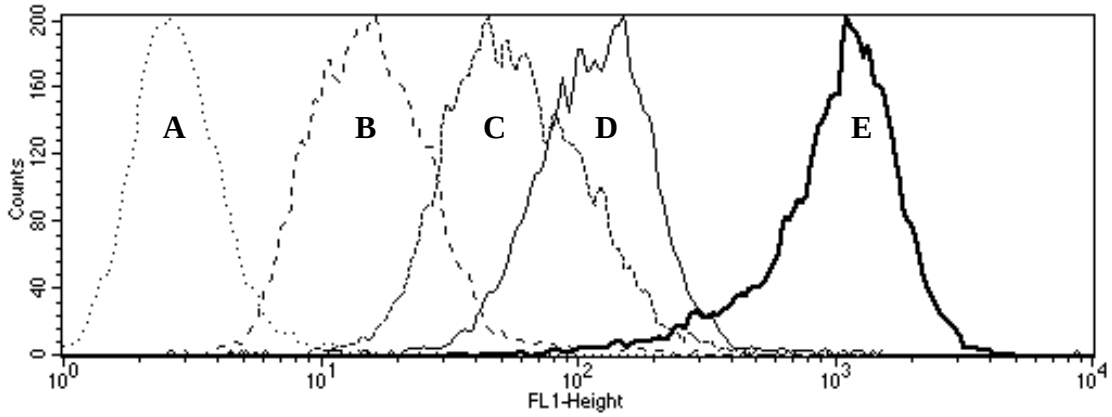

Figure 18. Flow cytometry profiles of OVCAR-3 cells incubated with fluorescein-labeled HPMA copolymer conjugates in RPMI 1640 culture medium for 1 h in the dark. (**A**) Control cells, (**B**) P-(GFLG-Mce_6)-FITC, (**C**) P-(GFLG-SOS)-FITC, (**D**) P-(GFLG-SOS)-(Fab'-FITC), (**E**) P-(GFLG-Mce_6)-(Fab'-FITC).

Table 5. IC_{50} values for Mce_6, SOS, and HPMA copolymer-Mce_6 or -SOS conjugates against OVCAR-3 cells.

Drug	**Incubation time (days)**	**IC_{50} or D_m (μM)[a]**
Mce_6	1	3.34 ± 0.43
P-GFLG-Mce_6		12.5 ± 1.06
P-(GFLG-Mce_6)-Fab’		1.35 ± 0.10
SOS	4	2.02 ± 0.17
P-GFLG-SOS		32.9 ± 4.94
P-(GFLG-SOS)-Fab’		43.8 ± 2.90

[a] IC_{50} or D_m values are the means ± SEM (n=6 in single experiment).

preliminary experiments on the relationship between exposure time and cell inhibition effect (data not shown). After 1-day Mce_6 exposure and 4-day SOS exposure, the cells were more susceptible to Mce_6 than SOS about 2 times. It is interesting to note the enormous difference in the activity of SOS toward OVCAR-3 cells and toward the human A498 renal cell line (177). Previous study on human renal A498 cells demonstrated that free SOS and P-GFLG-SOS conjugates were effective individually and in combination with free DOX and P-GFLG-DOX or free Mce_6 and P-GFLG-Mce_6, respectively (177). The IC_{50} values for Mce_6 toward both cell types (OVCAR-3 and A498 (177)) were similar. However, SOS was very effective toward A498 cells (IC_{50} = 3 nM) (177), but its activity toward OVCAR-3 was about 670 times lower. These data are consistent with the results of the NCI anticancer drug screen consisting of a panel of 60 human cancer cell lines. Rivera *et al.* showed that after a 2-day continuous exposure to SOS, OVCAR-3 cells were less sensitive to SOS than the A498 cells (77). These results reflect the different p53 status in these cell lines. The inhibitory effect of SOS is mediated through p53; the disruption of the p53-HDM-2 interactions results in increasing p53 accumulation in tumor cells (76). It was demonstrated that the p53 status of A498 cells and OVCAR-3 cells are wild-type and mutant, respectively (189). However, the study of the p53 gene in human ovarian carcinoma cell lines by Yaginuma and Westphal showed that the wild-type p53 protein was detectable in OVCAR-3 cells by immunoprecipitation analysis (190). These reports indicated that OVCAR-3 cells can be inhibited by higher concentrations of SOS, but have lower sensitivity when compared to the A498 cell line.

The IC_{50} doses of non-targeted conjugates, P-GFLG-Mce_6 and P-GFLG-SOS, were higher than those of free Mce_6 and SOS, respectively. These results reflect the different mechanisms of cell entry of free drugs *vs.* copolymer conjugates (96). In contrast, the targeted P-(GFLG-Mce_6)-Fab' conjugate was 2 and 9 times more effective than Mce_6 and P-GFLG-Mce_6, respectively. The cytotoxicity data with Mce_6 conjugates were in agreement with biorecognition data and internalization mechanisms (Figures 17 and 18). There was a discrepancy in data obtained for P-(GFLG-SOS)-Fab'. This conjugate showed faster internalization (Figure 17) and moderately better biorecognition (Figure 18) than P-GFLG-SOS; however, it possessed a slightly weaker inhibitory effect than P-GFLG-SOS (Table 5). One

explanation may be in the long drug exposure time. After long exposure times the intracellular drug content of targeted and non-targeted conjugates may be similar (191). Furthermore, the efficacies of SOS and its conjugates might be limited by the problem of SOS trafficking to the subcellular compartments where p53 is mainly located, such as nucleus and mitochondria (192). Subcellular targeting is very important for some active agents and macromolecular therapeutics that have to be transported to their assigned cell organelles. Once those molecules are delivered to the cytosol, various approaches to locate drugs in a particular subcellular organelle have been performed, such as the use of nuclear localization peptides (68, 193), cell-penetrating peptides (194), lipophilic cationic moieties (4), and mitochondrial localization agents (195).

The OA-3 surface antigen (CD47 or IAP) was chosen as delivery target in this study because it is overexpressed in about 90% of the ovarian tumors and only weakly expressed in normal tissue (183). Although a panel of anti-CD47 mAbs used in the study of Mawby *et al.*, such as NBTS/BRIC-125 (BRIC-125), NBTS/BRIC-126 (BRIC-126) and NBTS/BRIC-154 (BRIC-154), showed an extremely broad tissue distribution, not only in ovarian carcinomas studied, but also in all hematopoeitic cells, mesenchyme and epithelia at multiple sites (182). It is striking that the tissue distribution of ^{125}I-labeled OV-TL16 mAb in OVCAR-3 bearing nude mice 48 h after i.v. injection studied by Boerman *et al.* demonstrated that ^{125}I-labeled OV-TL16 mAb possessed tumor/non-tumor ratio of about 3-15 (183). Furthermore, the mAb OV-TL3 used by Campbell *et al.* to define OA3 showed little or no reactivity with normal tissues but reacted with most ovarian carcinomas (184). Slobbe *et al.* studied the structure of OV-TL3 and OV-TL16 antibodies and reported that both mAbs are able to bind to same epitopic regions on the ovarian carcinoma membrane antigen OA3, although structurally different in their VH regions (196).

The basis for the difference between mAbs used in the study of Mawby *et al.* and Boerman *et al.* or Campbell *et al.* is unknown and deserves further investigation. One possibility is that an unusual amino acid sequence in the OA3 isoforms is expressed in ovarian cancer cells, and that OV-TL3 and OV-TL16 recognize epitopes in this sequence (182).

1.4 *In vitro* Inhibition of OVCAR-3 Cell Growth with Drug Combinations

The investigation of possible synergistic, additive, or antagonistic effects of sequential combinations of SOS+Mce_6, P-GFLG-SOS+P-GFLG-Mce_6, or P-(GFLG-SOS)-Fab'+P-(GFLG-Mce_6)-Fab' against the ovarian carcinoma OVCAR-3 cell line was performed *in vitro* by exposing cells to SOS or its conjugates for 4 days, followed by exposure of cells to Mce_6 or its conjugates for 1 day, and finally, a 30-min irradiation. This sequential combination was chosen because the optimal exposure times of SOS/ P-GFLG-SOS/ P-(GFLG-SOS)-Fab' and Mce_6/ P-GFLG-Mce_6/ P-(GFLG-Mce_6)-Fab' were different (4 days for SOS and 1 day for Mce_6), as mentioned above. The dose ratios of each combination (Table 6) were based on their respective IC_{50} concentrations from Table 5 as a series of two-fold dilutions from 4 to 0.03125 times IC_{50}. Figure 19 shows the composite dose-response curves and median-effect plots of OVCAR-3 cells, indicating the anti-proliferative effects of single agents and their combinations. The dose-response curves for combined treatment were obtained by plotting % cell viability (*y*) *vs.* the combined dose of two single agents (*x*). The median-effect plots of single agents and combinations were derived from the linear part of dose-response curves. All of the combination treatments showed anti-proliferative activities toward OVCAR-3 cells. The dose ratio and D_m values of the combination treatments are shown in Table 6. The IC_{50} dose of each drug in combinations was significantly lower than those of each drug as single agents (compare Tables 5 and 6). These results clearly indicate that all of the combination treatments were effective against OVCAR-3 cells.

The CI analysis was used to assess the drug-drug interaction of the sequential combinations of free drugs, non-targeted and targeted copolymer conjugates towards OVCAR-3 cells *in vitro* (37, 38). In the CI analysis, values of CI < 1, CI = 1, and CI > 1 indicate synergy, additivity, and antagonism, respectively. Figure 20 shows the Fa-CI plots over all inhibition effect levels (f_a = 0.05-0.95 or 5-95% of inhibition effect) in OVCAR-3 cells. The sequential combinations of SOS+Mce_6 and P-GFLG-SOS+P-GFLG-Mce_6 yield CI values lower than 1 over the entire range of cytotoxicity, indicating very strong synergistic to synergistic effects. The P-(GFLG-SOS)-Fab'+P-(GFLG-Mce_6)-Fab' combination also displayed a strong synergism for f_a values up to

Table 6. Dose ratios and IC_{50} doses in combinations of free drugs (SOS+Mce_6), non-targeted copolymer conjugates (P-GFLG-SOS+P-GFLG-Mce_6), and targeted copolymer conjugates [P-(GFLG-SOS)-Fab'+P-(GFLG-Mce_6)-Fab'] in OVCAR-3 cells.

Drug combination		**Dose ratio**	**D_m (μM)[a]**
Drug A	**Drug B**		**(Dose A + Dose B)[b]**
SOS	Mce_6	1 : 1.61	0.096 ± 0.0077 (0.037 + 0.059)
P-GFLG-SOS	P-GFLG-Mce_6	1 : 0.38	1.69 ± 0.22 (1.22 + 0.47)
P-(GFLG-SOS)-Fab'	P-(GFLG-Mce_6)-Fab'	1 : 0.031	1.70 ± 0.38 (1.65 + 0.051)

[a] D_m represent the means ± SEM (*n*=6 in single experiment).

[b] Doses of drug A and drug B were calculated approximately from the D_m of each combination and dose ratio.

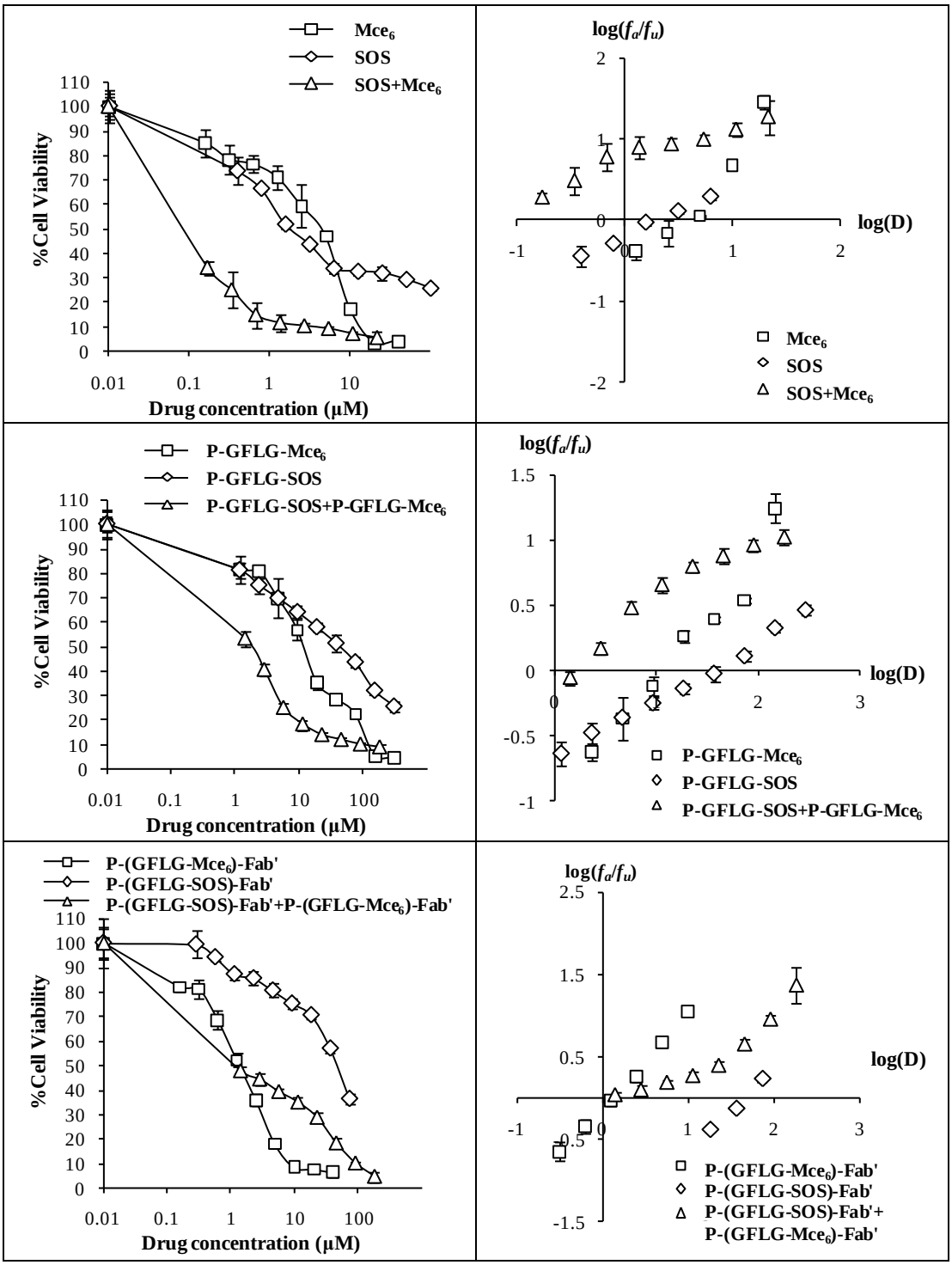

Figure 19. Dose response curves and median-effect plots of OVCAR-3 cells treated with Mce_6, SOS, P-GFLG-Mce_6, P-GFLG-SOS, P-(GFLG-Mce_6)-Fab', and P-(GFLG-SOS)-Fab' as single agents and sequential combinations at constant ratios of their respective IC_{50} concentrations. Bars represent standard error (n=6 in single experiment).

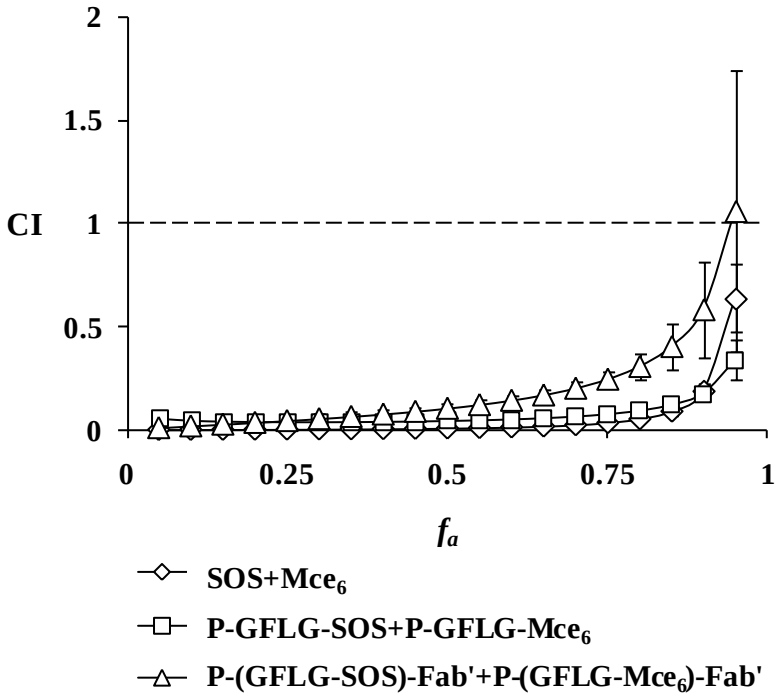

Figure 20. Combination index plots (Fa-CI plots) obtained from median-effect analysis. Chemotherapeutic drugs and their HPMA copolymer conjugates were gradually diluted at the ratio of their IC_{50} values as a series of two-fold dilutions from 4 to 0.03125 times IC_{50} and OVCAR-3 cells exposed to drugs sequentially as described. CI < 1, = 1 and > 1 indicates synergism, additive effect, and antagonism, respectively. The vertical bars indicate the 95% confidence intervals based on Sequential Deletion Analysis (180) and can be generated by using CompuSyn software.

about 0.85, but showed synergistic effect and nearly additive effect at f_a = 0.9 and 0.95, respectively.

The drug interactions may depend on the differences of drugs in the combination, such as physicochemical properties, the mechanisms of action, and the drug exposure schedules. All these differences may result in different antitumor activities. SOS and Mce_6 are hydrophobic low-molecular weight molecules, but both have different mechanisms and sites of action. SOS acts on p53 and DNA while Mce_6 can cause damage to biological molecules by generation of reactive oxygen species. In previous study, we compared the simultaneous combination of P-GFLG-SOS+P-GFLG-Mce_6 to SOS+Mce_6 against the human renal A498 carcinoma cell line. After 16-h cells exposure to the combinations, both combinations displayed synergism for f_a up to 0.8, but showed slight antagonism and near additivity at f_a = 0.95 (177). Many researchers have studied the antitumor activities following different drug exposure schedules. For example, the simultaneous and sequential exposures of irofulven with oxaliplatin or cisplatin against human breast, colon, and ovarian cancer cell lines showed that the sequence oxaliplatin followed by irofulven displayed better synergistic effect than the other schedules (197).

2. Combination Treatment of Human Renal Carcinoma Cells with Free Drugs and HPMA Copolymer Bound Drug Conjugates

According to results of Experiment A, SOS had shown the low cytotoxicity to OVCAR3 ovarian carcinoma cell line due to the mediator of SOS activity is through wild-type p53, which expresses only small amount on OVCAR3 cells. The A498 human renal carcinoma cell line expressing wild-type p53 was selected to study.

In this study, SOS, DOX, and Mce_6 were chosen as anticancer agents; these represent low-M_w compounds possessing different sites and/or mechanisms of action. The interactions between free and HPMA copolymer-bound SOS, DOX, and Mce_6 in binary combination against the A498 renal carcinoma cell line *in vitro* were evaluated using median-effect analysis. We hypothesized that a combination of these agents may produce synergistic effects and thereby reduce effective doses while maintaining efficacy, compared to the doses required for each agent alone to produce a given drug effect level.

2.1 Characteristics of HPMA Copolymer-SOS or –DOX or -Mce_6 Conjugates

P-GFLG-SOS, P-GFLG-DOX and P-GFLG-Mce_6 conjugates were synthesized as shown in Figures 10, 11 and 16. The GFLG oligopeptide sequence was chosen as the drug attachment/release site and incorporated in all three conjugates. This tetrapeptidyl linker was designed to be stable in blood plasma, but susceptible to cleavage by cathepsin B within the lysosomal compartment (112, 114, 115).

The characteristics of the conjugates, including the drug content in mole% and mole/gram of polymer conjugate, average amount of drug per macromolecule, molecular weight, and polydispersity, are summarized in Table 7. The drug content in all conjugates was similar. P-GFLG-SOS, P-GFLG-DOX and P-GFLG-Mce_6 conjugates contained 3.4, 3.0, and 2.9 drug molecules per macromolecule, respectively. The apparent M_w of polymer conjugates were estimated by size exclusion chromatography using ÄKTA system, equipped with a Superose 6 HR 10/30 column calibrated with poly(HPMA) samples. The apparent M_w of the polymer conjugates were between 23 and 32 kDa, whereas the polydispersity ranged from 1.2 to 1.5.

Table 7. Characterization of HPMA copolymer-drug conjugates.

Conjugates	Mol% of drug[a]	mmol drug per g polymer conjugate	Number of drug molecules per conjugate	Apparent M_w (kDa)[b]	Poly-dispersity[c]	% Yield
P-GFLG-SOS	1.62	0.106	3.4 (SOS)	32	1.50	69
P-GFLG-DOX	1.93	0.121	3.0 (DOX)	25	1.24	68
P-GFLG-Mce_6	2.04	0.125	2.9 (Mce_6)	23	1.34	61

[a] Determined by UV spectrophotometry: ε_{358} = 33 000 M^{-1} cm^{-1} in methanol for SOS, ε_{488} = 11 000 M^{-1} cm^{-1} in DI water for DOX, and ε_{395} = 158 000 M^{-1} cm^{-1} in methanol for Mce_6.

[b] Apparent M_w of polymers was estimated by size exclusion chromatography using ÄKTA/FPLC system equipped with a Superose 6 column, calibrated with polyHPMA fractions. Acetate buffer pH 5.5 + 30% (v) acetonitrile was used for P-GFLG-SOS. PBS buffer pH 7.3 + 30% (v) acetonitrile was used for P-GFLG-DOX and P-GFLG-Mce_6.

[c] Polydispersity = the ratio of weight-average to number-average molecular weight

2.2 *In Vitro* Inhibition of A498 Cell Growth by Drugs as Single Agents

Renal cell carcinoma is the predominant form of kidney cancer and highly refractory to chemotherapy due to the multidrug resistance. This is due to gp-170, a membranous glycoprotein encoded by the MDR1 gene (198). The A498 cell line is a primary renal carcinoma cell line that expresses a moderate level of gp-170 (199). Moreover, A498 cell has been reported to express a functional wild-type p53. The transcriptional activity of p53 in renal cell carcinoma is significantly regulated by MDM-2 (mouse double minute-2) (200).

SOS has a pronounced antitumor activity toward tumor cells lines expressing wild-type p53, especially the A498 human renal carcinoma cell line. *In vivo* study of SOS in mice xenografts of A498 cells showed that SOS exhibited strong antitumor activity and completed tumor regression of A498 tumor xenografts (77).

DOX is one of the most widely used chemotherapeutic agents with multiple mechanisms of action. *In vitro* studies of DOX cytotoxicity toward renal carcinoma cell lines have shown that they are sensitive to DOX, especially the A498 cell line (199, 201).

Mce_6 the second generation photosensitizer is activated by light to produce singlet oxygen, which can damage the biomolecules, and thus destroys the cells (59, 61). Its common side effects are prolonged cutaneous and systemic photosensitivities, which remain a problem in patients treated with low-M_w photosensitizers (202, 203). Binding Mce_6 to HPMA copolymers containing a targeting moiety can also limit its distribution in the body and reduce side effects (32, 125, 204).

The inhibitory effects of SOS, DOX, Mce_6, P-GFLG-SOS, P-GFLG-DOX, and P-GFLG-Mce_6 as single agents on the growth of A498 cells were evaluated after 16 h of drug exposure using the MTT assay. Values collected using untreated control cells corresponded to 100% cell viability. The IC_{50} values for the free drugs and the HPMA copolymer conjugates are shown in Table 8. The A498 cell line was highly susceptible to SOS and P-GFLG-SOS with IC_{50} values of 3 nM and 23 nM, respectively. The IC_{50} of SOS in this study was in agreement with that measured by Rivera *et al.*, who reported an IC_{50} of 2 nM in the A498 cell line after a 48 h exposure to SOS (77). In all experiments the linear correlation coefficient of the median-effect plot (r) was > 0.98, providing a reliable basis for further calculations.

SOS was 80 and 1170 times more effective than DOX and Mce_6, respectively; P-GFLG-SOS was 1170 and 320 times more effective than P-GFLG-DOX and P-GFLG-Mce_6, respectively (Table 8). The IC_{50} values of P-GFLG-SOS, P-GFLG-DOX and P-GFLG-Mce_6 were higher than those of free SOS, DOX, and Mce_6, respectively. These results reflect the different mechanisms of cellular internalization of free drugs *vs.* copolymer conjugates. Copolymer conjugates containing hydrophobic drugs/moieties are internalized by fluid-phase pinocytosis and adsorptive pinocytosis concurrently, which is slower than the diffusion process of free drugs (96). The relatively low disparity between the IC_{50} doses of Mce_6 and P-GFLG-Mce_6 (3.55 *vs.* 7.32 μM) reflects the fact that it is not necessary for Mce_6 molecules to be cleaved from copolymer backbone to generate a photodynamic effect. Polymer-bound Mce_6 can also produce singlet oxygen, albeit at a lower quantum yield than free Mce_6 (125).

The main advantages of HPMA copolymer-drug conjugates over their low-M_w drugs (reviewed in Kopeček (22), Putnam and Kopeček (24), Kopeček *et al*. (7), Duncan (102), Cuchelkar and Kopeček (25), Pan and Kopeček (26)) include: (*a*) enhanced water solubility of low soluble or insoluble drugs with concomitant improvement of drug bioavailability; (*b*) long-lasting circulation in the bloodstream (86, 92); (*c*) decreased non-specific toxicity of the conjugated drug and immunogenicity of the targeting moiety (34); (*d*) increased *passive* and/or *active* accumulation of the drug at the site of its action by the EPR effect and/or by targeting, respectively (30-32); (*e*) active uptake by fluid-phase pinocytosis (non-targeted polymer-bound drug) or receptor-mediated endocytosis (targeted polymer bound drug); (*f*) the potential to overcome efflux pump-mediated mechanism of drug resistance (8-10); and (*g*) ability to deliver several active components with different properties to the same target site that enhance the specific activity of the main drug (205, 206).

2.3 *In Vitro* Growth Inhibition of Agents in Combination

Experiments investigating the cytotoxicity potential of binary combinations of SOS, DOX, Mce_6, P-GFLG-SOS, P-GFLG-DOX, P-GFLG-Mce_6 against A498 cells were evaluated by exposing cells to combinations of free drugs/conjugates at ratios based on their respective IC_{50} concentrations (Table 8). Figure 21 shows the

Table 8. Cell proliferation IC_{50} values for SOS, DOX, Mce_6, and their HPMA copolymer conjugates against A498 cells.

Drug	**IC_{50} or D_m (μM)[a]**
SOS	0.003 ± 0.0003
DOX	0.24 ± 0.02
Mce_6	3.55 ± 0.08
P-GFLG-SOS	0.023 ± 0.0004
P-GFLG-DOX	26.8 ± 3.4
P-GFLG-Mce_6	7.32 ± 0.12

[a] IC_{50} or D_m values are the means ± SEM (n=6). The differences of means against control were statistically significant at p-value < 0.05 (Student's t-test).

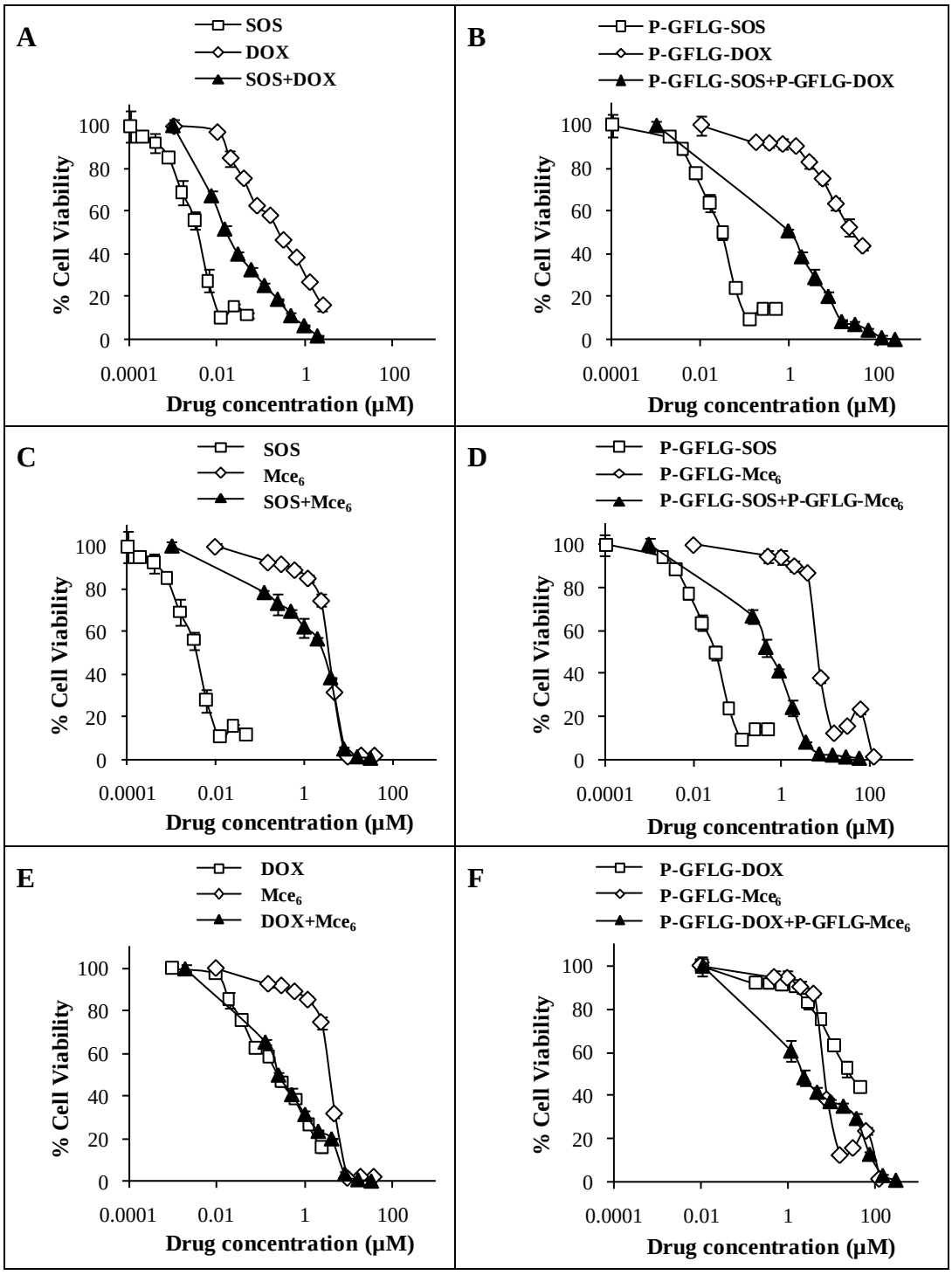

Figure 21. Dose-response curves of A498 cells treated with (**A**) SOS and DOX, (**B**) P-GFLG-SOS and P-GFLG-DOX, (**C**) SOS and Mce_6, (**D**) P-GFLG-SOS and P-GFLG-Mce_6, (**E**) DOX and Mce_6, (**F**) P-GFLG-DOX and P-GFLG-Mce_6, as single agents and binary combinations at constant ratios of their respective IC_{50} concentrations; bars represent the standard error (n=6).

composite dose-response curves of A498 cells indicating the anti-proliferative effects of single agents and their combinations. The dose-response curves for combined treatment were obtained by plotting cell viability (*y*) *vs.* the combined dose of two single agents (*x*). All of the binary combination treatments showed anti-proliferative activities toward the A498 cell line. The dose ratio, IC_{50} or D_m values of the combination treatment, and dose of each drug/conjugate combination that inhibit cell growth by 50% are shown in Table 9. The dose of each drug/conjugate in combination was substantially lower than the IC_{50} doses of the drugs as single agents (compare Tables 8 and 9). These results clearly indicate that all of the combination treatments were effective against A498 cells.

To evaluate potential synergy of the combinations of free drugs and copolymer conjugates towards A498 cells *in vitro*, the CI analysis was used (37, 38). In the CI analysis, values of CI < 1, CI = 1, and CI > 1 indicate synergy, additivity, and antagonism, respectively. Figure 22 and Table 10 show a graphic summary of the CI analyses over all levels of effect (f_a = 0.05-0.95 or 5-95% of inhibition effect) and CI values at 25%, 50%, 75% and 95% of growth inhibition effects in A498 cells, respectively. It should be noted that at very high and at very low drug effect levels, the method is less accurate due to logarithmic transformation (39). Consequently, we have chosen f_a from 0.05 to 0.95 for evaluation. The most synergistic binary combination was SOS+DOX. Simultaneous addition of SOS and DOX to A498 cells in a monolayer culture yielded CI values lower than 1 over the entire range of cytotoxicity, indicating a strong synergistic to moderate synergistic effect. The SOS+Mce_6 and P-GFLG-SOS+P-GFLG-Mce_6 combinations both displayed synergism for f_a values up to about 0.8, but showed slight antagonism and near additivity at f_a = 0.95, respectively. However, all other combinations were synergistic to varying degrees up to f_a < 0.9, and were additive at higher f_a values. The experimental data were also analyzed using the isobologram method (207). The result comparison (data not shown) indicated that both the CI and isobologram analyses produced very similar results.

The synergistic effects of combinations may depend on the cytotoxic mechanism of each agent. SOS, DOX, and Mce_6 have different sites of action, but produce similar cytotoxic intermediates and outcomes including: DNA damage,

Table 9. Dose ratios and IC_{50} doses in combinations of free drugs (SOS+DOX, SOS+Mce_6, DOX+Mce_6) and their copolymer conjugates (P-GFLG-SOS+P-GFLG-DOX, P-GFLG-SOS+P-GFLG-Mce_6, P-GFLG-DOX+P-GFLG-Mce_6) in A498 cells.

Drug combination		**Dose ratio**	**D_m (μM)[a]** **(Dose A + Dose B)[b]**
Drug A	**Drug B**		
SOS	DOX	1:80	0.0213 ± 0.002 (0.00027 + 0.021)
SOS	Mce_6	1:1330	0.270 ± 0.028 (0.00020 + 0.27)
DOX	Mce_6	1:16.7	0.392 ± 0.018 (0.022 + 0.37)
P-GFLG-SOS	P-GFLG-DOX	1:1200	1.37 ± 0.052 (0.0011 + 1.37)
P-GFLG-SOS	P-GFLG-Mce_6	1:280	1.48 ± 0.291 (0.0053 + 1.47)
P-GFLG-DOX	P-GFLG-Mce_6	1:0.23	3.71 ± 0.337 (3.01 + 0.70)

[a] D_m represent the means ± SEM (n=6). The statistical comparisons in D_m between single agent treatments (Table 8) and combination treatments (Table 9) were significant at p-value < 0.05 (ANOVA).

[b] D is the dose of each drug/conjugate in a combination that inhibits the cell growth by 50%.

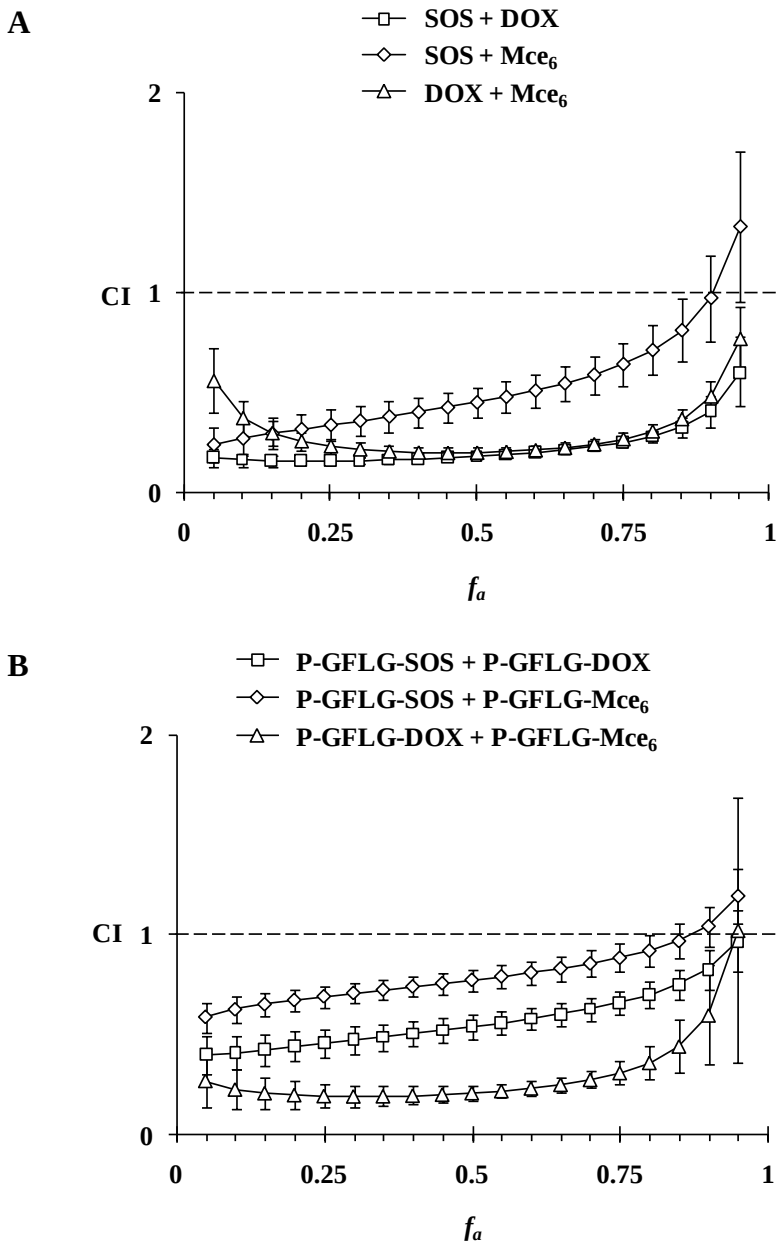

Figure 22. Fa-CI plots obtained from median-effect analysis. (**A**) free drug combinations, and (**B**) copolymer conjugate combinations. Chemotherapeutic drugs and their copolymer conjugates were gradually diluted at the ratio of their IC_{50} values as a series of two-fold dilutions from 8 to 0.03125 times IC_{50} and A498 cells exposed to drugs simultaneously for 16 h as described. CI < 1, = 1 and > 1 indicates synergism, additive effect and antagonism, respectively. The vertical bars indicate the 95% confidence intervals based on Sequential Deletion Analysis (180) and can be generated by using CompuSyn software.

Table 10. Combination index values at different effect levels for combination treatments of A498 cells with free and HPMA copolymer-bound drugs.

Drug combination		**Combination index (CI)[a] at**			
Drug A	**Drug B**	**IC_{25}**	**IC_{50}**	**IC_{75}**	**IC_{95}**
SOS	DOX	0.16 ± 0.02	0.18 ± 0.01	0.25 ± 0.02	0.60 ± 0.17
SOS	Mce_6	0.34 ± 0.08	0.45 ± 0.08	0.64 ± 0.11	1.33 ± 0.38
DOX	Mce_6	0.23 ± 0.04	0.20 ± 0.03	0.27 ± 0.03	0.77 ± 0.16
P-GFLG-SOS	P-GFLG-DOX	0.46 ± 0.07	0.54 ± 0.06	0.66 ± 0.06	0.97 ± 0.15
P-GFLG-SOS	P-GFLG-Mce_6	0.69 ± 0.05	0.77 ± 0.05	0.88 ± 0.07	1.19 ± 0.13
P-GFLG-DOX	P-GFLG-Mce_6	0.20 ± 0.06	0.21 ± 0.04	0.31 ± 0.06	1.02 ± 0.66

[a] CI values < 1, = 1, and > 1 characterize synergism, additive effect, and antagonism, respectively. CI values shown are mean ± SEM (*n*=6).

cellular damage, cell cycle arrest, and cell apoptosis. DOX+Mce_6 and P-GFLG-DOX+P-GFLG-Mce_6 combinations showed better synergistic effects compared to other combinations, probably due to the multiple mechanisms of action of DOX, including generation of reactive oxygen species (81), which is analogous to the activity of Mce_6. The mechanism of this synergistic effect is the potentiation of PDT by DOX and vice versa. In the cell, DOX can be reduced by NADPH cytochrome P450 reductase to semiquinone-free radicals. In the presence of molecular oxygen, the semiquinone radicals are capable of enhancing superoxide production (208, 209), which can cause damage to biological molecules. This suggests that DOX+Mce_6 and P-GFLG-DOX+P-GFLG-Mce_6 combinations produced similar cytotoxic intermediates with a concomitant enhancement of efficacy. Enhanced efficacy resulting from the combination of a photosensitizer and DOX has been demonstrated on various cell lines, such as Walker 256 carcinosarcoma cells (210), H-MESO-1 human malignant mesothelioma cells (211), murine L929 cells (212), and murine hepatoma MH-22A (213).

SOS+DOX and P-GFLG-SOS+P-GFLG-DOX combinations also showed synergistic effects. Both drugs act on DNA: SOS induces DNA-protein and DNA-DNA crosslinks with no detectable DNA strand breaks (75), but DOX can intercalate into DNA strands and also produce non-protein-associated and protein-associated DNA strand breaks (83). Regardless of the detailed mechanism, both SOS and DOX induce DNA damage, cell cycle arrest at G_1 and G_2, and, ultimately cell apoptosis.

Furthermore, many *in vivo* studies have described enhanced antitumor activity of DOX in combination with other chemotherapeutic agents. Examples include: the combination of immunoconjugate BR96-DOX and paclitaxel against MCF7 human breast carcinoma, L2987 human lung carcinoma, RCA and LS174T human colon carcinomas in athymic mice (214), doxorubicin with anti-fetal liver kinase 1 monoclonal antibody in human SKLMS-1 leiomysarcoma and RD rhabdomyosacoma xenografts in SCID mice (215), pegylated liposomal doxorubicin administered with nanoliposomal topotecan for treatment of intracranial brain tumor xenografts (216), and the combination of liposomal doxorubicin and topotecan, docetaxel, gemcitabine, capecitabine, or celecoxib for treatment of OVCAR-3 and ES-2 human ovarian carcinoma xenografts (217).

SOS+Mce_6 and P-GFLG-SOS+P-GFLG-Mce_6 combinations showed weaker synergistic effects than the other combinations. It is not clear how the facts, that SOS and Mce_6 have different mechanisms of action and produce different cytotoxic intermediates, relate to this phenomenon.

The DRI values in Table 11 indicate the fraction that the drug concentrations can be decreased by to achieve the IC_{50}. For example, the IC_{50} value was 0.003 µM SOS or 0.24 µM DOX in single agent treatments (Table 8), but a 1:80 combination of SOS+DOX can inhibit 50% of cell growth using 0.00027 µM SOS and 0.021 µM DOX. This represents an 11-fold decrease for both SOS and DOX concentrations. All combinations produced IC_{50} values with DRIs ranging from 4.5 to 20.5. These results indicated that the median effect dose of each agent could be reduced when used in combination and consequently reduce the non-specific side effect of each agent.

Previously, *in vitro* studies of the interaction between free DOX and Mce_6 using the isobologram method (148) and the cooperation between free and HPMA copolymer-DOX and HPMA copolymer-Mce_6 conjugates (31) in human ovarian OVCAR-3 carcinoma cells demonstrated that the combination DOX+Mce_6 decreased the percentage of viable cells and displayed synergistic-to-additive effects in the dose range tested. P-GFLG-DOX improved the efficacy of P-GFLG-Mce_6 when the variable dose of P-GFLG-DOX was simultaneously added to an effective dose of P-GFLG-Mce_6. By contrast, P-GFLG-Mce_6 did not significantly improve the efficacy profile of P-GFLG-DOX when the variable dose of P-GFLG-Mce_6 was simultaneously added to an effective dose of P-GFLG-DOX (31).

Recently, Vicent and collaborators (205, 206) have synthesized the HPMA copolymer conjugate containing both DOX and the aromatase inhibitor aminoglutethimide (AGM) attached to one macromolecule and evaluated its biological activity of toward MCF-7 and MCF-7ca breast cancer cells. Their results showed that HPMA copolymer bearing both DOX and AGM on one macromolecule showed increased cytotoxicity *in vitro*, while a combination of P-GFLG-DOX and HPMA copolymer-bound AGM (P-GFLG-AGM) exhibited low toxicity. The mechanism is unknown, but is probably related to differences in the subcellular pharmacokinetics of one conjugate *vs.* the combination of two conjugates possessing one drug.

Table 11. Dose-reduction index values at 50% effect levels of combinations of free drugs and their copolymer conjugates in A498 cells.

Drug combination		**Dose-reduction index (DRI)[a] for**	
Drug A	**Drug B**	**Drug A**	**Drug B**
SOS	DOX	11.16 ± 1.38	11.12 ± 0.42
SOS	Mce_6	14.96 ± 0.53	13.36 ± 1.73
DOX	Mce_6	10.74 ± 1.28	9.62 ± 1.30
P-GFLG-SOS	P-GFLG-DOX	20.50 ± 0.93	19.52 ± 1.37
P-GFLG-SOS	P-GFLG-Mce_6	4.46 ± 0.05	4.97 ± 0.42
P-GFLG-DOX	P-GFLG-Mce_6	8.90 ± 0.50	10.42 ± 1.61

[a] Dose-reduction index (DRI) values at IC_{50} (or D_m) represent means ± SEM (n=6).

Recently, many researchers have focused on drug combinations *in vivo* and in clinical trials to determine the synergism or antagonism of combined drugs in order to lower dosages and reduce side effects. A recently published review of clinical studies of combination treatments of renal cell carcinoma (218) showed five different combination regimens with 5% to 71% antitumor response along with acceptable toxicity profiles. Hainsworth *et al.* studied the clinical efficacy and toxicity of combined treatment of metastatic renal cell carcinoma with bevacizumab and erlotinib in a phase II trial. It was demonstrated that both targeted agents in combination were effective and well-tolerated (219). Using drug combinations with different drug exposure schedules, or simultaneous *vs.* consecutive exposure, may result in different antitumor activities. For example, the combination of a *bis*-phenazine (XR5944) with 5-fluorouracil (5-FU) and irinotecan, simultaneously or sequentially, against colon cancer HT29 cell line showed that simultaneous exposure of cells to XR5944 and 5-FU or irinotecan exhibited antagonism, while sequential exposure to either order of these drugs displayed additive effects or better (144).

CHAPTER V
CONCLUSION

HPMA copolymer bound drug conjugates are one of the most frequently evaluated polymer backbones in polymer-drug conjugates and established as one of the first-generation nanomedicines for the treatment of cancer. These studies were based on the concept of combinations using HPMA copolymer bound drug conjugates toward cancer cells.

Combination Treatment of Human Ovarian Carcinoma Cells with Fab'-Targeted HPMA Copolymer Bound Drug Conjugates

The biological activities of sequential combinations of anticancer drugs, SOS and Mce_6, in the form of free drugs, non-targeted HPMA copolymer-drug conjugates, P-GFLG-Mce_6 and P-GFLG-SOS, and Fab'-targeted HPMA copolymer-drug conjugates, P-(GFLG-Mce_6)-Fab' and P-(GFLG-SOS)-Fab', were evaluated against human ovarian carcinoma OVCAR-3 cells. Mce_6, SOS, P-GFLG-Mce_6, P-GFLG-SOS, P-(GFLG-Mce_6)-Fab' and P-(GFLG-SOS)-Fab' when used as single agents or in binary combination, exhibited cytotoxic activities against OVCAR-3 cells, as determined using a modified MTT assay. The cellular internalization studies of P-(GFLG-Mce_6)-Fab' and P-(GFLG-SOS)-Fab' by OVCAR-3 cells were showed that an enhanced biorecognition by OVCAR-3 cells of Fab'-targeted HPMA copolymer conjugates than non-targeted conjugates. These results confirmed the incorporation of antibody Fab' fragment into HPMA copolymer-drug conjugates results in specific delivery and enhancement of the amount of the polymeric conjugate being internalized by receptor-mediated endocytosis.

Combination chemotherapy and PDT with free SOS and Mce_6, their non-targeted and Fab'-targeted HPMA copolymer conjugates in human ovarian carcinoma OVCAR-3 cells was evaluated. The sequential combinations of these therapeutics produced very strong synergism to nearly additivity in the treatment of OVCAR-3

cells. The synergistic effects ranked in the order: P-GFLG-SOS+P-GFLG-Mce_6 > SOS+Mce_6 > P-(GFLG-SOS)-Fab'+P-(GFLG-Mce_6)-Fab'. The sequential combinations of SOS+Mce_6 and P-GFLG-SOS+P-GFLG-Mce_6 displayed very strong synergism to synergism in the entire range of cell inhibition levels. The P-(GFLG-SOS)-Fab'+P-(GFLG-Mce_6)-Fab' exhibited a strong synergism for f_a values up to about 0.85, but showed synergistic effect and nearly additive effect at f_a = 0.9 and 0.95, respectively. These observations support the continuation of *in vivo* investigations of SOS, Mce_6 and these conjugates combinations to determine the antitumor activity for the treatment of ovarian cancer.

Combination Treatment of Human Renal Carcinoma Cells with Free Drugs and HPMA Copolymer Bound Drug Conjugates

The synergism in anticancer effect toward human renal carcinoma A498 cells by binary combinations of free and HPMA copolymer-bound anticancer drugs, SOS, DOX, and Mce_6, was evaluated. When used as single agents or in combinations, both free drugs and HPMA copolymer conjugates exhibited cytotoxic activities against A498 cells. As single agents, SOS and P-GFLG-SOS were significantly more effective than the other agents evaluated. Combinations of free and HPMA copolymer-bound SOS, DOX, and Mce_6 produced synergistic effects in the treatment of A498 renal carcinoma cells. The synergistic effects ranked in the order SOS+DOX > P-GFLG-DOX+P-GFLG-Mce_6 ≈ DOX+Mce_6 > P-GFLG-SOS+P-GFLG-DOX ≈ SOS+Mce_6 > P-GFLG-SOS+P-GFLG-Mce_6. The combination of SOS+DOX proved to be synergistic over all cell growth inhibition levels. All other combinations exhibited synergism in a wide range of drug effect levels. The SOS+Mce_6 and P-GFLG-SOS+P-GFLG-Mce_6 combinations displayed synergism up to f_a values of about 0.8 and reached slight antagonism and nearly additivity at f_a = 0.95, respectively. However, all other combinations were synergistic up to f_a < 0.9 and were additive at higher f_a values. This bodes well for further development of macromolecular nanomedicines based on HPMA copolymers. Several HPMA copolymer drug conjugates underwent clinical testing, including DOX (27) and platinates (28). The advantages of combination therapy using HPMA copolymer conjugates have been demonstrated on animal models of ovarian carcinoma (32, 153-

156). The results presented here highlight the potential applications of synergistic combinations and dose reduction for combination therapy for renal carcinoma. These observations that most combinations produced synergistic effects may prove useful in the development of *in vivo* combination study protocols for the treatment of renal cancer and could be further confirmed in future clinical applications.

REFERENCES

1. Dollinger M, Rosenbaum EH, Tempero M, Mulvihill SJ. Everyone's Guide to Cancer Therapy: How Cancer is Diagnosed, Treated, and Managed Day to Day. (4th ed). Andrews McMeel Publishing; 2002.
2. Maeda H, Seymour LW, Miyamoto Y. Conjugates of anticancer agents and polymers: advantages of macromolecular therapeutics in vivo. Bioconjug Chem 1992;3(5):351-62.
3. Maeda H, Wu J, Sawa T, Matsumura Y, Hori K. Tumor vascular permeability and the EPR effect in macromolecular therapeutics: a review. J Control Release 2000;65(1-2):271-84.
4. Breunig M, Bauer S, Goepferich A. Polymers and nanoparticles: intelligent tools for intracellular targeting? Eur J Pharm Biopharm 2008;68(1):112-28.
5. Duncan R. Polymer conjugates as anticancer nanomedicines. Nat Rev Cancer 2006;6(9):688-701.
6. Kiick KL. Materials science. Polymer therapeutics. Science 2007;317(5842):1182-3.
7. Kopeček J, Kopečková P, Minko T, Lu Z. HPMA copolymer-anticancer drug conjugates: design, activity, and mechanism of action. Eur J Pharm Biopharm 2000;50(1):61-81.
8. Minko T, Kopečková P, Kopeček J. Chronic exposure to HPMA copolymer-bound adriamycin does not induce multidrug resistance in a human ovarian carcinoma cell line. J Control Release 1999;59(2):133-48.
9. Minko T, Kopečková P, Pozharov V, Kopeček J. HPMA copolymer bound adriamycin overcomes MDR1 gene encoded resistance in a human ovarian carcinoma cell line. J Control Release 1998;54(2):223-33.
10. Minko T, Kopečková P, Kopeček J. Efficacy of the chemotherapeutic action of HPMA copolymer-bound doxorubicin in a solid tumor model of ovarian carcinoma. Int J Cancer 2000;86(1):108-17.

11. Allen TM. Ligand-targeted therapeutics in anticancer therapy. Nat Rev Cancer 2002;2(10):750-63.
12. David A, Kopečková P, Minko T, Rubinstein A, Kopeček J. Design of a multivalent galactoside ligand for selective targeting of HPMA copolymer-doxorubicin conjugates to human colon cancer cells. Eur J Cancer 2004;40(1):148-57.
13. Krishnaiah YS, Satyanarayana V, Dinesh Kumar B, Karthikeyan RS, Bhaskar P. In vivo evaluation of guargum-based colon-targeted oral drug delivery systems of celecoxib in human volunteers. Eur J Drug Metab Pharmacokinet 2002;27(4):273-80.
14. Wirth M, Gerhardt K, Wurm C, Gabor F. Lectin-mediated drug delivery: influence of mucin on cytoadhesion of plant lectins in vitro. J Control Release 2002;79(1-3):183-91.
15. Wroblewski S, Říhová B, Rossmann P, Hudcovicz T, Rehakova Z, Kopečková P, et al. The influence of a colonic microbiota on HPMA copolymer lectin conjugates binding in rodent intestine. J Drug Target 2001;9(2):85-94.
16. Dharap SS, Qiu B, Williams GC, Sinko P, Stein S, Minko T. Molecular targeting of drug delivery systems to ovarian cancer by BH3 and LHRH peptides. J Control Release 2003;91(1-2):61-73.
17. Low PS, Antony AC. Folate receptor-targeted drugs for cancer and inflammatory diseases. Adv Drug Deliv Rev 2004;56(8):1055-8.
18. Lukyanov AN, Elbayoumi TA, Chakilam AR, Torchilin VP. Tumor-targeted liposomes: doxorubicin-loaded long-circulating liposomes modified with anti-cancer antibody. J Control Release 2004;100(1):135-44.
19. Mao W, Luis E, Ross S, Silva J, Tan C, Crowley C, et al. EphB2 as a therapeutic antibody drug target for the treatment of colorectal cancer. Cancer Res 2004;64(3):781-8.
20. Lu ZR, Kopečková P, Kopeček J. Polymerizable Fab' antibody fragments for targeting of anticancer drugs. Nat Biotechnol 1999;17(11):1101-4.

21. Lu ZR, Kopečková P, Kopeček J. Polymerizable Fab' antibody fragments targeted photodynamic cancer therapy in nude mice. STP Pharma Sciences 2003;13:69-75.
22. Kopeček J. Soluble biomedical polymers. Polim Med 1977;7(3):191-221.
23. Khandare J, Minko T. Polymer-drug conjugates: Progress in polymeric prodrugs. Prog Polym Sci 2006;31:359-97.
24. Putnam D, Kopeček J. Polymer Conjugates with Anticancer Activity. Adv Polym Sci 1995;122:55-123.
25. Cuchelkar V, Kopeček J. Polymer-Drug Conjugates. In: Uchegbu IF, Schätzlein AG, editors. Polymers in Drug Delivery. Florida: CRC Press; 2006. p.155-82.
26. Pan H, Kopeček J. Multifunctional Water-Soluble Polymers for Drug Delivery. In: Torchilin VP, editor. Multifunctional Pharmaceutical Nanocarriers. New York: Springer; 2008. p.81-142.
27. Vasey PA, Kaye SB, Morrison R, Twelves C, Wilson P, Duncan R, et al. Phase I clinical and pharmacokinetic study of PK1 [*N*-(2-hydroxypropyl)methacrylamide copolymer doxorubicin]: first member of a new class of chemotherapeutic agents-drug-polymer conjugates. Cancer Research Campaign Phase I/II Committee. Clin Cancer Res 1999;5(1):83-94.
28. Rademaker-Lakhai JM, Terret C, Howell SB, Baud CM, De Boer RF, Pluim D, et al. A Phase I and pharmacological study of the platinum polymer AP5280 given as an intravenous infusion once every 3 weeks in patients with solid tumors. Clin Cancer Res 2004;10(10):3386-95.
29. Satchi-Fainaro R, Puder M, Davies JW, Tran HT, Sampson DA, Greene AK, et al. Targeting angiogenesis with a conjugate of HPMA copolymer and TNP-470. Nat Med 2004;10(3):255-61.
30. Shiah JG, Dvořák M, Kopečková P, Sun Y, Peterson CM, Kopeček J. Biodistribution and antitumour efficacy of long-circulating *N*-(2-hydroxypropyl)methacrylamide copolymer-doxorubicin conjugates in nude mice. Eur J Cancer 2001;37(1):131-9.

31. Lu JM, Peterson CM, Guo-Shiah J, Gu ZW, Peterson CA, Straight RC, et al. Cooperativity between free and *N*-(2-hydroxypropyl)methacrylamide copolymer bound adriamycin and meso-chlorin e_6 monoethylene diamine induced photodynamic therapy in human epithelial ovarian carcinoma in vitro. Int J Oncol 1999;15(1):5-16.
32. Shiah JG, Sun Y, Kopečková P, Peterson CM, Straight RC, Kopeček J. Combination chemotherapy and photodynamic therapy of targetable *N*-(2-hydroxypropyl)methacrylamide copolymer-doxorubicin/mesochlorin e_6-OV-TL 16 antibody immunoconjugates. J Control Release 2001;74(1-3):249-53.
33. Chapman AP. PEGylated antibodies and antibody fragments for improved therapy: a review. Adv Drug Deliv Rev 2002;54(4):531-45.
34. Říhová B, Kopečková P, Strohalm J, Rossmann P, Větvička V, Kopeček J. Antibody-directed affinity therapy applied to the immune system: in vivo effectiveness and limited toxicity of daunomycin conjugated to HPMA copolymers and targeting antibody. Clin Immunol Immunopathol 1988;46(1):100-14.
35. Lu ZR, Shiah JG, Sakuma S, Kopečková P, Kopeček J. Design of novel bioconjugates for targeted drug delivery. J Control Release 2002;78(1-3):165-73.
36. Hansen MB, Nielsen SE, Berg K. Re-examination and further development of a precise and rapid dye method for measuring cell growth/cell kill. J Immunol Methods 1989;119(2):203-10.
37. Chou TC. Theoretical basis, experimental design, and computerized simulation of synergism and antagonism in drug combination studies. Pharmacol Rev 2006;58(3):621-81.
38. Chou TC, Talalay P. Quantitative analysis of dose-effect relationships: the combined effects of multiple drugs or enzyme inhibitors. Adv Enzyme Regul 1984;22:27-55.
39. Zhao L, Wientjes MG, Au JL. Evaluation of combination chemotherapy: integration of nonlinear regression, curve shift, isobologram, and combination index analyses. Clin Cancer Res 2004;10(23):7994-8004.

40. Foote M. Oncology basics part 1. What is cancer? AMWA Journal 2005;20(2):52-8.
41. Hakem R, Harrington L. Cell Death. In: Tannock IF, editor. The Basic of Science of Oncology. (3rd ed). Columbus: The McGraw-Hill Companies; 2005. p.194-230.
42. Bronchud MH. Selecting the Right Targets for Cancer Therapy. In: Bronchud MH, editor. Principles of Molecular Oncology. Totowa: Humana Press; 2003. p.3-50.
43. Schneider CM, Dennehy CA, Carter SD. Overview of Cancer Pathology. In: Schneider CM, Dennehy CA, Carter SD, editors. Exercise and Cancer Recovery. Champaign: Human Kinetics; 2003. p.1-10.
44. Heffner LJ. Ovarian neoplasms. Human Reproduction at a Glance. Boston: Blackwell Publishing; 2001. p.102-3.
45. Garcia AA, Hamid O, El-Khoueiry A. Ovarian Cancer. WebMD; http://www.emedicine.com/med/topic1698.htm#section~medication [online]. [accessed 3 July 2007].
46. Zweemer RP, Jacobs IJ. Familial Ovarian Cancer. In: Bartlett JM, editor. Ovarian Cancer. Totowa: Hamana Press; 2000. p.13-24.
47. Berek JS, Yao SF, Hacker NF. Ovarian cancer. In: Berek JS, Adashi EY, Hollard PA, editors. Novak's Gynecology. (12th ed). Baltimore: Williams & Wilkins; 1996. p.1155-230.
48. Jemal A, Siegel R, Ward E, Murray T, Xu J, Thun MJ. Cancer statistics, 2007. CA Cancer J Clin 2007;57(1):43-66.
49. Cohen HT, McGovern FJ. Renal-cell carcinoma. N Engl J Med 2005;353(23):2477-90.
50. Sachdeva K, Makhoul I, Javeed M, Curti B. Renal cell carcinoma. WebMD; http://www.emedicine.com/med/topic2002.htm#section~treatment [online]. [accessed 15 April 2007].
51. Kim WJ, Kakehi Y, Kinoshita H, Arao S, Fukumoto M, Yoshida O. Expression patterns of multidrug-resistance (MDR1), multidrug resistance-associated protein (MRP),glutathione-S-transferase-pi (GST-pi) and

DNA topoisomerase II (Topo II) genes in renal cell carcinomas and normal kidney. J Urol 1996;156(2 Pt 1):506-11.

52. Mickisch G, Bier H, Bergler W, Bak M, Tschada R, Alken P. P-170 glycoprotein, glutathione and associated enzymes in relation to chemoresistance of primary human renal cell carcinomas. Urol Int 1990;45(3):170-6.
53. Elson PJ, Witte RS, Trump DL. Prognostic factors for survival in patients with recurrent or metastatic renal cell carcinoma. Cancer Res 1988;48(24 Pt 1):7310-3.
54. Atzpodien J, Poliwoda H, Kirchner H. Alpha-interferon and interleukin-2 in renal cell carcinoma: studies in nonhospitalized patients. Semin Oncol 1991;18(5 Suppl 7):108-12.
55. Gleave ME, Elhilali M, Fradet Y, Davis I, Venner P, Saad F, et al. Interferon gamma-1b compared with placebo in metastatic renal-cell carcinoma. Canadian Urologic Oncology Group. N Engl J Med 1998;338(18):1265-71.
56. Bukowski RM. Natural history and therapy of metastatic renal cell carcinoma: the role of interleukin-2. Cancer 1997;80(7):1198-220.
57. Ramsey S, Aitchison M. Treatment for renal cancer: are we beyond the cytokine era? Nat Clin Pract Urol 2006;3(9):478-84.
58. Canti G, Lattuada D, Morelli S, Nicolin A, Cubeddu R, Taroni P, et al. Efficacy of photodynamic therapy against doxorubicin-resistant murine tumors. Cancer Lett 1995;93(2):255-9.
59. Hopper C. Photodynamic therapy: a clinical reality in the treatment of cancer. Lancet Oncol 2000;1:212-9.
60. Akhlynina TV, Jans DA, Statsyuk NV, Balashova IY, Toth G, Pavo I, et al. Adenoviruses synergize with nuclear localization signals to enhance nuclear delivery and photodynamic action of internalizable conjugates containing chlorin e6. Int J Cancer 1999;81(5):734-40.
61. Dolmans DE, Fukumura D, Jain RK. Photodynamic therapy for cancer. Nat Rev Cancer 2003;3(5):380-7.

62. Bonnett R. Photodynamic Action. Chemical Aspects of Photodynamic Therapy. Amsterdam: Gordon and Breach Science Publishers; 2000. p.57-88.
63. Oleinick NL, Morris RL, Belichenko I. The role of apoptosis in response to photodynamic therapy: what, where, why, and how. Photochem Photobiol Sci 2002;1(1):1-21.
64. Lukšienė Ž. Photodynamic therapy: mechanism of action and ways to improve the efficiency of treatment. Medicina (Kaunas) 2003;39(12):1137-50.
65. Dougherty TJ, Gomer CJ, Henderson BW, Jori G, Kessel D, Korbelik M, et al. Photodynamic therapy. J Natl Cancer Inst 1998;90(12):889-905.
66. Moan J, Berg K. The photodegradation of porphyrins in cells can be used to estimate the lifetime of singlet oxygen. Photochem Photobiol 1991;53(4):549-53.
67. Henderson BW, Dougherty TJ. How does photodynamic therapy work? Photochem Photobiol 1992;55(1):145-57.
68. Tijerina M, Kopečková P, Kopeček J. Correlation of subcellular compartmentalization of HPMA copolymer-Mce_6 conjugates with chemotherapeutic activity in human ovarian carcinoma cells. Pharm Res 2003;20(5):728-37.
69. Allison BA, Waterfield E, Richter AM, Levy JG. The effects of plasma lipoproteins on in vitro tumor cell killing and in vivo tumor photosensitization with benzoporphyrin derivative. Photochem Photobiol 1991;54(5):709-15.
70. Bachor R, Shea CR, Gillies R, Hasan T. Photosensitized destruction of human bladder carcinoma cells treated with chlorin e6-conjugated microspheres. Proc Natl Acad Sci U S A 1991;88(4):1580-4.
71. Lane DP, Fischer PM. Turning the key on p53. Nature 2004;427(6977):789-90.
72. Vassilev LT, Vu BT, Graves B, Carvajal D, Podlaski F, Filipovic Z, et al. In vivo activation of the p53 pathway by small-molecule antagonists of MDM2. Science 2004;303(5659):844-8.
73. Stoll R, Renner C, Hansen S, Palme S, Klein C, Belling A, et al. Chalcone derivatives antagonize interactions between the human oncoprotein MDM2 and p53. Biochemistry 2001;40(2):336-44.

74. Chi SW, Lee SH, Kim DH, Ahn MJ, Kim JS, Woo JY, et al. Structural details on mdm2-p53 interaction. J Biol Chem 2005;280(46):38795-802.

75. Nieves-Neira W, Rivera MI, Kohlhagen G, Hursey ML, Pourquier P, Sausville EA, et al. DNA protein cross-links produced by NSC 652287, a novel thiophene derivative active against human renal cancer cells. Mol Pharmacol 1999;56(3):478-84.

76. Issaeva N, Bozko P, Enge M, Protopopova M, Verhoef LG, Masucci M, et al. Small molecule RITA binds to p53, blocks p53-HDM-2 interaction and activates p53 function in tumors. Nat Med 2004;10(12):1321-8.

77. Rivera MI, Stinson SF, Vistica DT, Jorden JL, Kenney S, Sausville EA. Selective toxicity of the tricyclic thiophene NSC 652287 in renal carcinoma cell lines: differential accumulation and metabolism. Biochem Pharmacol 1999;57(11):1283-95.

78. Thigpen JT. Advances in novel anthracycline therapy - Innovations in anthracycline therapy: overview. Community Oncology 2005;2(1):3-7.

79. Neidle S. The molecular basis for the action of some DNA-binding drugs. Prog Med Chem 1979;16:151-221.

80. Tewey KM, Rowe TC, Yang L, Halligan BD, Liu LF. Adriamycin-induced DNA damage mediated by mammalian DNA topoisomerase II. Science 1984;226(4673):466-8.

81. Sinha BK, Katki AG, Batist G, Cowan KH, Myers CE. Differential formation of hydroxyl radicals by adriamycin in sensitive and resistant MCF-7 human breast tumor cells: implications for the mechanism of action. Biochemistry 1987;26(13):3776-81.

82. Blagosklonny MV. Sequential activation and inactivation of G_2 checkpoints for selective killing of p53-deficient cells by microtubule-active drugs. Oncogene 2002;21(41):6249-54.

83. Fornari FA, Randolph JK, Yalowich JC, Ritke MK, Gewirtz DA. Interference by doxorubicin with DNA unwinding in MCF-7 breast tumor cells. Mol Pharmacol 1994;45(4):649-56.

84. Larsen AK, Escargueil AE, Skladanowski A. From DNA damage to G_2 arrest: the many roles of topoisomerase II. Prog Cell Cycle Res 2003;5:295-300.

85. Shan K, Lincoff AM, Young JB. Anthracycline-induced cardiotoxicity. Ann Intern Med 1996;125(1):47-58.

86. Seymour LW, Ulbrich K, Strohalm J, Kopeček J, Duncan R. The pharmacokinetics of polymer-bound adriamycin. Biochem Pharmacol 1990;39(6):1125-31.

87. Siena S, Piccart MJ, Holmes FA, Glaspy J, Hackett J, Renwick JJ. A combined analysis of two pivotal randomized trials of a single dose of pegfilgrastim per chemotherapy cycle and daily Filgrastim in patients with stage II-IV breast cancer. Oncol Rep 2003;10(3):715-24.

88. Bhatt R, de Vries P, Tulinsky J, Bellamy G, Baker B, Singer JW, et al. Synthesis and in vivo antitumor activity of poly(l-glutamic acid) conjugates of 20S-camptothecin. J Med Chem 2003;46(1):190-3.

89. Seymour LW, Ferry DR, Anderson D, Hesslewood S, Julyan PJ, Poyner R, et al. Hepatic drug targeting: phase I evaluation of polymer-bound doxorubicin. J Clin Oncol 2002;20(6):1668-76.

90. Matsumura Y, Maeda H. A new concept for macromolecular therapeutics in cancer chemotherapy: mechanism of tumoritropic accumulation of proteins and the antitumor agent smancs. Cancer Res 1986;46(12 Pt 1):6387-92.

91. Duncan R, Pratten MK, Cable HC, Ringsdorf H, Lloyd JB. Effect of molecular size of 125I-labelled poly(vinylpyrrolidone) on its pinocytosis by rat visceral yolk sacs and rat peritoneal macrophages. Biochem J 1981;196(1):49-55.

92. Seymour LW, Duncan R, Strohalm J, Kopeček J. Effect of molecular weight (Mw) of *N*-(2-hydroxypropyl)methacrylamide copolymers on body distribution and rate of excretion after subcutaneous, intraperitoneal, and intravenous administration to rats. J Biomed Mater Res 1987;21(11):1341-58.

93. Seymour LW, Miyamoto Y, Maeda H, Brereton M, Strohalm J, Ulbrich K, et al. Influence of molecular weight on passive tumour accumulation of a soluble macromolecular drug carrier. Eur J Cancer 1995;31A(5):766-70.

94. Twaites B, de Las Heras Alarcón C, Alexander C. Synthetic polymers as drugs and therapeutics. J Mater Chem 2005;15:441-55.

95. de Duve C, de Barsy T, Poole B, Trouet A, Tulkens P, Van Hoof F. Commentary. Lysosomotropic agents. Biochem Pharmacol 1974;23(18):2495-531.

96. Duncan R, Rejmanová P, Kopeček J, Lloyd JB. Pinocytic uptake and intracellular degradation of *N*-(2-hydroxypropyl)methacrylamide copolymers. A potential drug delivery system. Biochim Biophys Acta 1981;678(1):143-50.

97. Duncan R, Cable HC, Rejmanová P, Kopeček J, Lloyd JB. Tyrosinamide residues enhance pinocytic capture of *N*-(2-hydroxypropyl)methacrylamide copolymers. Biochim Biophys Acta 1984;799(1):1-8.

98. McCormick LA, Seymour LCW, Duncan R, Kopeček J. Interaction of a cationic *N*-(2-hydroxypropyl)methacrylamide copolymer with rat visceral yolk sac cultured in vitro and rat liver in vivo. J Bioact Comp Polym 1986;1:4-19.

99. Omelyanenko V, Gentry C, Kopečková P, Kopeček J. HPMA copolymer-anticancer drug-OV-TL16 antibody conjugates. II. Processing in epithelial ovarian carcinoma cells in vitro. Int J Cancer 1998;75(4):600-8.

100. Říhová B. Targeting of drugs to cell surface receptors. Crit Rev Biotechnol 1997;17(2):149-69.

101. Allen TM, Cullis PR. Drug delivery systems: entering the mainstream. Science 2004;303(5665):1818-22.

102. Duncan R. The dawning era of polymer therapeutics. Nat Rev Drug Discov 2003;2(5):347-60.

103. Kopeček J, Bažilová H. Poly[*N*-(2-hydroxypropyl)methacrylamide]- I, Radical polymerization and copolymerization. Eur Polym J 1973;9(1):7-14.

104. Říhová B, Bilej M, Větvička V, Ulbrich K, Strohalm J, Kopeček J, et al. Biocompatibility of *N*-(2-hydroxypropyl)methacrylamide copolymers containing adriamycin. Immunogenicity, and effect on haematopoietic stem cells in bone marrow in vivo and mouse splenocytes and human peripheral blood lymphocytes in vitro. Biomaterials 1989;10(5):335-42.

105. Huang Y, Nan A, Rosen GM, Winalski CS, Schneider E, Tsai P, et al. *N*-(2-Hydroxypropyl)methacrylamide (HPMA) Copolymer-Linked Nitroxides: Potential Magnetic Resonance Contrast Agents. Macromol Biosci 2003;3(11):647-52.

106. Zarabi B, Nan A, Zhuo J, Gullapalli R, Ghandehari H. Macrophage targeted *N*-(2-hydroxypropyl)methacrylamide conjugates for magnetic resonance imaging. Mol Pharm 2006;3(5):550-7.

107. Foster S, Lloyd JB. Solute transport across the mammalian lysosome membrane. Biochim Biophys Acta 1988;947(3):465-91.

108. Willner D, Trail PA, Hofstead SJ, King HD, Lasch SJ, Braslawsky GR, et al. (6-Maleimidocaproyl)hydrazone of doxorubicin--a new derivative for the preparation of immunoconjugates of doxorubicin. Bioconjug Chem 1993;4(6):521-7.

109. Shen WC, Ryser HJ. cis-Aconityl spacer between daunomycin and macromolecular carriers: a model of pH-sensitive linkage releasing drug from a lysosomotropic conjugate. Biochem Biophys Res Commun 1981;102(3):1048-54.

110. Shen WC, Ryser HJ, LaManna L. Disulfide spacer between methotrexate and poly(D-lysine). A probe for exploring the reductive process in endocytosis. J Biol Chem 1985;260(20):10905-8.

111. Duncan R, Cable HC, Lloyd JB, Rejmanová P, Kopeček J. Polymers containing enzymatically degradable bonds. 7. Design of oligopeptide side-chains in poly[*N*-(2-hydroxypropyl)methacrylamide] copolymers to promote efficient degradation by lysosomal enzymes. Makromol Chem 1983;184:1997-2008.

112. Kopeček J, Rejmanová P. Enzymatically Degradable Bonds in Synthetic Polymers. In: Bruck SD, editor. Controlled Drug Delivery. Florida: CRC Press; 1983. p.81-124.
113. Rejmanová P, Kopeček J, Duncan R, Lloyd JB. Stability in rat plasma and serum of lysosomally degradable oligopeptide sequences in *N*-(2-hydroxypropyl) methacrylamide copolymers. Biomaterials 1985;6(1):45-8.
114. Rejmanová P, Pohl J, Baudyš M, Kostka V, Kopeček J. Polymers containing enzymatically degradable bonds. 8. Degradation of oligopeptide sequences in *N*-(2-hydroxypropyl)methacrylamide copolymers by bovine spleen cathepsin B. Makromol Chem 1983;184(10):2009-20.
115. Kopeček J. Controlled biodegradability of polymers--a key to drug delivery systems. Biomaterials 1984;5(1):19-25.
116. Seymour LW, Ulbrich K, Steyger PS, Brereton M, Subr V, Strohalm J, et al. Tumourtropism and anti-cancer efficacy of polymer-based doxorubicin prodrugs in the treatment of subcutaneous murine B16F10 melanoma. Br J Cancer 1994;70(4):636-41.
117. Chytrý V, Letourneur D, Vraná A, Jozefonvicz J. Insulin bound to chiral polymer with *N*-acetyl-D-glucosaminyl units. Lacks of mitogenic activity on rat aorta smooth muscle cell proliferation. J Control Release 1998;50(1-3):197-203.
118. Duncan R, Kopeček J, Rejmanová P, Lloyd JB. Targeting of *N*-(2-hydroxypropyl)methacrylamide copolymers to liver by incorporation of galactose residues. Biochim Biophys Acta 1983;755(3):518-21.
119. Eavarone DA, Yu X, Bellamkonda RV. Targeted drug delivery to C6 glioma by transferrin-coupled liposomes. J Biomed Mater Res 2000;51(1):10-4.
120. Gabizon A, Horowitz AT, Goren D, Tzemach D, Mandelbaum-Shavit F, Qazen MM, et al. Targeting folate receptor with folate linked to extremities of poly(ethylene glycol)-grafted liposomes: in vitro studies. Bioconjug Chem 1999;10(2):289-98.

121. Akhlynina TV, Rosenkranz AA, Jans DA, Sobolev AS. Insulin-mediated intracellular targeting enhances the photodynamic activity of chlorin e6. Cancer Res 1995;55(5):1014-9.

122. Blessing T, Kursa M, Holzhauser R, Kircheis R, Wagner E. Different strategies for formation of pegylated EGF-conjugated PEI/DNA complexes for targeted gene delivery. Bioconjug Chem 2001;12(4):529-37.

123. Gijsens A, Missiaen L, Merlevede W, de Witte P. Epidermal growth factor-mediated targeting of chlorin e6 selectively potentiates its photodynamic activity. Cancer Res 2000;60(8):2197-202.

124. Duncan R, Seymour LC, Scarlett L, Lloyd JB, Rejmanová P, Kopeček J. Fate of *N*-(2-hydroxypropyl)methacrylamide copolymers with pendent galactosamine residues after intravenous administration to rats. Biochim Biophys Acta 1986;880(1):62-71.

125. Krinick NL, Říhová B, Ulbrich K, Strohalm J, Kopeček J. Targetable photoactivatable drugs, 2. Synthesis of *N*-(2-hydroxypropyl)methacrylamide copolymer anti-thy 1.2 antibody-chlorin e_6 conjugates and a preliminary study of their photodynamic effect on mouse splenocytes in vitro. Makromol Chem 1990;191(4):839-56.

126. Duncan R, Coatsworth JK, Burtles S. Preclinical toxicology of a novel polymeric antitumour agent: HPMA copolymer-doxorubicin (PK1). Hum Exp Toxicol 1998;17(2):93-104.

127. Hopewel JW, Duncan R, Wilding D, Chakrabarti K. Preclinical evaluation of the cardiotoxicity of PK2: a novel HPMA copolymer-doxorubicin-galactosamine conjugate antitumour agent. Hum Exp Toxicol 2001;20(9):461-70.

128. Meerum Terwogt JM, ten Bokkel Huinink WW, Schellens JH, Schot M, Mandjes IA, Zurlo MG, et al. Phase I clinical and pharmacokinetic study of PNU166945, a novel water-soluble polymer-conjugated prodrug of paclitaxel. Anticancer Drugs 2001;12(4):315-23.

129. Bissett D, Cassidy J, de Bono JS, Muirhead F, Main M, Robson L, et al. Phase I and pharmacokinetic (PK) study of MAG-CPT (PNU 166148): a

polymeric derivative of camptothecin (CPT). Br J Cancer 2004;91(1):50-5.

130. Sarapa N, Britto MR, Speed W, Jannuzzo M, Breda M, James CA, et al. Assessment of normal and tumor tissue uptake of MAG-CPT, a polymer-bound prodrug of camptothecin, in patients undergoing elective surgery for colorectal carcinoma. Cancer Chemother Pharmacol 2003;52(5):424-30.
131. Schoemaker NE, van Kesteren C, Rosing H, Jansen S, Swart M, Lieverst J, et al. A phase I and pharmacokinetic study of MAG-CPT, a water-soluble polymer conjugate of camptothecin. Br J Cancer 2002;87(6):608-14.
132. Wachters FM, Groen HJ, Maring JG, Gietema JA, Porro M, Dumez H, et al. A phase I study with MAG-camptothecin intravenously administered weekly for 3 weeks in a 4-week cycle in adult patients with solid tumours. Br J Cancer 2004;90(12):2261-7.
133. Campone M, Rademaker-Lakhai JM, Bennouna J, Howell SB, Nowotnik DP, Beijnen JH, et al. Phase I and pharmacokinetic trial of AP5346, a DACH-platinum-polymer conjugate, administered weekly for three out of every 4 weeks to advanced solid tumor patients. Cancer Chemother Pharmacol 2007;60(4):523-33.
134. Rice JR, Gerberich JL, Nowotnik DP, Howell SB. Preclinical efficacy and pharmacokinetics of AP5346, a novel diaminocyclohexane-platinum tumor-targeting drug delivery system. Clin Cancer Res 2006;12(7 Pt 1):2248-54.
135. Schacht E, Ruys L, Vermeersch J, Remon JP, Duncan R. Use of polysaccharides as drug carriers. Dextran and inulin derivatives of procainamide. Ann N Y Acad Sci 1985;446:199-212.
136. Yang F, Zhuo R. Synthesis and Antitumor Activity of Poly(L-cysteine) Bonded Covalently 5-Fluorouracil. Polymer J 1990;22(7):572-7.
137. Pietersz GA. The linkage of cytotoxic drugs to monoclonal antibodies for the treatment of cancer. Bioconjug Chem 1990;1(2):89-95.
138. Pietersz GA, Cunningham Z, McKenzie IF. Specific in vitro anti-tumour activity of methotrexate-monoclonal antibody conjugates prepared using human

serum albumin as an intermediary. Immunol Cell Biol 1988;66 (Pt 1):43-9.

139. Ulbrich K, Šubr V, Strohalm J, Plocová D, Jelínková M, Říhová B. Polymeric drugs based on conjugates of synthetic and natural macromolecules. I. Synthesis and physico-chemical characterisation. J Control Release 2000;64(1-3):63-79.
140. Omelyanenko V, Kopečková P, Gentry C, Shiah JG, Kopeček J. HPMA copolymer-anticancer drug-OV-TL16 antibody conjugates. 1. influence of the method of synthesis on the binding affinity to OVCAR-3 ovarian carcinoma cells in vitro. J Drug Target 1996;3(5):357-73.
141. Lu ZR, Shiah JG, Kopečková P, Kopeček J. Preparation and biological evaluation of polymerizable antibody Fab' fragment targeted polymeric drug delivery system. J Control Release 2001;74(1-3):263-8.
142. Hansen HH, Bajorin DF, Muss HB, Purkalne G, Schrijvers D, Stahel R. Recommendations for a Global Core Curriculum in Medical Oncology. Ann Oncol 2004;15(11):1603-12.
143. Mason E, Routledge PA. Combination therapy of diseases: general concepts. In: Majkowski J, Bourgeois BF, Patsalos PN, Mattson RH, editors. Antiepileptic Drugs: Combination Therapy and Interactions. Cambridge: Cambridge University Press; 2005. p.3-15.
144. Harris SM, Mistry P, Freathy C, Brown JL, Charlton PA. Antitumour activity of XR5944 in vitro and in vivo in combination with 5-fluorouracil and irinotecan in colon cancer cell lines. Br J Cancer 2005;92(4):722-8.
145. Shanks RH, Rizzieri DA, Flowers JL, Colvin OM, Adams DJ. Preclinical evaluation of gemcitabine combination regimens for application in acute myeloid leukemia. Clin Cancer Res 2005;11(11):4225-33.
146. Jin ML, Yang BQ, Zhang W, Ren P. Combined treatment with photodynamic therapy and chemotherapy for advanced cardiac cancers. J Photochem Photobiol B 1992;12(1):101-6.
147. Nahabedian MY, Cohen RA, Contino MF, Terem TM, Wright WH, Berns MW, et al. Combination cytotoxic chemotherapy with cisplatin or

doxorubicin and photodynamic therapy in murine tumors. J Natl Cancer Inst 1988;80(10):739-43.

148. Peterson CM, Lu JM, Gu ZW, Shiah JG, Lythgoe K, Peterson CA, et al. Isobolographic assessment of the interaction between adriamycin and photodynamic therapy with meso-chlorin e_6 monoethylene diamine in human epithelial ovarian carcinoma (OVCAR-3) in vitro. J Soc Gynecol Investig 1995;2(6):772-7.
149. Welt S, Ritter G, Williams C, Jr., Cohen LS, Jungbluth A, Richards EA, et al. Preliminary report of a phase I study of combination chemotherapy and humanized A33 antibody immunotherapy in patients with advanced colorectal cancer. Clin Cancer Res 2003;9(4):1347-53.
150. Colasanti A, Kisslinger A, Quarto M, Riccio P. Combined effects of radiotherapy and photodynamic therapy on an in vitro human prostate model. Acta Biochim Pol 2004;51(4):1039-46.
151. Buchegger F, Allal AS, Roth A, Papazyan JP, Dupertuis Y, Mirimanoff RO, et al. Combined radioimmunotherapy and radiotherapy of liver metastases from colorectal cancer: a feasibility study. Anticancer Res 2000;20(3B):1889-96.
152. Kopeček J, Krinick NL, inventors; Drug delivery system for the simultaneous delivery of drugs activatable by enzymes and light patent 5,258,453. 2 Nov 1993.
153. Krinick NL, Sun Y, Joyner D, Spikes JD, Straight RC, Kopeček J. A polymeric drug delivery system for the simultaneous delivery of drugs activatable by enzymes and/or light. J Biomater Sci Polym Ed 1994;5(4):303-24.
154. Peterson CM, Lu JM, Sun Y, Peterson CA, Shiah JG, Straight RC, et al. Combination chemotherapy and photodynamic therapy with *N*-(2-hydroxypropyl)methacrylamide copolymer-bound anticancer drugs inhibit human ovarian carcinoma heterotransplanted in nude mice. Cancer Res 1996;56(17):3980-5.
155. Shiah JG, Sun Y, Peterson CM, Straight RC, Kopeček J. Antitumor activity of *N*-(2-hydroxypropyl)methacrylamide copolymer-mesochlorine e_6 and

adriamycin conjugates in combination treatments. Clin Cancer Res 2000;6(3):1008-15.

156. Shiah JG, Sun Y, Peterson CM, Kopeček J. Biodistribution of free and *N*-(2-hydroxypropyl)methacrylamide copolymer-bound mesochlorin e_6 and adriamycin in nude mice bearing human ovarian carcinoma OVCAR-3 xenografts. J Control Release 1999;61(1-2):145-57.
157. Larsen JC. Basic concepts and terminology used to describe the combined action of chemicals in mixtures. Combined Actions and Interactions of Chemicals in Mixtures. The Toxiclogical Effects of Exposure to Mixtures of Industrial and Environmental Chemicals. (1st ed): Schultz; 2003. p.20-32.
158. Groten JP, Feron VJ, Suhnel J. Toxicology of simple and complex mixtures. Trends Pharmacol Sci 2001;22(6):316-22.
159. Berenbaum MC. What is synergy? Pharmacol Rev 1989;41(2):93-141.
160. Greco WR, Bravo G, Parsons JC. The search for synergy: a critical review from a response surface perspective. Pharmacol Rev 1995;47(2):331-85.
161. Webb JL. Effect of more than one inhibitor. Enzymes and Metabolic Inhibitors. New York: Academic Press; 1963. p.55-79.
162. Fitzgerald JB, Schoeberl B, Nielsen UB, Sorger PK. Systems biology and combination therapy in the quest for clinical efficacy. Nat Chem Biol 2006;2(9):458-66.
163. Goldoni M, Johansson C. A mathematical approach to study combined effects of toxicants in vitro: evaluation of the Bliss independence criterion and the Loewe additivity model. Toxicol In Vitro 2007;21(5):759-69.
164. Fraser TR. The antagosnism between the actions of active substances. Br Med J 1872;2:485-7.
165. Tallarida RJ. Drug synergism: its detection and applications. J Pharmacol Exp Ther 2001;298(3):865-72.
166. Berenbaum MC. Criteria for analyzing interactions between biologically active agents. Adv Cancer Res 1981;35:269-335.

167. Meadows SL, Gennings C, Carter WH, Jr., Bae DS. Experimental designs for mixtures of chemicals along fixed ratio rays. Environ Health Perspect 2002;110 Suppl 6:979-83.
168. Chou TC. Derivation and properties of Michaelis-Menten type and Hill type equations for reference ligands. J Theor Biol 1976;59(2):253-76.
169. Chou TC. On the determination of availability of ligand binding sites in steady-state systems. J Theor Biol 1977;65(2):345-56.
170. Reynolds CP, Maurer BJ. Evaluating response to antineoplastic drug combinations in tissue culture models. Methods Mol Med 2005;110:173-83.
171. Chou TC, Talalay P. Analysis of combined drug effects: a new look at a very old problem. Trends Pharmacol Sci 1983;4:450-4.
172. Topaly J, Fruehauf S, Ho AD, Zeller WJ. Rationale for combination therapy of chronic myelogenous leukaemia with imatinib and irradiation or alkylating agents: implications for pretransplant conditioning. Br J Cancer 2002;86(9):1487-93.
173. Dasmahapatra GP, Didolkar P, Alley MC, Ghosh S, Sausville EA, Roy KK. In vitro combination treatment with perifosine and UCN-01 demonstrates synergism against prostate (PC-3) and lung (A549) epithelial adenocarcinoma cell lines. Clin Cancer Res 2004;10(15):5242-52.
174. Poindessous V, Koeppel F, Raymond E, Cvitkovic E, Waters SJ, Larsen AK. Enhanced antitumor activity of irofulven in combination with 5-fluorouracil and cisplatin in human colon and ovarian carcinoma cells. Int J Oncol 2003;23(5):1347-55.
175. Kopeček J. Targetable polymeric anticancer drugs. Temporal control of drug activity. Ann N Y Acad Sci 1991;618:335-44.
176. Kopeček J, Rejmanová P, Strohalm J, Ulbrich K, Říhová B, Chytrý V, et al., inventors; Synthetic polymeric drugs. patent 5,037,883. 6 Aug 1991.
177. Hongrapipat J, Kopečková P, Prakongpan S, Kopeček J. Enhanced antitumor activity of combinations of free and HPMA copolymer-bound drugs. Int J Pharm 2008;351(1-2):259-70.

178. Alley MC, Hollingshead MG, Dykes DJ, Waud WR. Human tumor xenograft models in NCI drug development. In: Teicher BA, Andrews PA, editors. Anticancer Drug Development Guide: Preclinical Screening, Clinical Trials, and Approval. (2nd ed). New Jersey: Humana Press; 2004. p.125-52.

179. Chou JH, Chou TC. Computerized simulation of dose reduction index (DRI) in synergistic drug combinations. Pharmacologist 1988;30:A231.

180. Chou TC, Martin N. A Computer Program for Quantitation of Synergism and Antagonism in Drug Combinations, and the Determination of IC_{50} and ED_{50} values. New York: ComboSyn, Inc.; 2006.

181. Dahl KN, Westhoff CM, Discher DE. Fractional attachment of CD47 (IAP) to the erythrocyte cytoskeleton and visual colocalization with Rh protein complexes. Blood 2003;101(3):1194-9.

182. Mawby WJ, Holmes CH, Anstee DJ, Spring FA, Tanner MJ. Isolation and characterization of CD47 glycoprotein: a multispanning membrane protein which is the same as integrin-associated protein (IAP) and the ovarian tumour marker OA3. Biochem J 1994;304 (Pt 2):525-30.

183. Boerman O, Massuger L, Makkink K, Thomas C, Kenemans P, Poels L. Comparative in vitro binding characteristics and biodistribution in tumor-bearing athymic mice of anti-ovarian carcinoma monoclonal antibodies. Anticancer Res 1990;10(5A):1289-95.

184. Campbell IG, Freemont PS, Foulkes W, Trowsdale J. An ovarian tumor marker with homology to vaccinia virus contains an IgV-like region and multiple transmembrane domains. Cancer Res 1992;52(19):5416-20.

185. Roth MG. Clathrin-mediated endocytosis before fluorescent proteins. Nat Rev Mol Cell Biol 2006;7(1):63-8.

186. Soldati T, Schliwa M. Powering membrane traffic in endocytosis and recycling. Nat Rev Mol Cell Biol 2006;7(12):897-908.

187. Liu J, Pan H, Kopečková P, Kopeček J, editors. Internalization and Subcellular Fate of HPMA Copolymer-Doxorubicin Conjugates. International Symposium on Polymer Therapeutics ISPT-07; 2007 February 19-21;

Berlin, Germany. Institute of Chemistry and Biochemistry, Freie Universität Berlin.

188. Omelyanenko V, Kopečková P, Gentry C, Kopeček J. Targetable HPMA copolymer-adriamycin conjugates. Recognition, internalization, and subcellular fate. J Control Release 1998;53(1-3):25-37.
189. O'Connor PM, Jackman J, Bae I, Myers TG, Fan S, Mutoh M, et al. Characterization of the p53 tumor suppressor pathway in cell lines of the National Cancer Institute anticancer drug screen and correlations with the growth-inhibitory potency of 123 anticancer agents. Cancer Res 1997;57(19):4285-300.
190. Yaginuma Y, Westphal H. Abnormal structure and expression of the p53 gene in human ovarian carcinoma cell lines. Cancer Res 1992;52(15):4196-9.
191. Marecos E, Weissleder R, Bogdanov A, Jr. Antibody-mediated versus nontargeted delivery in a human small cell lung carcinoma model. Bioconjug Chem 1998;9(2):184-91.
192. Shmueli A, Oren M. Regulation of p53 by Mdm2: fate is in the numbers. Mol Cell 2004;13(1):4-5.
193. Tijerina M, Kopečková P, Kopeček J. Mechanisms of cytotoxicity in human ovarian carcinoma cells exposed to free Mce_6 or HPMA copolymer-Mce_6 conjugates. Photochem Photobiol 2003;77(6):645-52.
194. Nori A, Jensen KD, Tijerina M, Kopečková P, Kopeček J. Tat-conjugated synthetic macromolecules facilitate cytoplasmic drug delivery to human ovarian carcinoma cells. Bioconjug Chem 2003;14(1):44-50.
195. Callahan J, Kopeček J. Semitelechelic HPMA copolymers functionalized with triphenylphosphonium as drug carriers for membrane transduction and mitochondrial localization. Biomacromolecules 2006;7(8):2347-56.
196. Slobbe R, Poels L, ten Dam G, Boerman O, Nieland L, Leunissen J, et al. Analysis of idiotope structure of ovarian cancer antibodies: recognition of the same epitope by two monoclonal antibodies differing mainly in their heavy chain variable sequences. Clin Exp Immunol 1994;98(1):95-103.

197. Serova M, Calvo F, Lokiec F, Koeppel F, Poindessous V, Larsen AK, et al. Characterizations of irofulven cytotoxicity in combination with cisplatin and oxaliplatin in human colon, breast, and ovarian cancer cells. Cancer Chemother Pharmacol 2006;57(4):491-9.
198. Vugrin D. Systemic therapy of metastatic renal cell carcinoma. Semin Nephrol 1987;7(2):152-62.
199. Yu DS, Chang SY, Ma CP. The expression of mdr-1-related gp-170 and its correlation with anthracycline resistance in renal cell carcinoma cell lines and multidrug-resistant sublines. Br J Urol 1998;82(4):544-7.
200. Warburton HE, Brady M, Vlatkovic N, Linehan WM, Parsons K, Boyd MT. p53 regulation and function in renal cell carcinoma. Cancer Res 2005;65(15):6498-503.
201. Mertins SD, Myers TG, Hollingshead M, Dykes D, Bodde E, Tsai P, et al. Screening for and identification of novel agents directed at renal cell carcinoma. Clin Cancer Res 2001;7(3):620-33.
202. Chiarello K. In between the light and the dark. Pharm Technol 2004;28(12):48-54.
203. Dougherty TJ, Cooper MT, Mang TS. Cutaneous phototoxic occurrences in patients receiving Photofrin. Lasers Surg Med 1990;10(5):485-8.
204. Goff BA, Bamberg M, Hasan T. Photoimmunotherapy of human ovarian carcinoma cells ex vivo. Cancer Res 1991;51(18):4762-7.
205. Greco F, Vicent MJ, Penning NA, Nicholson RI, Duncan R. HPMA copolymer-aminoglutethimide conjugates inhibit aromatase in MCF-7 cell lines. J Drug Target 2005;13(8-9):459-70.
206. Vicent MJ, Greco F, Nicholson RI, Paul A, Griffiths PC, Duncan R. Polymer therapeutics designed for a combination therapy of hormone-dependent cancer. Angew Chem International Ed Engl 2005;44(26):4061-6.
207. Loewe S. The problem of synergism and antagonism of combined drugs. Arzneimittelforschung 1953;3(6):285-90.
208. Bartoszek A. Metabolic activation of adriamycin by NADPH-cytochrome P450 reductase; overview of its biological and biochemical effects. Acta Biochim Pol 2002;49(2):323-31.

209. Berlin V, Haseltine WA. Reduction of adriamycin to a semiquinone-free radical by NADPH cytochrome P-450 reductase produces DNA cleavage in a reaction mediated by molecular oxygen. J Biol Chem 1981;256(10):4747-56.

210. Edell ES, Cortese DA. Combined effects of hematoporphyrin derivative phototherapy and adriamycin in a murine tumor model. Lasers Surg Med 1988;8(4):413-7.

211. Brophy PF, Keller SM. Adriamycin enhanced in vitro and in vivo photodynamic therapy of mesothelioma. J Surg Res 1992;52(6):631-4.

212. Lanks KW, Gao JP, Sharma T. Photodynamic enhancement of doxorubicin cytotoxicity. Cancer Chemother Pharmacol 1994;35(1):17-20.

213. Kirveliene V, Grazeliene G, Dabkeviciene D, Micke I, Kirvelis D, Juodka B, et al. Schedule-dependent interaction between Doxorubicin and mTHPC-mediated photodynamic therapy in murine hepatoma in vitro and in vivo. Cancer Chemother Pharmacol 2006;57(1):65-72.

214. Trail PA, Willner D, Bianchi AB, Henderson AJ, TrailSmith MD, Girit E, et al. Enhanced antitumor activity of paclitaxel in combination with the anticarcinoma immunoconjugate BR96-doxorubicin. Clin Cancer Res 1999;5(11):3632-8.

215. Zhang L, Yu D, Hicklin DJ, Hannay JA, Ellis LM, Pollock RE. Combined anti-fetal liver kinase 1 monoclonal antibody and continuous low-dose doxorubicin inhibits angiogenesis and growth of human soft tissue sarcoma xenografts by induction of endothelial cell apoptosis. Cancer Res 2002;62(7):2034-42.

216. Yamashita Y, Krauze MT, Kawaguchi T, Noble CO, Drummond DC, Park JW, et al. Convection-enhanced delivery of a topoisomerase I inhibitor (nanoliposomal topotecan) and a topoisomerase II inhibitor (pegylated liposomal doxorubicin) in intracranial brain tumor xenografts. Neuro Oncol 2007;9(1):20-8.

217. Saucier JM, Yu J, Gaikwad A, Coleman RL, Wolf JK, Smith JA. Determination of the optimal combination chemotherapy regimen for treatment of

platinum-resistant ovarian cancer in nude mouse model. J Oncol Pharm Pract 2007;13(1):39-45.

218. Amato RJ. Renal cell carcinoma: review of novel single-agent therapeutics and combination regimens. Ann Oncol 2005;16(1):7-15.

219. Hainsworth JD, Sosman JA, Spigel DR, Edwards DL, Baughman C, Greco A. Treatment of metastatic renal cell carcinoma with a combination of bevacizumab and erlotinib. J Clin Oncol 2005;23(31):7889-96.

BIOGRAPHY

NAME	Jarunee Hongrapipat
DATE OF BIRTH	16 March 1980
PLACE OF BIRTH	Surin, Thailand
INSTITUTUION ATTENDED	Srinakharinwirot University, 1997-2001 Bachelor of Pharmacy (Second class honors) Mahidol University, 2002-2007 Doctor of Philosophy (Pharmaceutics)
POSITION & OFFICE	Srinakharinwirot University, 2001-2002 Ongkharak, Nakhornnayok, 26120 Thailand Position: Lecturer
HOME ADDRESS	227-228 Tepnimit Road, Sikhoraphum, Surin, 32110 Thailand Tel. (664)-456-1015 E-mail: jarunee.hongrapipat@gmail.com

GRADUATION GRANT	Thailand Research Fund through the Royal Golden Jubilee Ph.D. Program (Grant. No. PHD/0176/2545) NIH Grant CA51578 from the National Cancer Institute